THE UNIVERSITY OF ADELAIDE

DEPARTMENT OF MECHANICAL ENGINEERING

AN INVESTIGATION INTO THE DEVELOPMENT OF LAMINAR NATURAL CONVECTION IN HEATED VERTICAL DUCTS

by

J. Ross Dyer, B.E., B.Ec.

Thesis for the Degree of Doctor of Philosophy

October, 1971

TABLE OF CONTENTS

SUMMARY

An account of a theoretical and experimental study of the development of laminar natural-convective flow in heated vertical ducts is presented in this thesis. The ducts studied were open-ended and circular in cross-section, and the heated internal surface either had a uniform temperature or dissipated heat uniformly. In addition, the effect of restricting the flow at entry was studied in the case of ducts with uniform surface temperatures. In this work the flow restriction was provided by keeping the lower part of the duct at ambient temperature.

Relationships between Nusselt and Rayleigh numbers were derived by relaxing the governing equations. The general solutions obtained on a computer were corroborated at both small and large Rayleigh numbers by theoretical analysis.

For uniform surface temperature ducts two distinct laminar flow regimes were observed. At small Rayleigh numbers the flow was fully developed and at large Rayleigh numbers boundary layer flow occurred. An entry restriction had the effect of lowering the Nusselt

number. However, it was found that the flow ceased to be laminar when the entry restriction reached a certain size and that the size of the largest entry restriction for laminar flow decreased with increasing Rayleigh numbers.

Besides confirming the theoretical work, the experimental studies supported the hypothesis that entry restrictions that were too large to allow laminar flow throughout the duct produced a mixing flow above where the laminar flow degenerated. Furthermore, it was found that, if the entry restriction were very large, an unsteady open-thermosyphon flow occurred in the top part of the duct. In this case, the open-thermosyphon flow dissipated heat in the upper part of the duct as did the restricted-entry flow in the lower part.

Prandtl numbers greater than about 0.7 were found to have only a small effect on the theoretical relationship between the Nusselt and Rayleigh numbers. However, the influence that the Prandtl number had on the relationship was shown to increase significantly as the Prandtl number decreased below 0.7.

In uniform surface heat flux ducts, it is not

possible to obtain fully developed flow because the fluid is receiving heat along the entire length of the duct. However, small Rayleigh numbers produced a flow that resembled fully developed flow. At the other extreme, large Rayleigh numbers produced a boundary layer flow. For boundary layer flow, it was found that the Nusselt number relationship for the uniform surface temperature ducts could be satisfactorily used if the entire surface were assumed to be at the mean surface temperature.

DECLARATION OF ORIGINALITY

This thesis contains no material that has been accepted by another University for the award of a degree or a diploma. Also, to the best of the author's knowledge and belief, this thesis contains no material previously published or written by another person, except where due reference has been made in the text of the thesis.

J.R. Dyer
October, 1971

ACKNOWLEDGEMENTS

The work described in this thesis was carried out in the Department of Mechanical Engineering at the University of Adelaide under the aegis of Professor H.H. Davis. The author is grateful to Professor Davis for allowing him to undertake the research.

The author is greatly indebted to Dr J. Mannam, Reader in the Department of Mechanical Engineering at the University of Adelaide, for his encouragement and for his help and advice on many occasions.

The author thanks Messrs R.C. Fitton, R.H. Schumann, H. Bode and other members of the staff of the Mechanical Engineering Workshop for their valuable contributions to the experimental work.

For making the experimental ducts and for carrying out some of the tests, Messrs I.G. Stanley, S.G. Lim, C.E.T. Ong and R.K. Inverarity, former undergraduate students in the Department of Mechanical Engineering at the University of Adelaide, are gratefully acknowledged.

For proof reading and helping to prepare the material for publication, the author is much indebted to his wife, Elizabeth.

A special word of thanks is due to Mrs G.M. Duncan who, when typing the text, kept a careful watch for inconsistencies in the manuscript.

Finally, the author thanks the Australian Institute of Nuclear Science and Engineering for providing financial grants, without which this work would not have been possible.

1. INTRODUCTION

1.1 Scope of the investigation - In many industrial applications, the internal surfaces of vertical ducts have to be cooled by natural convection. Since there is little information in the literature on the subject of natural convection in open-ended vertical ducts, it was considered profitable to carry out a theoretical and experimental study into the mechanism of laminar natural convection in such ducts. The results of this study, including those which have previously been published (1,2)[1], are presented in this thesis.

All the work to be described was undertaken on ducts of circular cross-section, and the following specific problems in natural-convective heat transfer were examined:

1. Ducts with uniform surface temperatures and plain entries
2. Ducts with uniform surface temperatures and restricted entries
3. Ducts with uniform surface heat fluxes and plain entries

---

[1] References, shown on page 173.

Shown in Fig. 1.1 are sectional views of these ducts. It will be seen in Fig. 1.1(b) that the entry restriction is simply an unheated section of the duct.

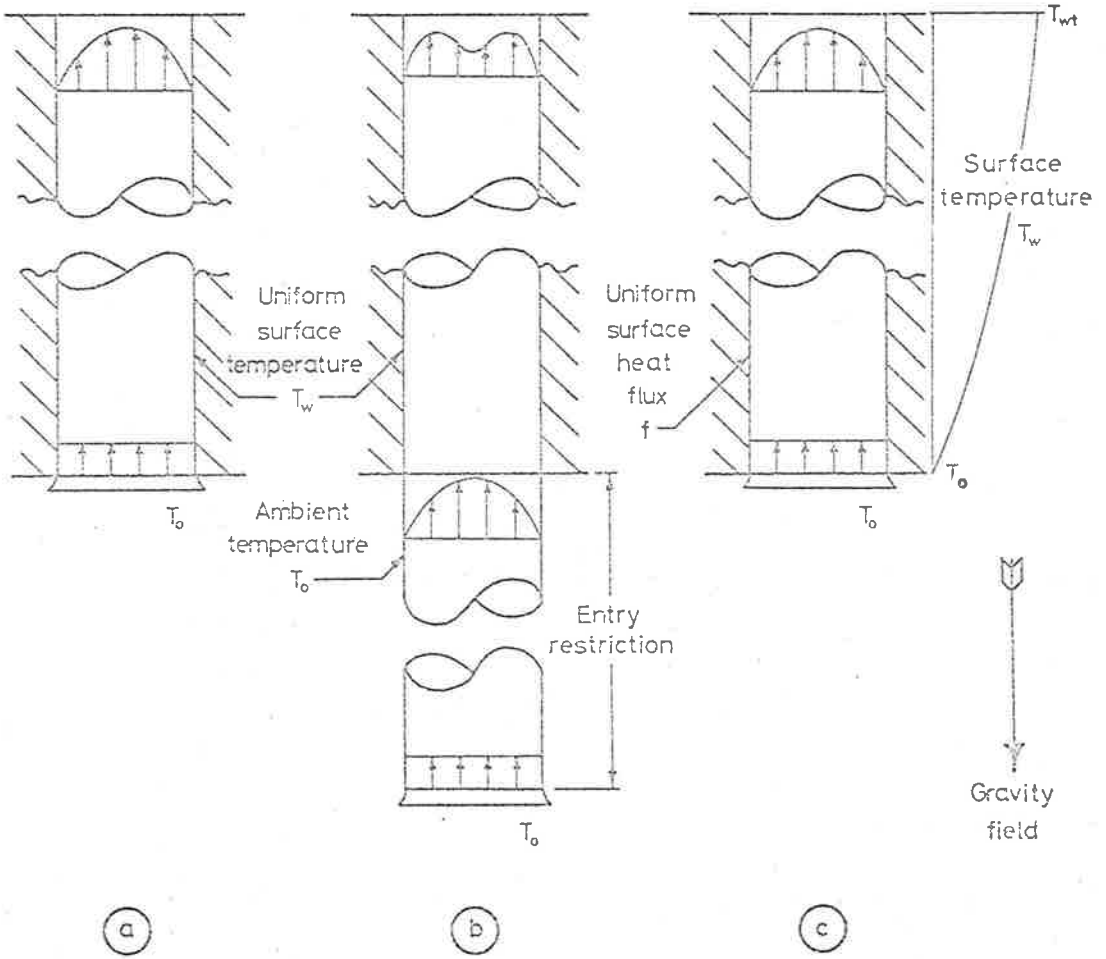

Fig. 1.1 Diagrammatic sectioned views of the heated ducts

(a) Plain-entry duct with a uniform surface temperature
(b) Restricted-entry duct with a uniform surface temperature
(c) Plain-entry duct with a uniform surface heat flux

1.2 List of symbols

General:

a	Cross-sectional area of the duct
A	Internal surface area of the heated section of the duct
c_p	Specific heat at constant pressure
C	Constant
g	Acceleration of gravity
h_x	Heat dissipated by convection from the bottom of the duct to a particular elevation per unit time
k	Thermal conductivity of the fluid
ℓ	Length of the heated section of the duct
ℓ_i	Length of the unheated section of the duct (entry-restriction)
p	Pressure
p_d	Pressure defect, $(p-p_o)$
p_o	Hydrostatic pressure
Pr	Prandtl number, $\mu c_p/k$
q	Volume flow
r	Radial coordinate
R	Dimensionless radial coordinate, r/r_w
T	Temperature
u	Velocity of the fluid in the x- direction
v	Velocity of the fluid in the radial direction

V Dimensionless fluid velocity in the radial direction, $r_w v/\nu$

x Vertical coordinate; x=0 at the bottom of the heated section

β Coefficient of thermal buoyancy of the fluid

μ Dynamic viscosity of the fluid

ν Kinematic viscosity of the fluid, μ/ρ

ρ Density of the fluid

Applicable only to ducts with uniform surface temperatures:

Gr Grashof number based on both the heated length and the radius of the duct, $g\beta(T_w-T_o)r_w^4/\nu^2\ell$

Gr_ℓ Grashof number based on only the heated length of the duct, $g\beta(T_w-T_o)\ell^3/\nu^2$

H_x Dimensionless heat dissipated from the bottom of the duct to a particular elevation per unit time, $h_x/\rho c_p \nu \ell Gr(T_w-T_o)$

L Dimensionless length of the heated section of the duct, $1/Gr$

L_i Dimensionless length of the unheated section of the duct, $\ell_i/\ell Gr$

Nu Nusselt number based on the radius of the duct, $h_t r_w/A(T_w-T_o)k$, which reduces to $h_t/2\Pi\ell(T_w-T_o)k$

Nu_ℓ Nusselt number based on the heated length of the duct, $h_t\ell/A(T_w-T_o)k$, which reduces to $h_t/2\pi r_w(T_w-T_o)k$

P Dimensionless pressure, $pr_w^4/\rho\ell^2\nu^2Gr^2$

P_d Dimensionless pressure defect, $p_d r_w^4/\rho\ell^2\nu^2Gr^2$

Q Dimensionless volume flow, $q/\ell\nu Gr$

Ra Rayleigh number, Gr Pr

Re_r Reynolds number based on the radius of the duct, $u_m r_w/\nu$ or $GrQ\ell/\pi r_w$

U Dimensionless velocity of the fluid in the X-direction, $ur_w^2/\ell\nu Gr$

X Dimensionless vertical coordinate, $x/\ell Gr$; X=0 at the bottom of the heated section

θ Dimensionless temperature, $(T-T_o)/(T_w-T_o)$

Applicable only to uniform surface heat flux ducts[1]

f Uniform surface heat flux

F Dimensionless uniform heat flux, 1/Pr

Gr* Grashof number based on both the length and the radius of the duct, $g\beta f r_w^5/\nu^2\ell k$

---

1 The symbols for the dimensionless variables that are not common to those for ducts having uniform surface temperatures are identified by * for variables based on the uniform heat flux and by + for variables based on the mean temperature of the surface.

Gr^*_ℓ Grashof number based on only the length of the duct, $g\beta f\ell^4/\nu^2 k$

Gr^+ Gr^*/Nu^*

H^*_x Dimensionless heat dissipated from the bottom of the duct to a particular elevation per unit time, $h_x/Ra^* f\ell r_w$

H^+_x $H^*_x(Nu^*)^2$

L^* Dimensionless length of the duct, $1/Gr^*$

Nu^* Nusselt number based on the radius of the duct, $fr_w/(T_{wm}-T_o)k$

Nu^*_ℓ Nusselt number based on the length of the duct, $f\ell/(T_{wm}-T_o)k$

P^* Dimensionless pressure, $pr_w^4/\rho\ell^2\nu^2 Gr^{*2}$

P^*_d Dimensionless pressure defect, $p_d r_w^4/\rho\ell^2\nu^2 Gr^{*2}$

Q^* Dimensionless volume flow, $q/\ell\nu Gr^*$

Q^+ Q^*Nu^*

Ra^* Rayleigh number, Gr^*Pr

Ra^+ Ra^*/Nu^*

Re^*_r Reynolds number based on the radius of the duct, $u_m r_w/\nu$ or $Gr^*Q^*\ell/\Pi r_w$

U^* Dimensionless fluid velocity in X-direction, $r_w^2 u/\ell\nu Gr^*$

X^* Dimensionless vertical coordinate, $x/\ell Gr^*$; $X^*=0$ at the bottom of the heated section

θ^* Dimensionless temperature, $(T-T_o)k/fr_w$

θ^+ $\theta^* Nu^*$

Subscripts:

ct	On the vertical axis and at the top of the duct
cx	On the vertical axis and at elevation x, X, or X*
d	Defect (pressure)
e	Refers to the smaller diameter entrance used in the experimental study
i	Refers to the unheated section of the duct
j	j^{th} row of the relaxation grid
k	k^{th} column of the relaxation grid
ℓ	Based on the heated length of the duct
m	Mean value
me	At mid-elevation
o	Refers to ambient conditions
opt	Optimum value
p	Constant pressure
r	Based on the radius of the duct
t	At the top of the duct
w	Refers to the internal surface of the duct
wm	On the internal surface, and the mean value of the variable
wt	On the internal surface and at the top of the duct
wx	On the internal surface and at elevation x, X or X*

Abbreviations:

UST Uniform surface temperature

USHF Uniform surface heat flux

2. THEORETICAL CONSIDERATIONS

2.1 General

Heating the surfaces of the vertical ducts shown in Fig. 1.1 will produce an upward natural-convective flow through the ducts. The buoyancy forces giving rise to the flow are produced by density differences in the gravitational field.

In the case of the partly heated duct shown in Fig. 1.1(b), the flow, and consequently the heat transfer, will be reduced owing to the resistance presented by the unheated section. If, however, the restriction exceeds a certain size, the flow will cease to be laminar and fluid may even enter the top of the duct. This produces a flow in the upper part of the heated section similar to that in an open-thermosyphon duct (3) (a vertical duct that is open at the top and closed at the bottom).

Elenbaas (4) established the heat dissipating characteristics of plain-entry ducts of circular and other cross-sectional shapes with uniform surface temperatures. This was done by transforming the results of his theoretical study of natural-convective flow through heated vertical channels formed by two parallel and infinitely wide flat plates (5). It was not possible, however, to obtain temperature and velocity profiles in a

duct by using this method of solution.

This short-coming of Elenbaas's method (4) can now be remedied by relaxing the governing equations on a high-speed digital computer. Hence in the present work the development of laminar flow in vertical ducts of circular cross-section was determined by relaxation. The method adopted was similar to that used by Bodoia and Osterle (6) in their study of natural-convective flow through heated vertical channels.

2.2 Laminar flow equations

Throughout the analysis to be presented the following simplifying assumptions have been made:

(a) The fluid is Newtonian

(b) Fluid properties, except density, are independent of temperature

(c) Density variations are significant only in producing the buoyancy forces

(d) Flow in the duct is steady, incompressible and axisymmetrical

(e) Heat generated by internal friction is negligible

(f) Pressure variations in the duct are too small to have any effect on the properties of the fluid

The entry restriction shown in Fig. 1.1(b) was chosen because it allowed laminar flow to be produced in both sections of the duct, and thereby the mathematical analysis was simplified. It should be noted that a similar type of flow restriction was used by Dyer and Fowler (7) in their analysis of the problem of the restricted-entry vertical channel.

Fig. 2.1 describes the system of cylindrical coordinates used in the analysis. Using the assumptions on page 12, the equations of continuity, momentum and energy in cylindrical coordinates for laminar flow (8) are:

Continuity equation

$$\frac{\partial u}{\partial x} + \frac{1}{r}\frac{\partial rv}{\partial r} = 0 \qquad \ldots (2.1)$$

Momentum equations

$$\rho\left(u\frac{\partial u}{\partial x} + v\frac{\partial u}{\partial r}\right) = -\frac{\partial p}{\partial x} + \mu\left[\frac{1}{r}\frac{\partial}{\partial r}\left(r\frac{\partial u}{\partial r}\right) + \frac{\partial^2 u}{\partial x^2}\right] - g\rho \qquad \ldots (2.2)$$

$$\rho\left(u\frac{\partial v}{\partial x} + v\frac{\partial v}{\partial r}\right) = -\frac{\partial p}{\partial r} + \mu\left[\frac{\partial}{\partial r}\left(\frac{1}{r}\frac{\partial rv}{\partial r}\right) + \frac{\partial^2 v}{\partial x^2}\right] \qquad \ldots (2.3)$$

Energy equation

$$u \frac{\partial T}{\partial x} + v \frac{\partial T}{\partial r} = \frac{k}{\rho c_p} \left[\frac{\partial^2 T}{\partial r^2} + \frac{1}{r} \frac{\partial T}{\partial r} + \frac{\partial^2 T}{\partial x^2} \right] \quad \ldots (2.4)$$

The fluid entering and leaving the duct is under hydrostatic pressure. However, as the flow is confined, the pressure within the duct (p) will be less than the hydrostatic pressure (p_o) at the same elevation. The difference between the two pressures ($p-p_o$) will be called the pressure defect (p_d) (6).

The hydrostatic pressure decreases with elevation (9) according to the equation

$$\frac{dp_o}{dx} = - \rho_o g \quad \ldots (2.5)$$

Hence adding both $\frac{\partial p_o}{\partial x}$ and $\rho_o g$ to the right hand side of Eq. (2.2) yields

$$\rho \left(u \frac{\partial u}{\partial x} + v \frac{\partial u}{\partial r} \right) = - \frac{\partial (p-p_o)}{\partial x} + \mu \left[\frac{1}{r} \frac{\partial}{\partial r} \left(r \frac{\partial u}{\partial r} \right) + \frac{\partial^2 u}{\partial x^2} \right] + g(\rho_o - \rho) \quad \ldots (2.6)$$

The last term on the right hand side of Eq. (2.6) is the buoyancy force. It can be expressed in terms of

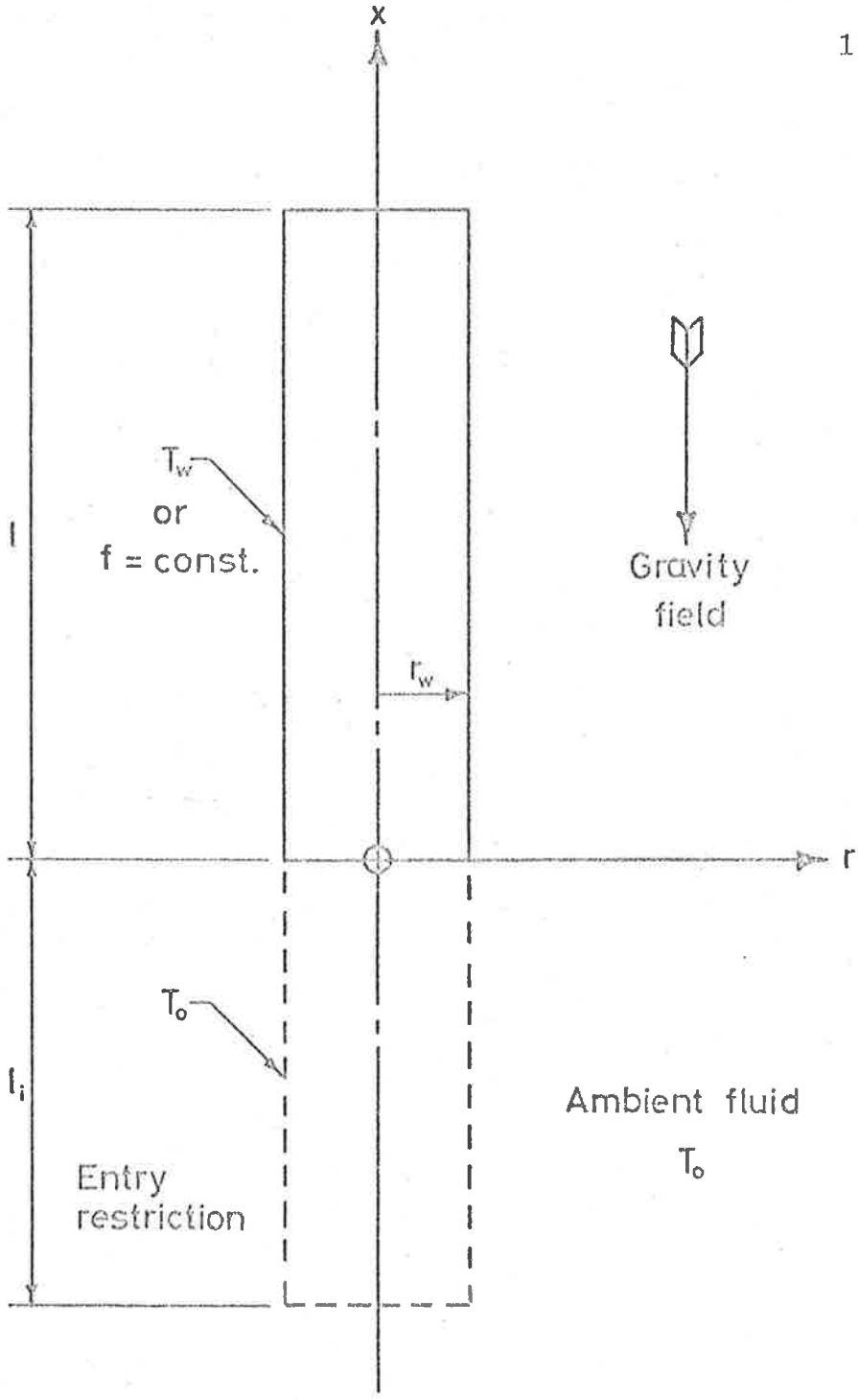

Fig. 2.1 System of cylindrical coordinates

the temperature difference $(T-T_o)$ by introducing the coefficient of thermal buoyancy (9) which is defined by the equation

$$\beta = - \frac{1}{\rho} \left(\frac{\partial \rho}{\partial T}\right)_p \qquad \ldots (2.7)$$

As an approximation for the small density difference caused by a temperature variation (9), the following relationship can be written:

$$(\rho_o - \rho) = \rho\beta(T-T_o) \qquad \ldots (2.8)$$

Substituting Eq. (2.8) into Eq. (2.6) yields

$$\rho\left(\frac{\partial u}{\partial x} + v \frac{\partial u}{\partial r}\right) = - \frac{\partial P_d}{\partial x} + \mu \left[\frac{1}{r} \frac{\partial}{\partial r}\left(r \frac{\partial u}{\partial r}\right) + \frac{\partial^2 u}{\partial x^2}\right] + g\rho\beta(T-T_o) \qquad \ldots (2.9)$$

Eqs. (2.1), (2.9), (2.3) and (2.4) can be expressed in the following dimensionless forms by using the dimensionless variables in the List of Symbols on pages 4 to 10.

The dimensionless equations for uniform surface temperature (UST) ducts reduce to:

$$\frac{\partial U}{\partial X} + \frac{V}{R} + \frac{\partial V}{\partial R} = 0 \qquad \ldots (2.10)$$

$$U \frac{\partial U}{\partial X} + V \frac{\partial U}{\partial R} = - \frac{\partial P_d}{\partial X} + \frac{\partial^2 U}{\partial R^2} + \frac{1}{R} \frac{\partial U}{\partial R} + \theta \qquad \ldots (2.11)$$

$$\frac{\partial P_d}{\partial R} = 0 \qquad \ldots (2.12)$$

$$U \frac{\partial \theta}{\partial X} + V \frac{\partial \theta}{\partial R} = \frac{1}{Pr} \left[\frac{\partial^2 \theta}{\partial R^2} + \frac{1}{R} \frac{\partial \theta}{\partial R} \right] \qquad \ldots (2.13)$$

Using another set of dimensionless variables, the equations for uniform surface heat flux (USHF) ducts reduce to:

$$\frac{\partial U^*}{\partial X^*} + \frac{V}{R} + \frac{\partial V}{\partial R} = 0 \qquad \ldots (2.14)$$

$$U^* \frac{\partial U^*}{\partial X^*} + V \frac{\partial U^*}{\partial R} = - \frac{\partial P_d^*}{\partial X^*} + \frac{\partial^2 U^*}{\partial R^2} + \frac{1}{R} \frac{\partial U^*}{\partial R} + \theta^* \qquad \ldots (2.15)$$

$$\frac{\partial P_d^*}{\partial R} = 0 \qquad \ldots (2.16)$$

$$U^* \frac{\partial \theta^*}{\partial X^*} + V \frac{\partial \theta^*}{\partial R} = \frac{1}{Pr} \left[\frac{\partial^2 \theta^*}{\partial R^2} + \frac{1}{R} \frac{\partial \theta^*}{\partial R} \right] \qquad \ldots (2.17)$$

The reason that some of the symbols in Eqs. (2.14) to (2.17) are without an asterisk is that they are common to both UST and USHF ducts. (Symbols with an asterisk are applicable only to USHF ducts).

Terms containing $r_w/\ell Gr$ and $r_w/\ell Gr^*$ were omitted

from the foregoing sets of dimensionless equations. This is permissible because in most practical situations these parameters, which are raised to the second power, are very much less than unity as illustrated in the following example. A 2 in. diameter duct has an internal surface temperature of 200°F and stands in a fluid whose temperature is 100°F. Calculations show that:

$$\text{for air,} \quad r_w/\ell Gr = 2 \times 10^{-5}$$

$$\text{for water,} \quad r_w/\ell Gr = 3 \times 10^{-8}$$

In each case the value of the parameter will be seen to be very much less than unity.

3. PLAIN-ENTRY DUCTS WITH UNIFORM SURFACE TEMPERATURES

3.1 General Nusselt relationship

The plain-entry duct with a uniform surface temperature illustrated in Fig. 1.1(a) has a dimensionless length (L), which, by definition (see List of Symbols), is the reciprocal of the Grashof number (Gr). This Grashof number is the product of $g\beta(T_w-T_o)r_w^3/\nu^2$, which is a Grashof number of the conventional form, and the ratio r_w/ℓ (6).

Since it has been assumed that the density of the fluid does not vary (see page 12), the dimensionless flow volume (Q) is constant throughout the duct and is given by

$$Q = 2\Pi \int_0^1 U\ R\ dR \qquad \ldots (3.1)$$

It follows from Eq. (3.1) that the dimensionless heat dissipated by the surface from the bottom of the duct to a particular elevation (X) is given by

$$H_X = 2\Pi \int_0^1 U\ \theta\ R\ dR \qquad \ldots (3.2)$$

The Nusselt number of the duct with the radius as the characteristic dimension is given by

$$Nu = \frac{h_t \, r_w}{A(T_w - T_o)k} \qquad \ldots (3.3)$$

where h_t is the rate at which the internal surface of the duct dissipates heat. When the surface area (A) is replaced by $2\Pi r_w \ell$, Eq. (3.3) becomes

$$Nu = \frac{h_t}{2\Pi \ell (T_w - T_o)k} \qquad \ldots (3.4)$$

Expressing h_t in terms of the dimensionless rate (H_t), Eq. (3.4) becomes

$$Nu = \frac{Gr \; Pr \; H_t}{2\Pi} \qquad \ldots (3.5)$$

Replacing Gr Pr by the Rayleigh number (Ra), Eq. (3.5) reduces to

$$Nu = \frac{Ra \; H_t}{2\Pi} \qquad \ldots (3.6)$$

Since the relationship between Nu and Ra alone is required, Eqs. (2.10) to (2.13) will be solved for the following boundary conditions based on the geometry of the duct shown in Fig. 2.1.

Boundary conditions

$X=0$ and $R=1$; $U=0$, $V=0$, $\theta=1$, $P_d=0$. (a)

$X=0$ and $1<R\leqslant 0$; $U=\frac{Q}{\Pi}$, $V=0$, $\theta=0$, $P_d=0$. (b)

$0<X<L$ and $R=1$; $U=0$, $V=0$, $\theta=1$, $P_d<0$. (c)

$0<X<L$ and $R=0$; $V=0$, $P_d<0$, $\frac{\partial U}{\partial R}=0$, $\frac{\partial \theta}{\partial R}=0$. (d)

$X=L$ and $R=1$; $U=0$, $V=0$, $\theta=1$, $P_d=0$. (e)

$X=L$ and $R=0$; $V=0$, $P_d=0$, $\frac{\partial U}{\partial R}=0$, $\frac{\partial \theta}{\partial R}=0$. (f)

$0\leqslant X\leqslant L$; Q is a constant. (g)

The assumption that the fluid enters the duct with a uniform velocity ($U=Q/\Pi$) was based on the practice usually adopted in analysing the development of forced-convective flow in pipes (9).

Before beginning the general solution of Eqs. (2.10) to (2.13), simplified solutions for the extreme values of the ratio ℓ/r_w will be obtained. The Nusselt relationships yielded by this analysis are useful for the corroboration of the results of the general solution.

3.2 Nusselt relationship for fully developed flow

Fully developed flow is obtained when the ratio

ℓ/r_w is made sufficiently large. This will produce a duct that has a small Ra.

When the flow is fully developed, the temperature of the fluid is the same as that of the surface, that is $\theta=1$, and the velocity profile is parabolic. Thus, for fully developed flow Eq. (2.11) reduces to

$$\frac{\partial P_d}{\partial X} = \frac{\partial^2 U}{\partial R^2} + \frac{1}{R}\frac{\partial U}{\partial R} + 1 \qquad \ldots (3.7)$$

and the velocity at a radius R for a volume flow (Q) is given by

$$U = \frac{2Q}{\Pi}(1-R^2) \qquad \ldots (3.8)$$

Substituting Eq. (3.8) into Eq. (3.7) yields

$$\frac{\partial P_d}{\partial X} = 1 - \frac{8Q}{\Pi} \qquad \ldots (3.9)$$

Clearly, the positive pressure gradient in the upper part of the duct will decrease as the length of the duct is increased and in the limit will approach zero. Thus, making $\partial P_d/\partial X$ equal to zero in Eq. (3.9) yields $Q = \Pi/8$, which will be the maximum value of Q. Comparing Eqs. (3.1) and (3.2) will show that both Q and H_x have the

same value when $\theta=1$. Thus H_x will be equal to $\Pi/8$ for fully developed flow and, since the fluid cannot absorb any more heat when the temperature of the fluid has reached $\theta=1$, H_t also will be equal to $\Pi/8$. Substituting $H_t=\Pi/8$ into Eq. (3.6) gives the Nusselt relationship

$$Nu = \frac{Ra}{16} \qquad \ldots (3.10)$$

which shows that for fully developed flow a linear relationship exists between Nu and Ra.

3.3 Nusselt relationship for boundary layer flow

Boundary layer flow occurs in a duct that has a small ℓ/r_w ratio and consequently a large value of Ra. The temperature and velocity distributions near the surface will be similar to those in the natural-convective boundary layer on a heated vertical flat surface. Thus, if the duct is opened out to form a vertical flat surface, there should be very little difference between the rate of heat transfer from the flat surface thus formed and the duct. Therefore, Nu will be independent of the radius of the duct and consequently can be expressed by the equation

$$Nu = C_1 Ra^{\frac{1}{4}} \qquad \ldots (3.11)$$

where C_1 is a constant. Expanding Eq. (3.11) and multiplying both sides by ℓ gives

$$\left[\frac{h_t\, r_w}{A(T_w-T_o)k}\right]\ell = C_1 \left[\frac{g\beta(T_w-T_o)r_w^4}{\nu^2\ell}\right]^{\frac{1}{4}} Pr^{\frac{1}{4}}\ell \qquad \ldots (3.12)$$

which, on eliminating r_w, reduces to

$$\frac{h_t\ell}{A(T_w-T_o)k} = C_1 \left[\frac{g\beta(T_w-T_o)\ell^3}{\nu^2}\right]^{\frac{1}{4}} Pr^{\frac{1}{4}} \qquad \ldots (3.13)$$

or

$$Nu_\ell = C_1\, Ra_\ell^{\frac{1}{4}} \qquad \ldots (3.14)$$

The subscript ℓ in Eq. (3.14) indicates that the characteristic dimension is now only the length of the duct. It should be noted that Eq. (3.14) has the same form as the simple relationship for a vertical flat surface, for which an accepted value of the constant is 0.59 (10). Hence putting C_1 equal to 0.59 in Eq. (3.11) gives the following relationship between Nu and Ra for a duct in which boundary layer flow occurs:

$$Nu = 0.59Ra^{\frac{1}{4}} \qquad \ldots (3.15)$$

The Nu-Ra relationships for fully developed flow and for boundary layer flow, given by Eq. (3.10) and Eq. (3.15), are illustrated in Fig. 3.1. The actual relationship should be approximately asymptotic to the two straight lines in this figure.

3.4 Method of solving the flow equations

In order to obtain Nu for all laminar flow values of Ra, and to study the flow development, Eqs. (2.10) to (2.13) were solved for the boundary conditions given in Section 3.1 by relaxation on the CDC 6400 computer at the University of Adelaide.

Finite difference forms of Eqs. (2.10) to (2.13) are given in Appendix A and the relaxation procedure is described in Appendix B.

3.5 Theoretical results

Examination of Eq. (2.13) will show that the Prandtl number (Pr) of the fluid is a parameter of the problem. Since air is the fluid in many natural-convective processes, most of the computations were based on Pr = 0.7. However, to study the influence that Pr has on the Nu-Ra relationship, some calculations were made using other values of Pr.

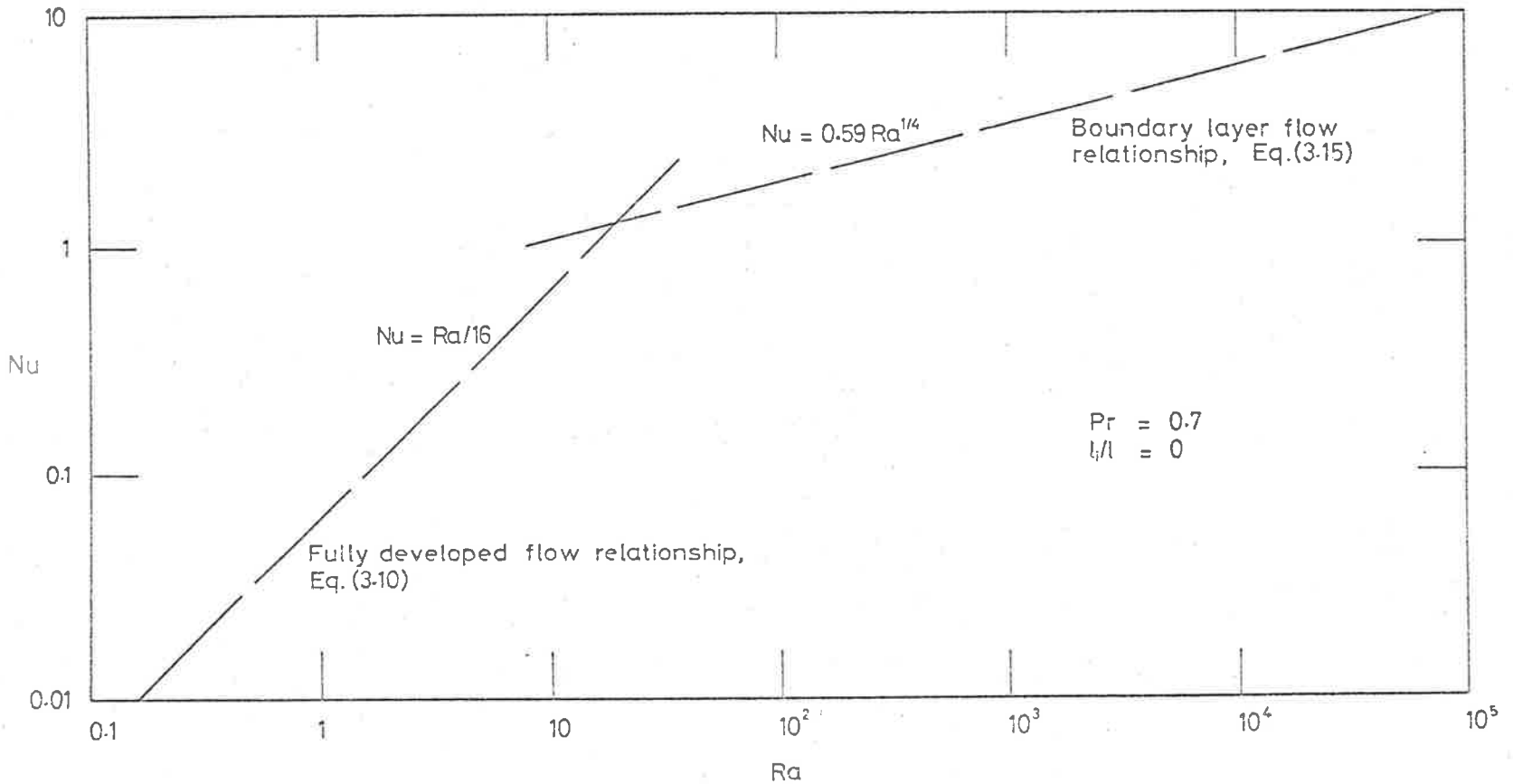

Fig. 3.1 Nusselt number against Rayleigh number for laminar fully developed flow and laminar boundary layer flow in plain-entry ducts with uniform surface temperatures

Fig. 3.2 shows the laminar flow relationship between Nu and Ra for Pr = 0.7. For small Ra, the curve will be seen to be asymptotic to the relationship Nu = Ra/16, which was derived in Section 3.2 for large values of the ratio ℓ/r_w. However, for large Ra, it is asymptotic to

$$Nu = 0.63\ Ra^{\frac{1}{4}} \qquad \ldots (3.16)$$

and not $Nu = 0.59\ Ra^{\frac{1}{4}}$, which was derived in Section 3.3 for small values of the ratio ℓ/r_w. The discrepancy between the equations, however, is insignificant bearing in mind that the constant 0.59 was based on the vertical flat surface relationship.

It will be seen in Fig. 3.3 that, for $Pr \geqslant 0.7$, Pr exerts only a small influence on the Nu-Ra relationship. In fact, changing Pr from 100 to 0.7 produces only a zero to a 10% reduction in Nu as Ra increases from 1 to 10^4. However, it will be observed that the influence of Pr becomes increasingly significant as Pr decreases below 0.7; when $Ra = 10^4$, a change in Pr from 0.7 to 0.01 (Pr = 0.01 is a typical value for a liquid metal) produces a 40% decrease in Nu. Thus for $Pr \geqslant 0.7$ a relationship of the form Nu = f(Ra) is satisfactory.

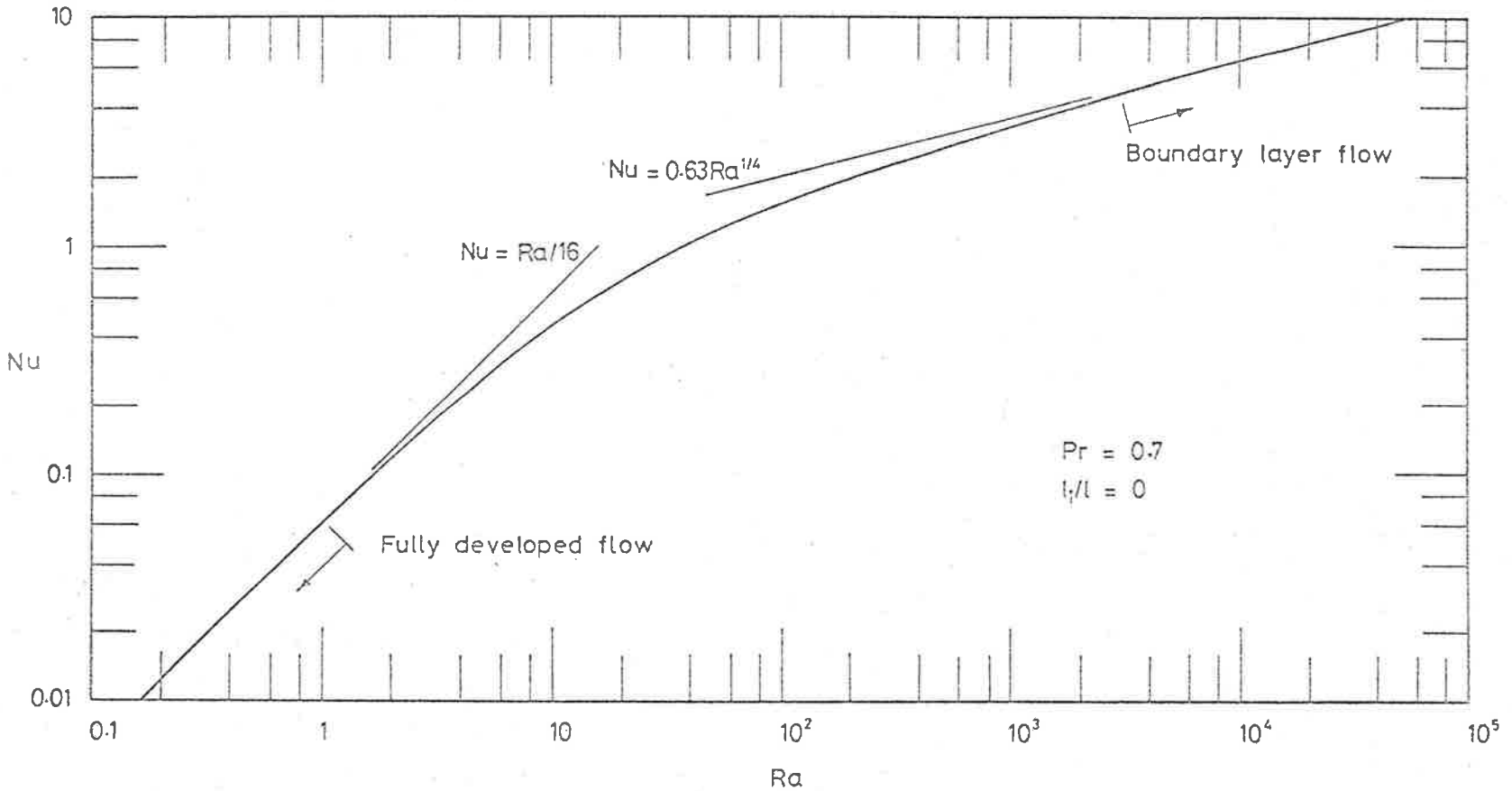

Fig. 3.2 Nusselt number against Rayleigh number for laminar flow in plain-entry ducts with uniform surface temperatures

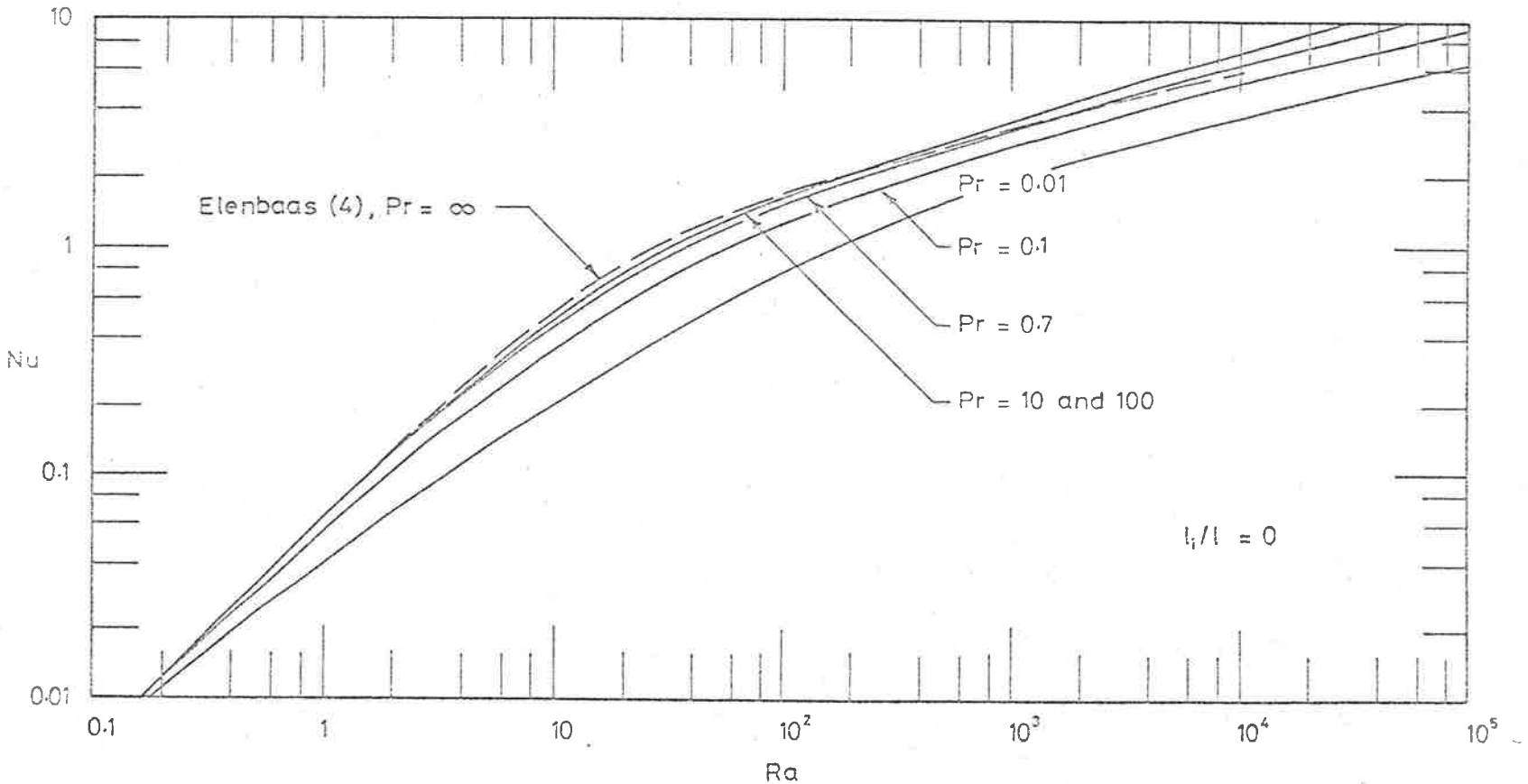

Fig. 3.3 Nusselt number against Rayleigh number for Prandtl numbers of 0.01, 0.1, 0.7, 10 and 100 for laminar flow in plain-entry ducts with uniform surface temperatures

For Pr < 0.7, however, the viscous forces become less important in relation to the inertia and buoyancy forces (9) and the relationship has the form

$$Nu = f(Ra, Pr) \qquad \ldots (3.17)$$

Elenbaas's relationship for Pr = ∞ (4) has been reproduced in Fig. 3.3, and it is interesting to note that the curve lies very close to the relationship derived in the present study for Pr = 10 and 100.

Fig. 3.4 shows the dimensionless volume flow (Q) and total heat transfer (H_t) plotted against Ra. Both curves at small values of Ra will be seen to converge and approach $\pi/8$, which was shown in Section 3.2 to be their maximum value.

Heat transfer from the bottom to various positions along the duct is presented in Fig. 3.5. It will be seen that h_x/h_t rapidly approaches unity as the value of Ra decreases below 10 and that h_x/h_t is almost independent of Ra in the boundary layer regime.

Fig. 3.6 compares the temperature and velocity profiles at the top of the duct for a wide range of Ra. In this figure both fully developed and boundary layer profiles will be seen. The temperature growth in the

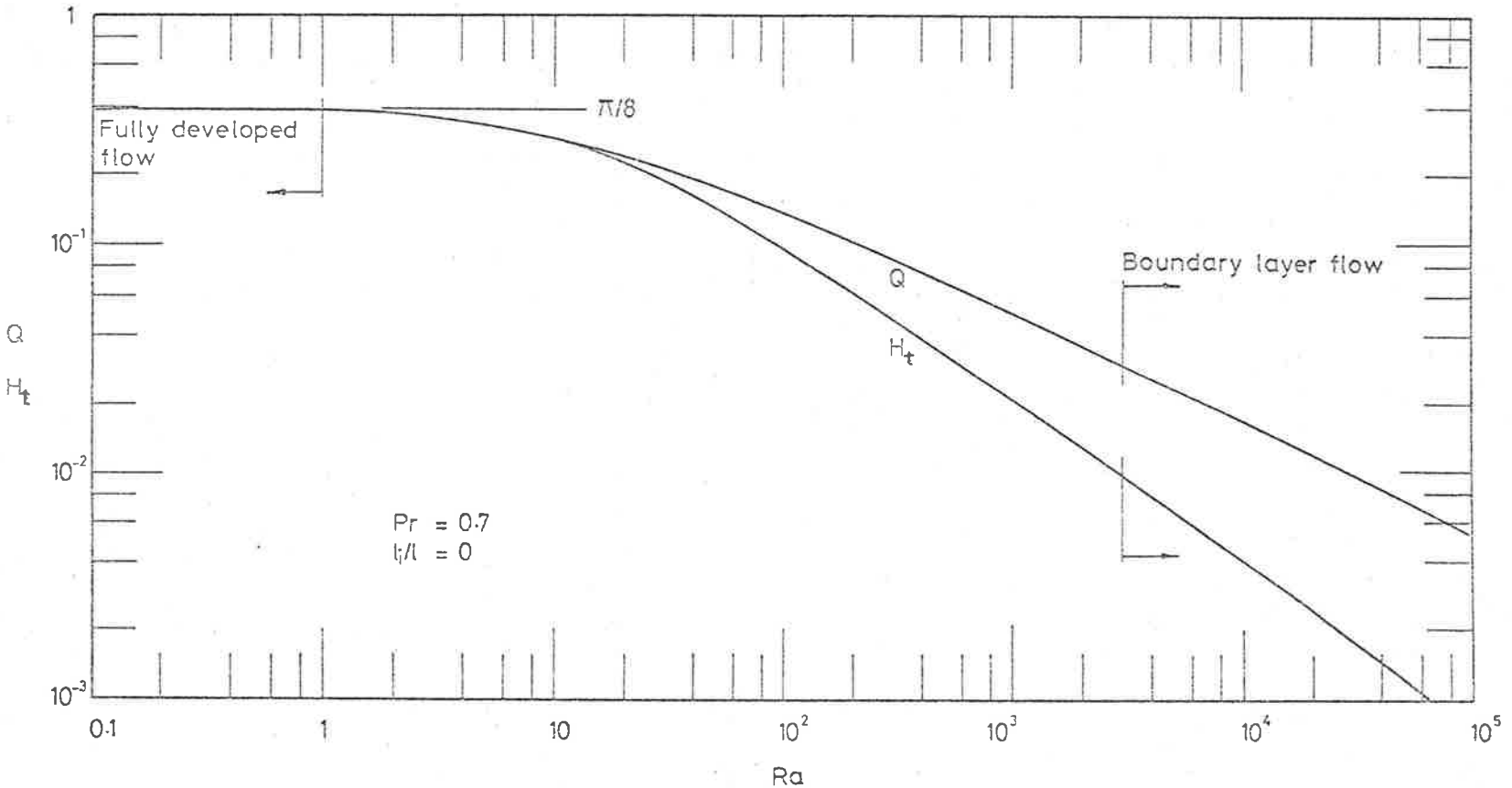

Fig. 3.4 Dimensionless flow (Q) and total heat transfer (H_t) against Rayleigh number for laminar flow in plain-entry ducts with uniform surface temperatures

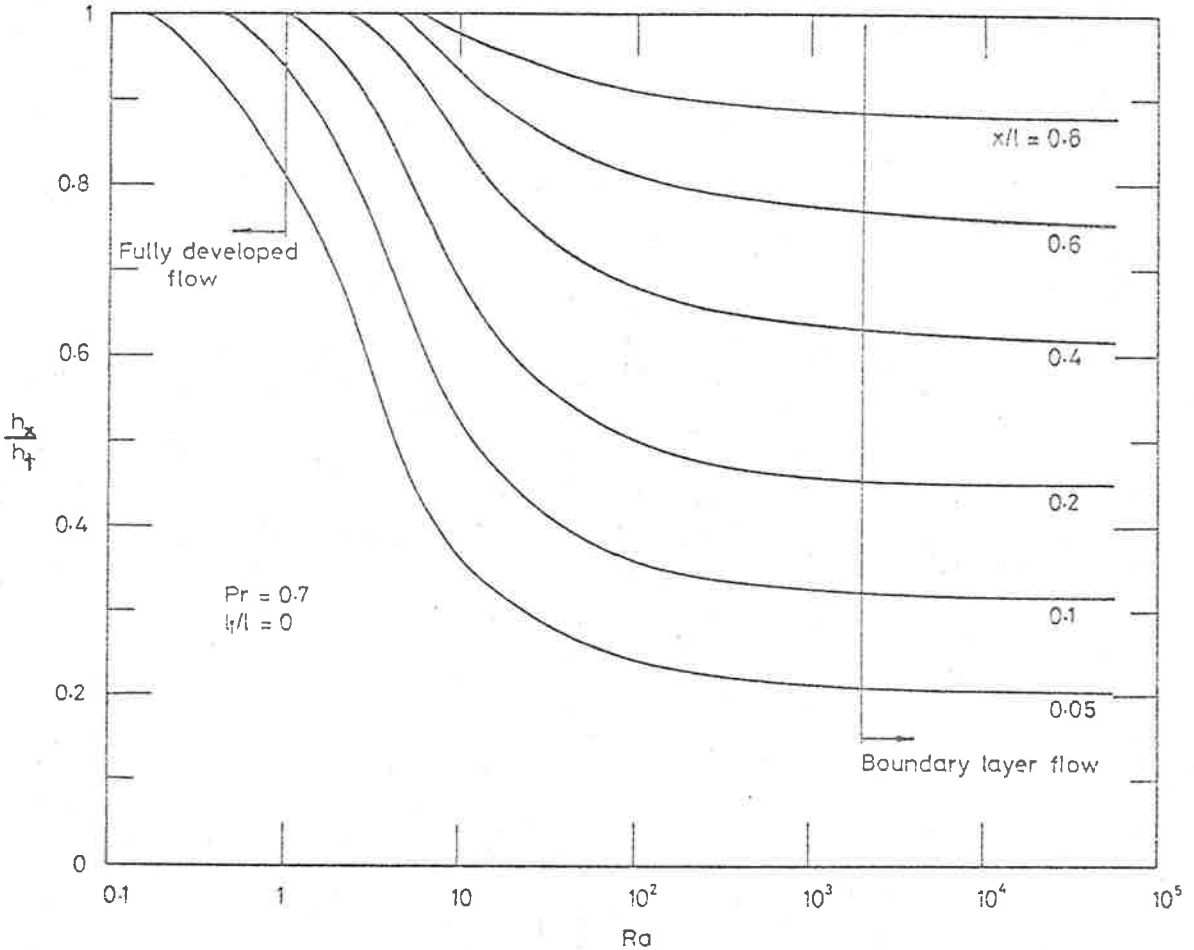

Fig. 3.5 Ratio of the heat transfer up to a particular elevation (H_x) to the total heat transfer (h_t) against Rayleigh number for plain-entry ducts with uniform surface temperatures

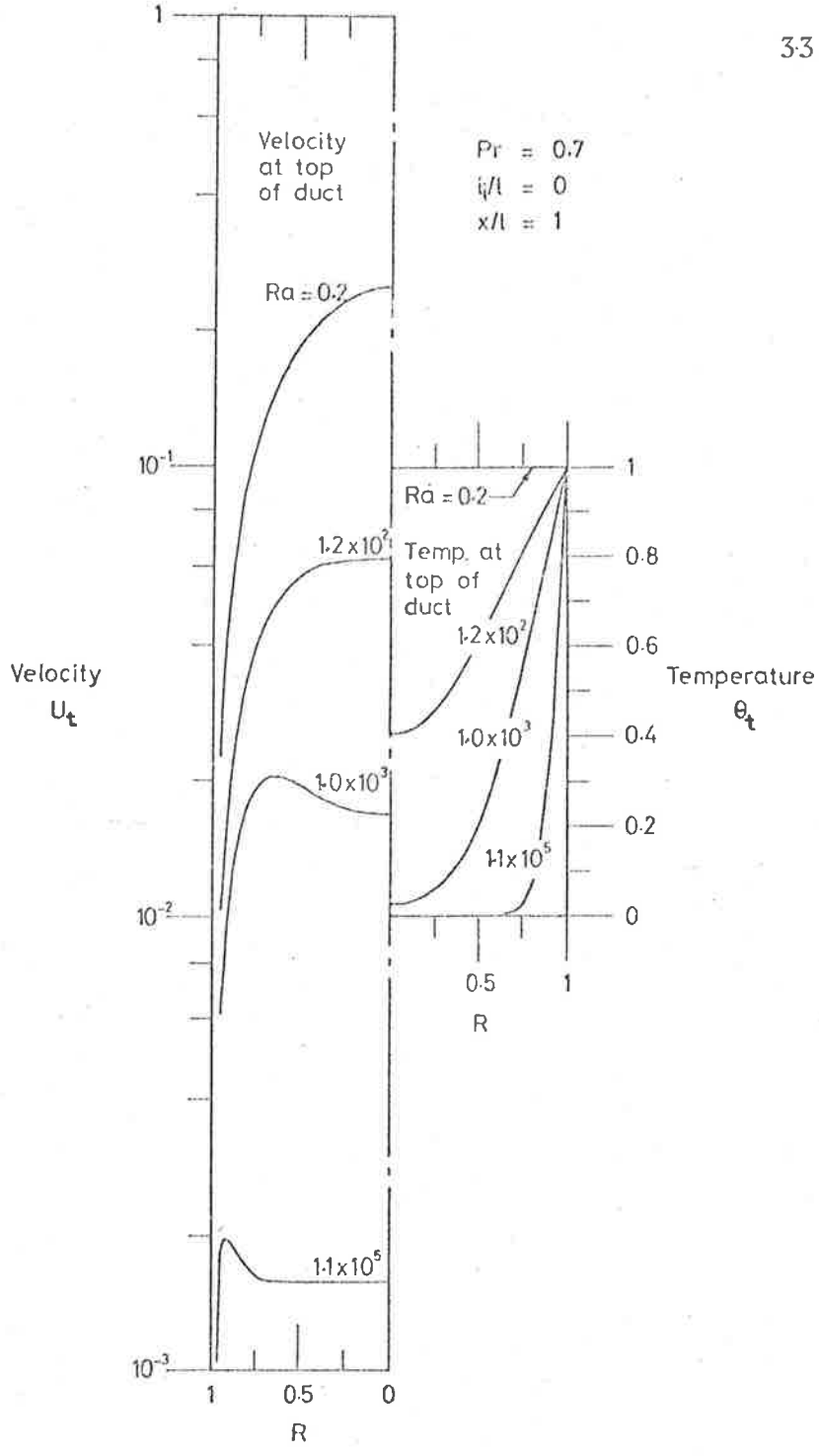

Fig. 3.6 Laminar-flow velocity and temperature profiles for various Rayleigh numbers at the top of plain-entry ducts with uniform surface temperatures

fluid along the axis of the duct for these Ra is shown in Fig. 3.7. It is interesting to observe in this figure that when Ra reaches 10^3 the temperature of the fluid in the centre part of the duct rises barely above ambient.

Fig. 3.8 shows the pressure defects along ducts for a small and a large value of Ra. The pressure gradient for Ra = 0.2 will be seen to be constant above $x/\ell=0.05$. This condition, it should be recalled, was assumed in Section 3.2 to derive the Nu-Ra relationship for fully developed flow.

Heat transfer per unit flow area

For given values of the length and surface temperature of a duct, there will be a radius which maximises the rate of heat transfer (h_t) per unit flow area (a). The optimum radius of the duct is determined by the Ra which yields the maximum value of

$$\frac{h_t}{a} = \frac{h_t}{\pi r_w^2} \qquad \ldots (3.18)$$

Expressing h_t on the right hand side of Eq. (3.18) in dimensionless form yields

$$\frac{h_t}{a} = \frac{H_t \; Gr \; \rho \; c_p \; \nu\ell(T_w-T_o)}{\pi r_w^2} \qquad \ldots (3.19)$$

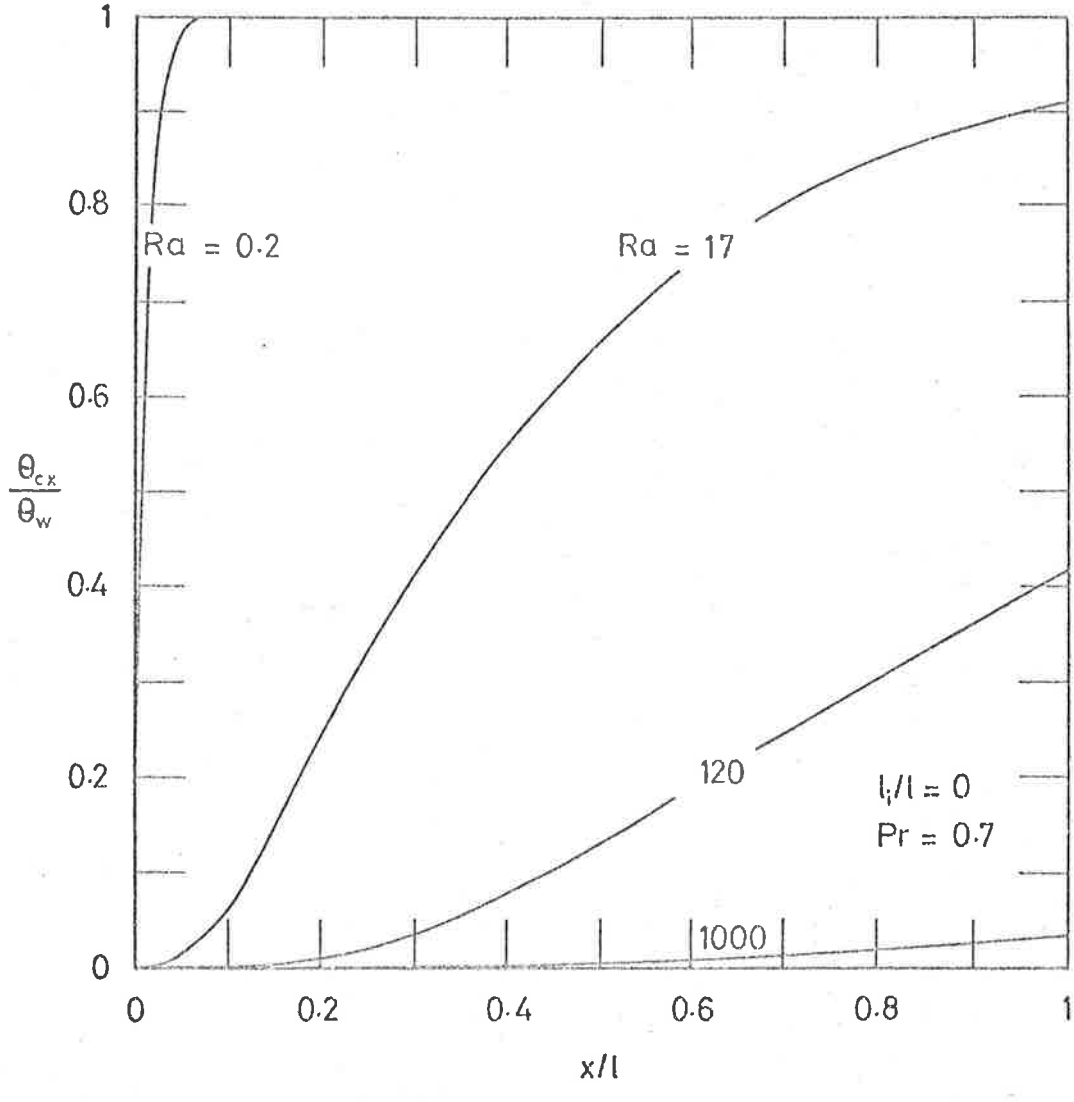

Fig. 3.7 Temperature development along the axes of plain-entry ducts with uniform surface temperatures for various Rayleigh numbers

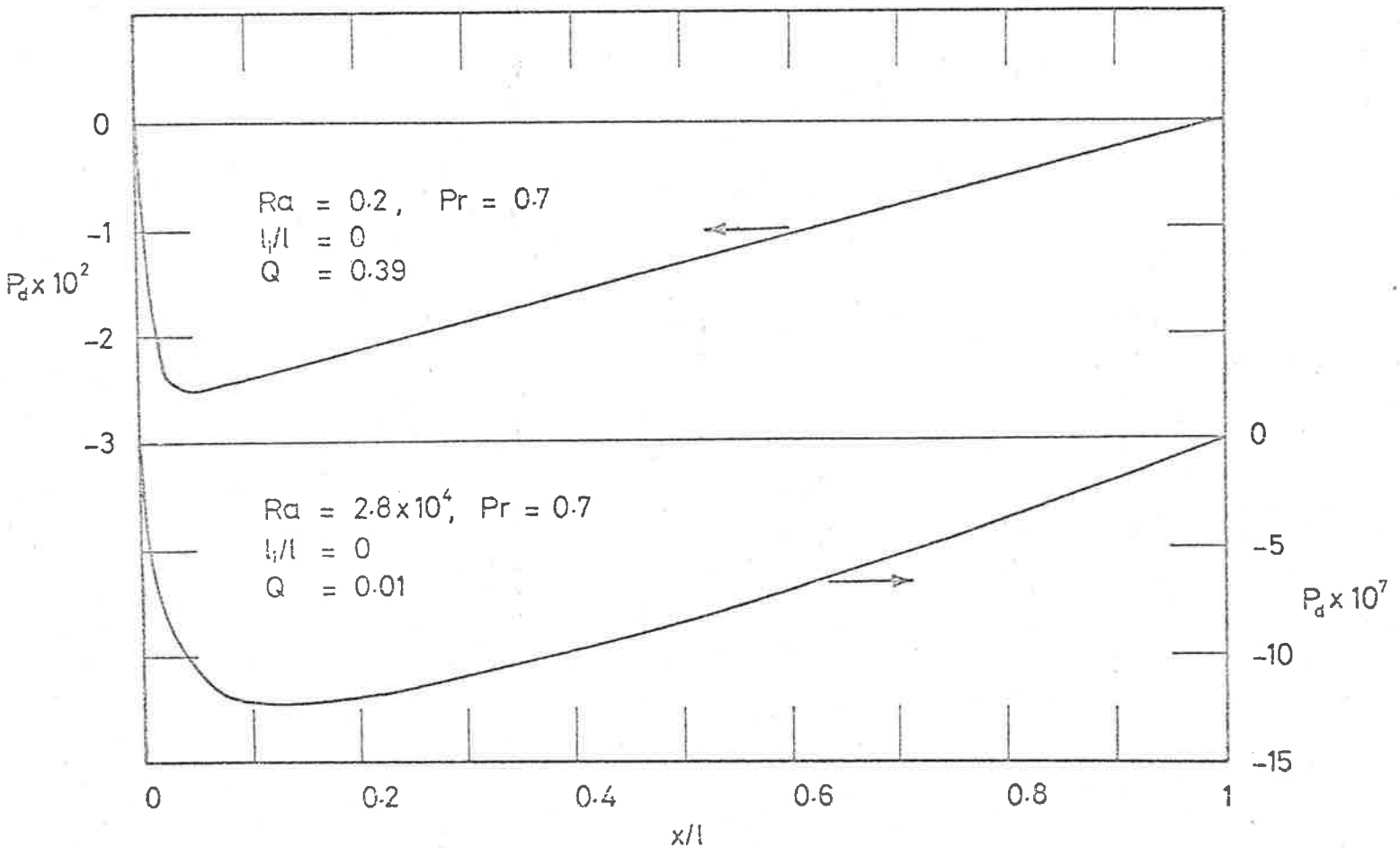

Fig. 3.8 Distribution of the dimensionless pressure defect (P_d) in plain-entry ducts with uniform surface temperatures for laminar fully developed flow (Ra = 0.2) and laminar boundary layer flow (Ra = 2.8×10^4)

From Eq. (3.5),

$$H_t \, Gr = \frac{2\Pi \, Nu}{Pr} \qquad \ldots (3.20)$$

and substituting Eq. (3.20) into Eq. (3.19) yields

$$\frac{h_t}{a} = 2 \frac{Nu}{Pr} \cdot \frac{\rho \, c_p \, \nu \ell (T_w - T_o)}{r_w^2} \qquad \ldots (3.21)$$

Multiplying the numerator and denominator of the right hand side of Eq. (3.21) by $\sqrt{Ra}$ yields

$$\frac{h_t}{a} = 2 \frac{Nu}{\sqrt{Ra}} \rho \, c_p \left[\frac{\beta g \ell \, (T_w - T_o)^3}{Pr} \right]^{\frac{1}{2}} \qquad \ldots (3.22)$$

Inspection of Eq. (3.22) will show that, for given values of ℓ and $(T_w - T_o)$ and for constant fluid properties, the terms to the right of $Nu/\sqrt{Ra}$ are invariant. Hence it follows that

$$\frac{h_t}{a} \propto \frac{Nu}{\sqrt{Ra}} \qquad \ldots (3.23)$$

It will be seen in Fig. 3.9 that, for a given Pr, the parameter $Nu/\sqrt{Ra}$ has a maximum value. Hence a duct can have a Rayleigh number (Ra_{opt}) for which the heat transfer per unit flow area is a maximum for given values

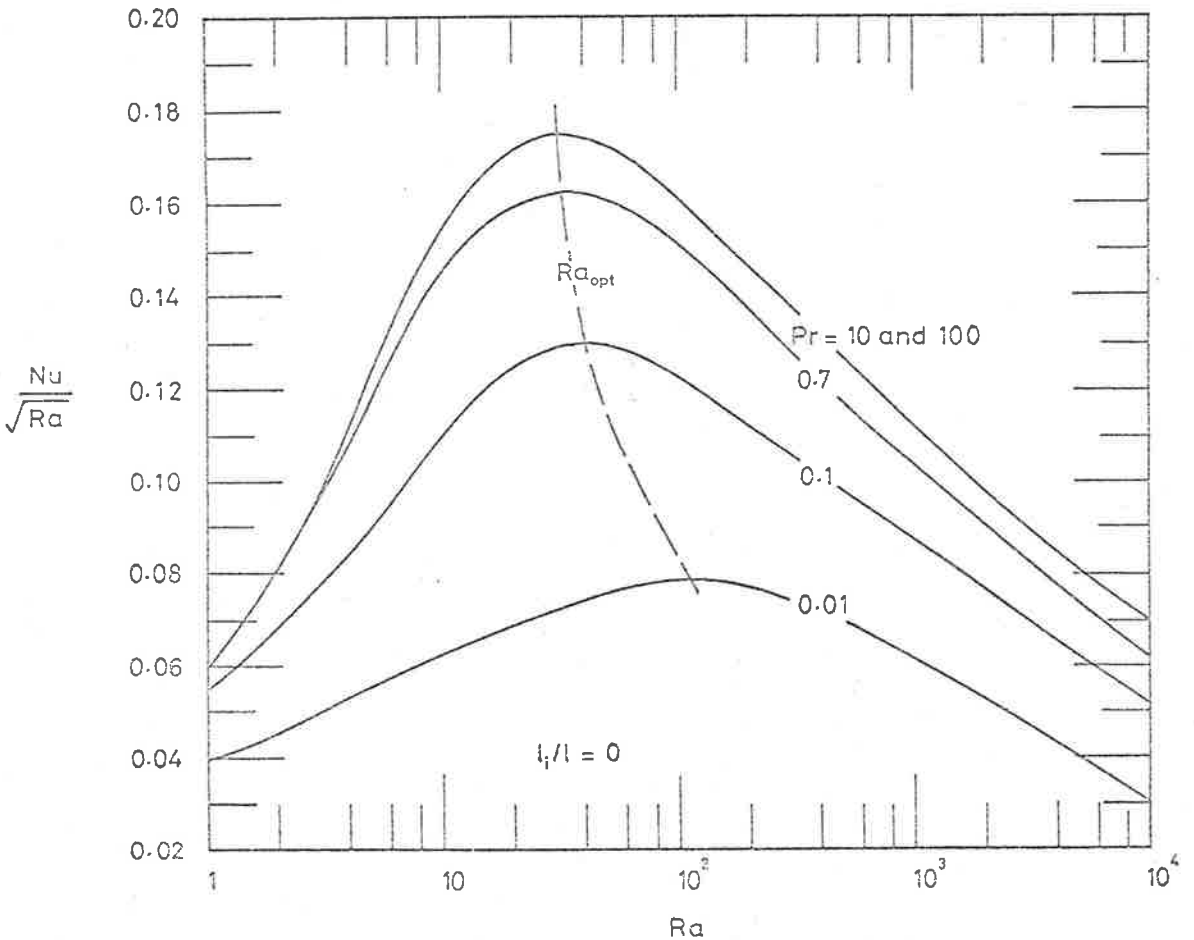

Fig. 3.9 Parameter $Nu/\sqrt{Ra}$, which is proportional to the rate of heat transfer per unit flow area, against Rayleigh number for plain-entry ducts with uniform surface temperatures

of ℓ and $(T_w - T_o)$. Fig. 3.9 shows that Ra_{opt} is almost independent of Pr for $Pr \geq 0.7$ but increases as Pr decreases below 0.7. When Pr has the value 0.7

$$Ra_{opt} = 32 \qquad \ldots (3.24)$$

and therefore the optimum radius of the duct is given by

$$r_{w\ opt} = \sqrt[4]{\frac{32\ \nu^2 \ell}{g\beta(T_w - T_o)Pr}} \qquad \ldots (3.25)$$

It is interesting to note that both the present study for Pr = 10 and 100 and the work of Elenbaas for Pr = ∞ (4) gave 30 as the value of Ra_{opt}.

Reynolds number

Based on the radius of the duct, Reynolds number (Re_r) is given by

$$Re_r = \frac{u_m\ r_w}{\nu} \qquad \ldots (3.26)$$

The mean flow velocity (u_m) is

$$u_m = \frac{q}{\Pi r_w^2} \qquad \ldots (3.27)$$

Substituting Eq. (3.27) into Eq. (3.26) yields

$$Re_r = \frac{q}{\Pi r_w \nu} \qquad \ldots (3.28)$$

Expressing q in Eq. (3.28) in dimensionless terms yields

$$Re_r = \frac{Gr\ Q}{\Pi} \cdot \frac{\ell}{r_w} \qquad \ldots (3.29)$$

or

$$Re_r = \frac{Ra\ Q}{\Pi\ Pr} \cdot \frac{\ell}{r_w} \qquad \ldots (3.30)$$

Fig. 3.10 shows the parameter (Re_r Pr r_w/ℓ) plotted against Ra.

Critical values of Re_r can be estimated in the following manner. Since both natural convection in vertical ducts and forced convection in pipes produce parabolic velocity profiles for fully developed laminar flow, it is reasonable to assume that the two flow conditions will have the same critical value of Reynolds number. Hence the critical Re_r for fully developed flow in ducts should be about 1150 (9). However, for boundary layer flow the critical Re_r is likely to be less than 1150 because the flow has a less stable velocity profile, as shown in Fig. 3.6.

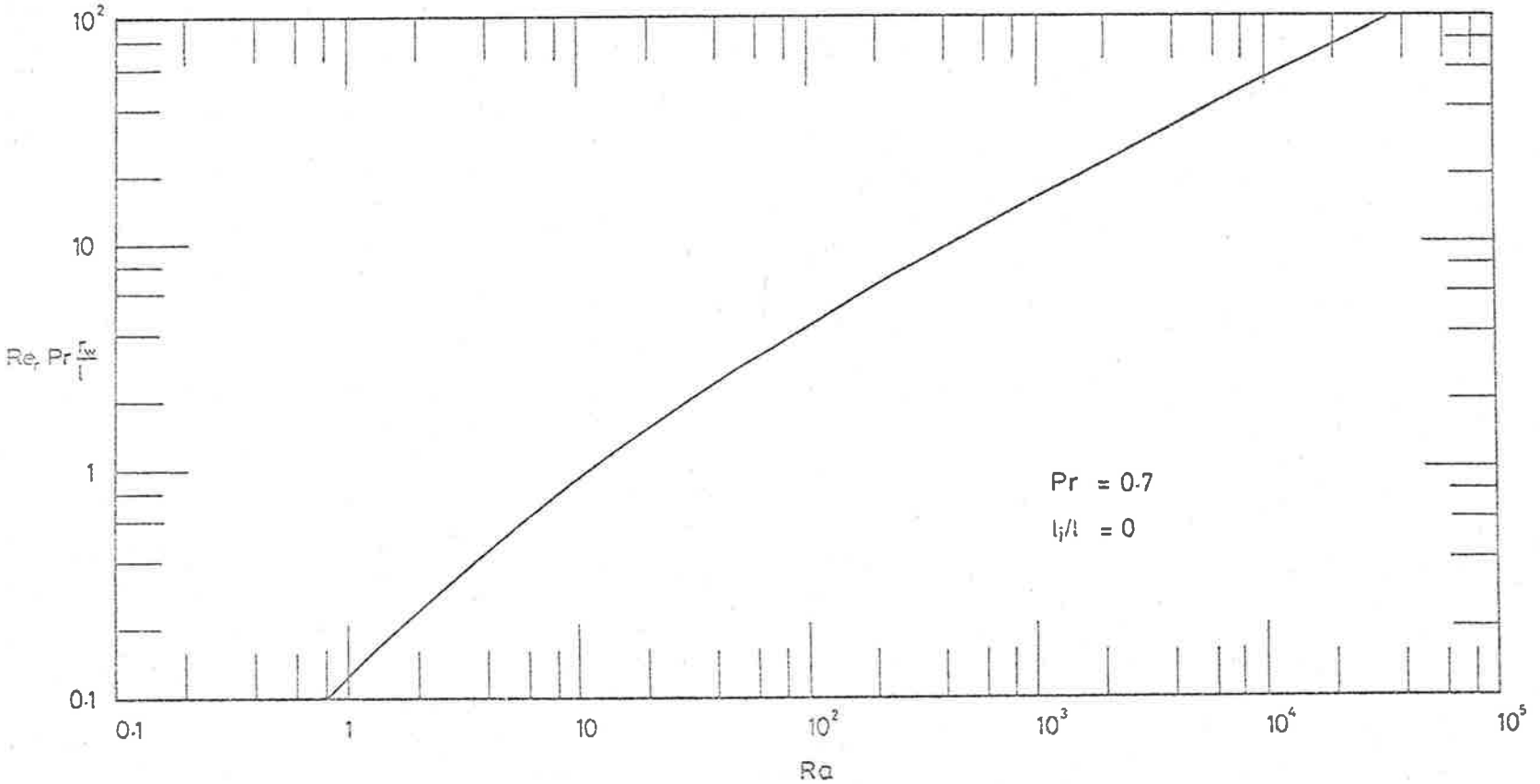

Fig. 3.10 Parameter $\mathrm{Re_r Pr}\, r_w/\ell$ against Rayleigh number for laminar flow in plain-entry ducts with uniform surface temperatures

4. RESTRICTED-ENTRY DUCTS WITH UNIFORM SURFACE TEMPERATURES

4.1 Introduction

The entry restriction, as shown in Fig. 1.1(b), is provided by leaving the lower part of the vertical duct unheated. The sketches of the velocity profiles in Fig. 1.1(b) show that the fluid enters with a uniform velocity and that the flow develops in the unheated section. If the length of the unheated section (ℓ_i) is large compared with the radius of the duct (r_w), the flow will be fully developed when it reaches the heated section. It should be noted that, as the unheated section presents a resistance to the flow, the pressure defect will increase along its length.

A restricted-entry duct can be classified by two dimensionless parameters: the Rayleigh number (Ra) and the ratio of the lengths of the unheated and heated sections (ℓ_i/ℓ). It should be emphasised here that ℓ in the denominator of Ra is the length of the heated section (ℓ), and not the overall length of the duct ($\ell_i+\ell$).

Considering the extreme values of the ratio ℓ_i/ℓ, if ℓ_i/ℓ is made equal to zero the duct will become a plain-entry duct and if the ratio is made infinitely large the duct will closely resemble an open thermosyphon duct (3).

As in the case of the analysis of plain-entry ducts, the Nu-Ra relationships for fully developed flow and for boundary layer flow will be derived to corroborate the general solution for the extreme values of Ra.

4.2 Nusselt relationship for fully developed flow

To obtain fully developed flow in both the heated and the unheated sections, the ratios ℓ/r_w and ℓ_i/ℓ are made large. The large ℓ/r_w means that the duct will have a small Ra.

The momentum equation for fully developed flow in the heated section is the same as that given by Eq. (3.9) for the plain-entry duct namely,

$$\left.\frac{\partial P_d}{\partial X}\right|_{\text{heated}} = 1 - \frac{8Q}{\Pi} \qquad \ldots (4.1)$$

The corresponding equation for the unheated section is derived in the same manner as Eq. (3.9), except that the dimensionless temperature (θ) is made equal to zero instead of to one. Thus the momentum equation for the unheated section becomes

$$\left.\frac{\partial P_d}{\partial X}\right|_{\text{unheated}} = - \frac{8Q}{\Pi} \qquad \ldots (4.2)$$

According to Eqs. (4.1) and (4.2), and as illustrated in Fig. 4.1, the pressure gradient in each section is constant. Hence the pressure defect at the top of the unheated section is

$$P_{d,X=0} = -\frac{8Q}{\Pi}\ell_i \qquad \ldots (4.3)$$

and at the bottom of the heated section the pressure defect is

$$P_{d,X=0} = -\left(1 - \frac{8Q}{\Pi}\right)\ell \qquad \ldots (4.4)$$

Since the pressure defects given by Eqs. (4.3) and (4.4) are equal, it follows that

$$Q = \frac{\Pi}{8\left(1 + \frac{\ell_i}{\ell}\right)} \qquad \ldots (4.5)$$

Eq. (4.5) shows that for fully developed flow, the value of Q is a function of only the ratio of the lengths of the two sections of the duct.

Inspection of Eqs. (3.1) and (3.2) will show that for $\theta=1$, Q and H_x have the same value. But H_x is equal to H_t for that part of the heated section in which the flow is fully developed and therefore H_t and Q will have

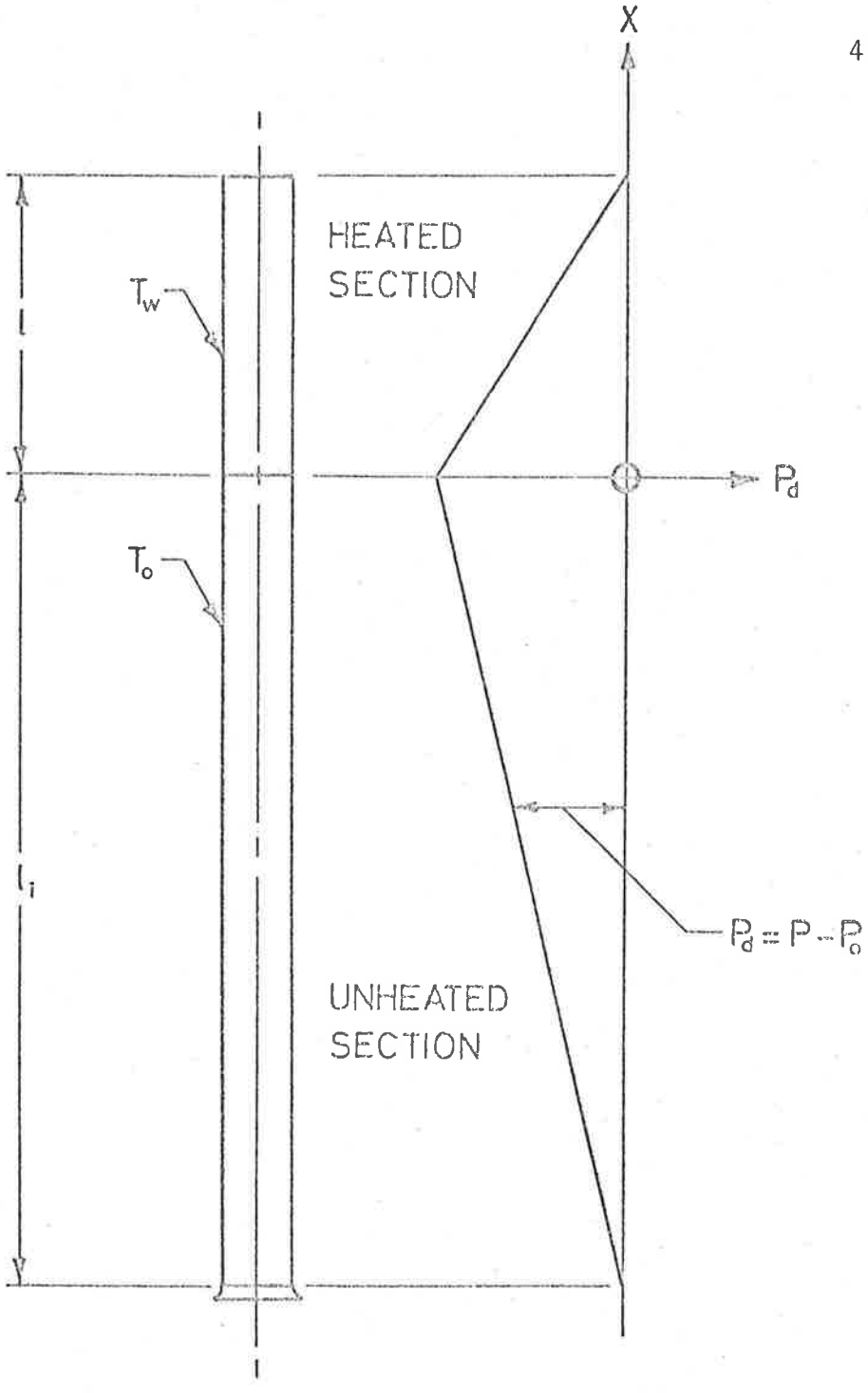

Fig. 4.1 Diagrammatic distribution of the dimensionless pressure defect (P_d) in a restricted-entry duct in which the flow in each section is laminar and fully developed

the same value. Substituting H_t for Q in Eq. (4.5) yields

$$H_t = \frac{\Pi}{8\left(1 + \frac{\ell_i}{\ell}\right)} \qquad \ldots (4.6)$$

and substituting Eq. (4.6) into Eq. (3.6) gives the following relationship between Nu and Ra for fully developed laminar flow:

$$Nu = \frac{Ra}{16\left(1 + \frac{\ell_i}{\ell}\right)} \qquad \ldots (4.7)$$

It is interesting to note that as ℓ_i/ℓ approaches zero Eq. (4.7) reduces to Eq. (3.10), which is the Nu-Ra relationship for a plain-entry duct. Obviously, Eq. (4.7) cannot be valid for all values of ℓ_i/ℓ. For example, if ℓ_i/ℓ were to approach infinity, Nu, according to Eq. (4.7), would approach zero. In practice this would not be the case, because an open-thermosyphon flow (3) would develop in the upper part of the duct and heat would be dissipated accordingly. A discussion on the largest values of ℓ_i/ℓ giving laminar flow will be deferred until a later section.

4.3 Nusselt relationship for boundary layer flow

To obtain boundary layer flow in the heated section, the ratio ℓ/r_w is made small. Thus Ra will be large.

It is reasonable to assume that the form of the Nu-Ra relationship will be the same as that for plain-entry ducts. However, the values of Nu will be smaller owing to the entry restriction reducing the flow rate. Thus it follows from Eq. (3.11) that the Nusselt relationship is given by

$$Nu = C_2 \, Ra^{\frac{1}{4}} \qquad \ldots (4.8)$$

where C_2 is a constant for a given value of ℓ_i/ℓ. The maximum value of C_2 will be 0.63, which is the value given by Eq. (3.16) for the case of $\ell_i/\ell = 0$. However, the lower limit of C_2 can be obtained only by solving the flow equations. This will be done in a later section.

4.4 Method of solving the flow equations

The procedure used to solve Eqs. (2.10) to (2.13) to give the general solution for the following boundary conditions is described in Appendix B.

Boundary conditions

$X=-L_i$ and $R=1$; $U=0$, $V=0$, $\theta=0$, $P_d=0$. (a)

$X=-L_i$ and $1<R\leqslant 0$; $U=\frac{Q}{\Pi}$, $V=0$, $\theta=0$, $P_d=0$. (b)

$-L_i<X<0$ and $R=1$; $U=0$, $V=0$, $\theta=0$, $P_d<0$. (c)

$-L_i<X<0$ and $R=0$; $V=0$, $\theta=0$, $P_d<0$, $\frac{\partial U}{\partial R}=0$. (d)

$0\leqslant X<L$ and $R=1$; $U=0$, $V=0$, $\theta=1$, $P_d<0$. (e)

$0\leqslant X<L$ and $R=0$; $V=0$, $P_d<0$, $\frac{\partial U}{\partial R}=0$, $\frac{\partial \theta}{\partial R}=0$. (f)

$X=L$ and $R=1$; $U=0$, $V=0$, $\theta=1$, $P_d=0$. (g)

$X=L$ and $R=0$; $V=0$, $P_d=0$, $\frac{\partial U}{\partial R}=0$, $\frac{\partial \theta}{\partial R}=0$. (h)

$-L_i\leqslant X\leqslant L$; Q is constant. (i)

4.5 Theoretical results

Fig. 4.2 shows Nu as a function of both Ra and the volume flow (Q) for Pr = 0.7. The top curve describes the relationship for plain-entry ducts ($\ell_i/\ell = 0$), and branching off it are constant volume flow (Q) curves for restricted-entry ducts. In the fully developed regime, Nu will be seen to be proportional to Ra for a constant value of Q. The explanation for this is obtained from Eqs. (4.5), (4.6) and (3.6). According to Eqs. (4.5) and (4.6), Q and H_t have the same value when the flow is fully developed. Hence it follows from Eq. (3.6) that Nu for small Ra is proportional to Ra for a given value of Q.

The relationship between ℓ_i/ℓ and Ra for various values of Q is shown in Fig. 4.3. As Ra decreases, it will be observed that the constant Q curves become independent of Ra and that the value of Q is determined only by the ratio ℓ_i/ℓ. This finding is consistent with Eq. (4.5). Further, at large values of Ra it will be seen that the curves for $Q < 0.021$ terminate when ℓ_i/ℓ is between 2 and 4.

The Nu-Ra relationship in a more practical form, with ℓ_i/ℓ instead of Q as the third parameter, is shown

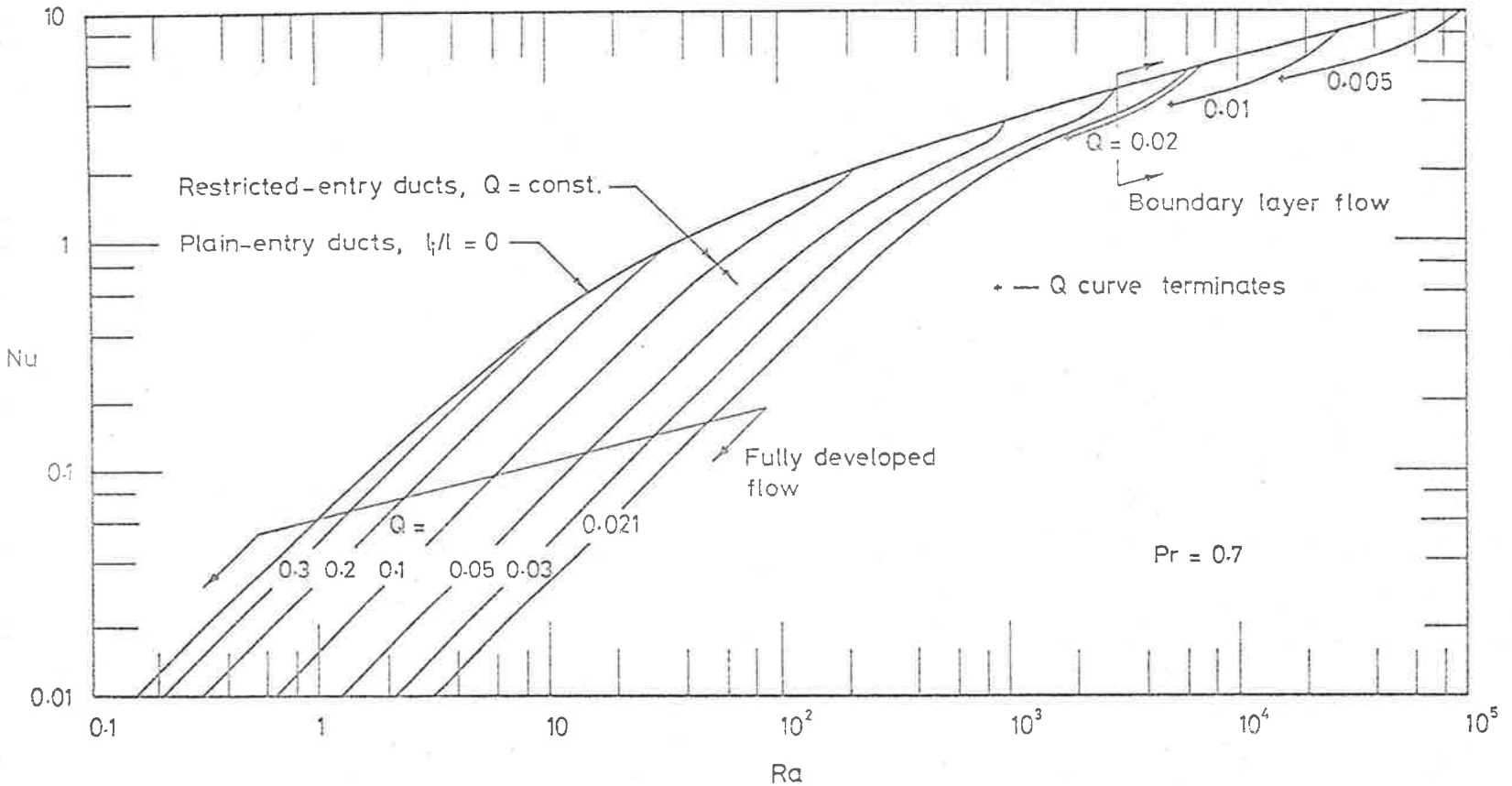

Fig. 4.2 Nusselt number as a function of the Rayleigh number and the dimensionless flow (Q) for laminar flow in restricted-entry ducts

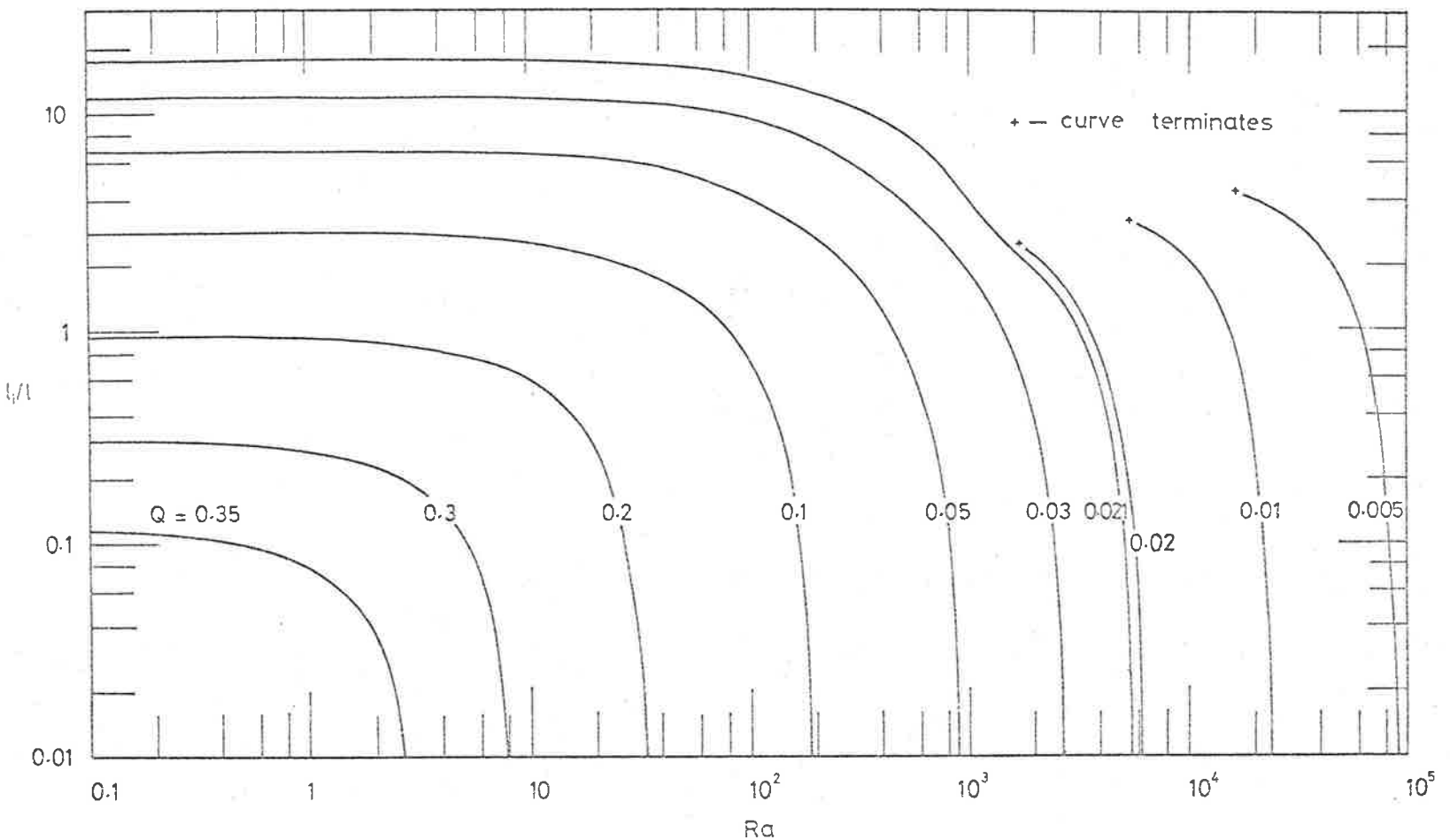

Fig. 4.3 Relationship between the dimensionless flow (Q), the ratio of the lengths of the unheated and heated sections (ℓ_i/ℓ) and the Rayleigh number for laminar flow in restricted-entry ducts

in Fig. 4.4. (In cross-plotting this figure from Figs. 4.2 and 4.3, the maximum value of ℓ_i/ℓ in the boundary layer regime was taken to be 2). The relationship agrees with Eqs. (4.7) and (4.8), which were derived for fully developed flow and boundary layer flow respectively. As the entry restriction increases, the fully developed flow regime will be seen to extend to larger Ra. This is readily explained by the fact that the flow becomes more developed as the flow rate decreases.

Further, the maximum value of ℓ_i/ℓ for a given Ra will be seen in Fig. 4.4 to decrease progressively from 18 in the fully developed flow regime to 2 in the boundary layer regime. Hence it follows that if a duct has a ratio of ℓ_i/ℓ greater than the values shown in Fig. 4.4, the flow will not be laminar. The reason for this will be discussed later.

An entry-restriction can reduce the value of Nu for fully developed laminar flow by a factor of 19 as shown by the following equations:

$$Nu = \frac{Ra}{16} \qquad \text{when } \ell_i/\ell = 0 \qquad \ldots (4.9)$$

$$Nu = \frac{Ra}{304} \qquad \text{when } \ell_i/\ell = 18 \qquad \ldots (4.10)$$

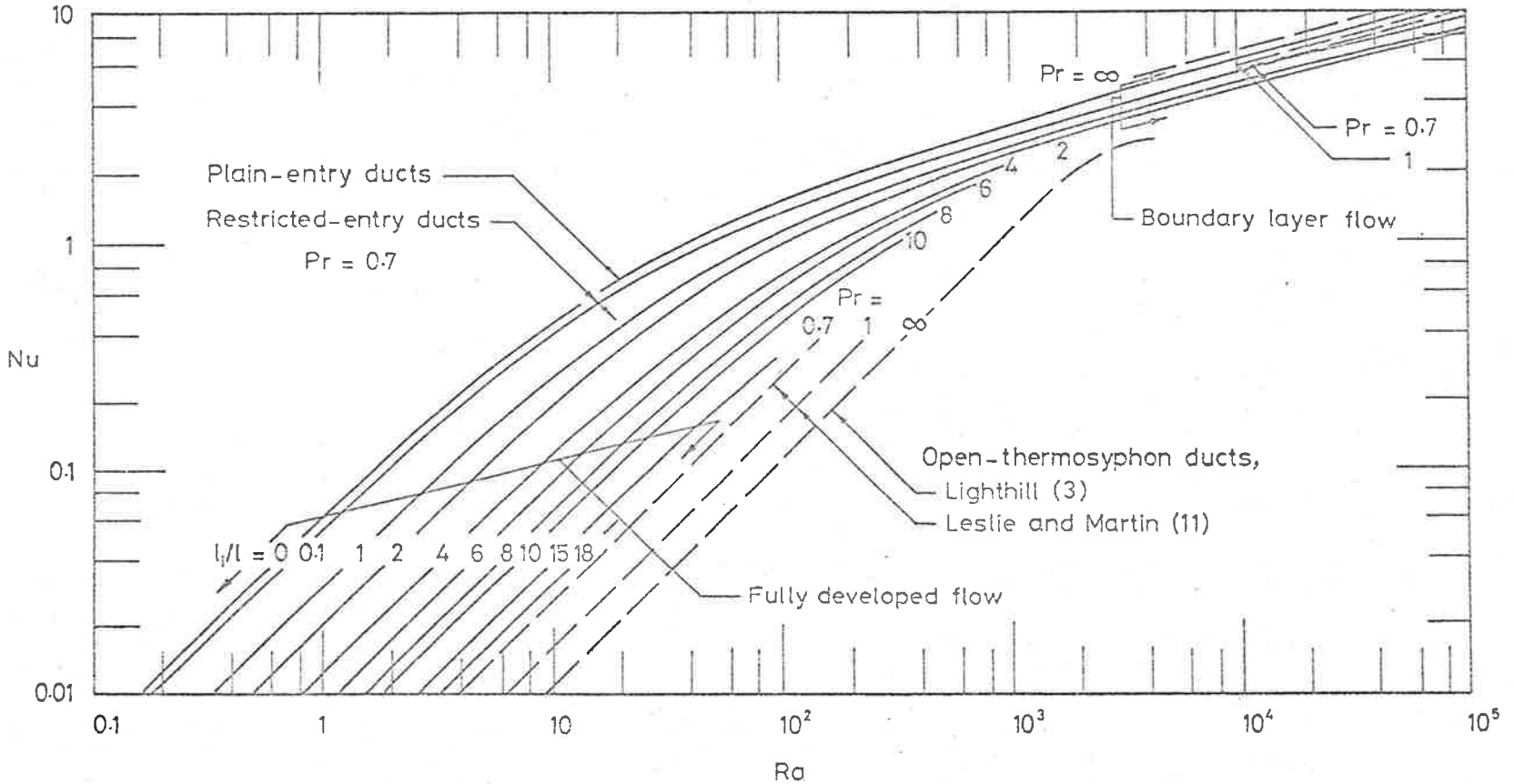

Fig. 4.4 Nusselt number as a function of the Rayleigh number and the ratio of the lengths of the unheated and heated sections (ℓ_i/ℓ) for laminar flow in restricted-entry ducts

However, for laminar boundary layer flow, Nu can be decreased by a factor of only 1.3 as shown by the following equations:

$$Nu = 0.63\ Ra^{\frac{1}{4}} \quad \text{when } \ell_i/\ell = 0 \qquad \ldots (4.11)$$

$$Nu = 0.48\ Ra^{\frac{1}{4}} \quad \text{when } \ell_i/\ell = 2 \qquad \ldots (4.12)$$

The laminar flow Nu-Ra relationship in Fig. 4.4 is valid only if it lies above the relationship for open-thermosyphon ducts. In order to test this criterion, the theoretical relationships between Nu and Ra for open-thermosyphon ducts which were derived by Lighthill (3) for $Pr = \infty$ and Leslie and Martin (11) for $Pr = 0.7$ and 1 are also shown in Fig. 4.4 (the latter did not provide data on non-similarity flow). It will be observed that for $Ra < 4 \times 10^3$ these curves lie below those for the restricted-entry ducts. Consequently, for any Ra below 4×10^3, a restricted-entry duct for which the ratio ℓ_i/ℓ is within the range of values allowed by Fig. 4.4 will produce laminar flow. On the other hand, the situation for $Ra > 4 \times 10^3$ is more complicated. Comparing Fig. 4.4 with Fig. 3.3, it will be found that for $Pr > 0.7$ the curves for open-thermosyphon ducts lie just below those

for restricted-entry ducts. Therefore, for Pr > 0.7 laminar boundary layer flow for ducts with small entry restrictions appears possible. In the case of Pr = 0.7, it will be observed in Fig. 4.4 that the open-thermosyphon curve almost coincides with the curve for $\ell_i/\ell = 0.1$. However, Lighthill (3) showed theoretically and Martin and Cohen (12) experimentally that for Pr less than about 1, the laminar boundary layer regime of the open-thermosyphon duct cannot occur and its place is taken by the impeding flow regime. In this regime inter-action between the upward and downward moving streams reduces the rate of flow in and out of the duct, and this causes a marked reduction in the rate of heat transfer. The resulting lower Nu-Ra relationship persists until Ra is sufficiently large for a turbulent boundary layer regime to establish itself. Hence, it would appear that the relationships shown in Fig. 4.4 for restricted-entry ducts for Pr = 0.7 are valid.

It will be recalled in Fig. 4.4 that the ℓ_i/ℓ curves ranging from 4 to 18 are not continuous. Each curve reaches a maximum Ra, which increases with decreasing ℓ_i/ℓ. An explanation for this result can be obtained by considering Figs. 4.2, 4.5 and 4.6.

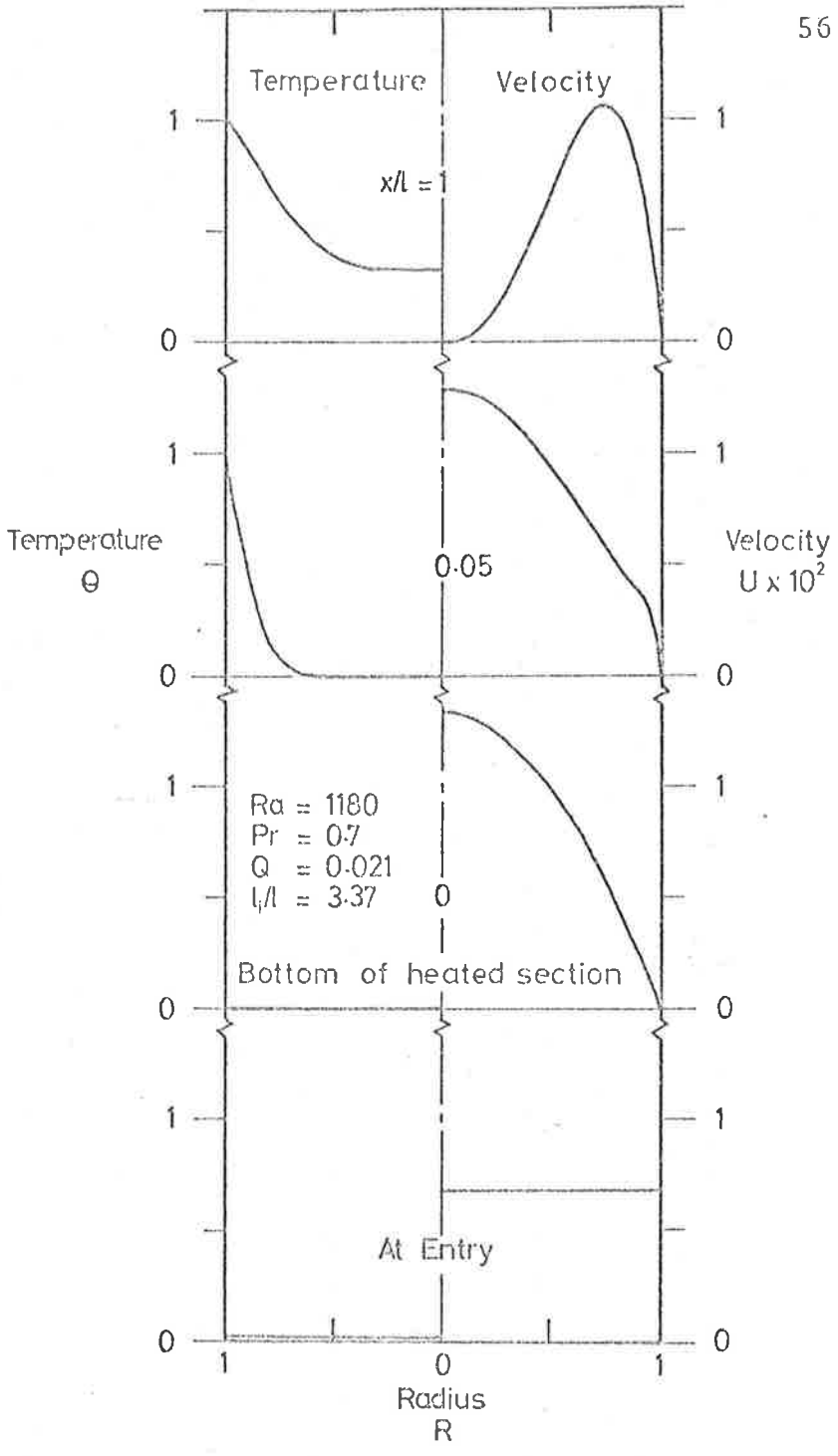

Fig. 4.5 Dimensionless temperature (θ) and velocity (U) profiles for laminar flow in a restricted-entry duct in which the velocity on the axis falls to zero at the top of the duct

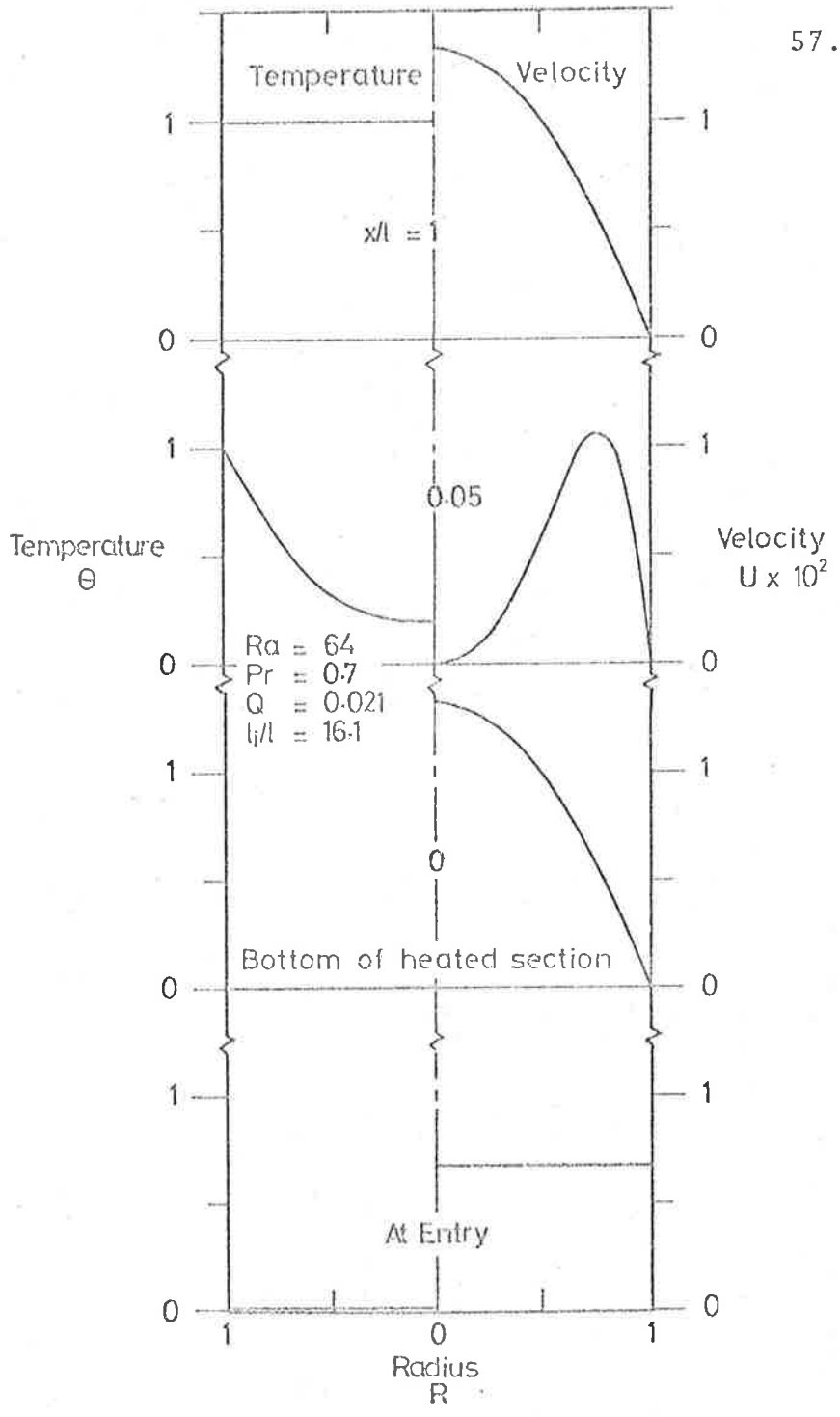

Fig. 4.6 Dimensionless temperature (θ) and velocity (U) profiles for laminar flow in a restricted-entry duct in which the velocity on the axis falls to zero near the bottom of the heated section and fully developed flow occurs near the top of the duct

In Fig. 4.2 it will be observed that the constant Q curves ranging from 0.021 to 0.3 emanate from the curve $\ell_i/\ell = 0$ and continue into the fully developed flow region. On the other hand, the curves which have Q values less than 0.021 terminate in the boundary layer region. In an attempt to obtain Nu-Ra values beyond the termination points, it was found that the relaxation (described in Appendix B) ran out of control. It was conjectured that the flow situation had changed when the point of termination was reached. To explain this phenomenon further, the temperature and velocity profiles in Figs. 4.5 and 4.6 for the continuous curve Q = 0.021 will be examined. It will be seen in Fig. 4.5 that the velocity distribution for Ra = 1180 changes from a fully developed parabolic profile at the bottom of the heated section to a boundary layer profile. At the top of the duct the velocity on the axis has fallen to zero. The effect on the velocity and temperature profiles of reducing Ra to 64 and maintaining the same value of Q (Q=0.021) is shown in Fig. 4.6. Again the velocity profile is parabolic at the entry to the heated section, but in this case the boundary layer profile with zero velocity on the axis occurs near the bottom of the heated

section at $x/\ell = 0.05$. Further up the duct, velocities in the centre region begin to increase and the fluid reaches the top of the duct with a fully developed profile. It should be noted in studying Fig. 4.6 that there is a radial outward component of the velocity of the fluid between $x/\ell = 0$ and 0.05, and a radial inward component above $x/\ell = 0.05$ to the formation of the fully developed flow. On the other hand, by increasing Ra above 1180 and maintaining $Q = 0.021$, boundary layer flow was produced similar to that shown in Fig. 4.5 except that the velocity on the axis did not drop to zero at the top of the duct.

Consideration will now be given to the curve $Q = 0.020$, which according to Fig. 4.2 terminates at about $Ra = 2 \times 10^3$. At this value of Ra, the velocity profiles were similar to those already shown in Fig. 4.5 with the velocity dropping to zero at the top of the duct. For the same Q of 0.020 and a larger flow restriction to give a smaller Ra, boundary layer flow with zero velocity on the axis was found to occur below the top of the duct. However, instead of the velocity increasing above this point as it did for the curve $Q = 0.021$, as shown in Fig. 4.6, velocities in the centre region of the duct

became negative and the computer solution ran out of control because reverse flow is incompatible with increasing temperatures. Under these conditions, laminar flow could no longer be sustained and the flow degenerated, as illustrated in Fig. 4.7, into what will be referred to as mixing flow. Describing it in another way, degeneration occurs when the laminar boundary layer is still growing but there is no flow in the centre region from which the boundary layer can draw fluid. This condition can occur only when Q is less than 0.021.

In Fig. 4.8, showing the pressure defect along a restricted-entry duct for a small Ra, it will be observed that the pressure gradient in each section is almost constant. This distribution of the pressure defect is in accord with the assumption made in Section 4.2 to derive the Nu-Ra relationship for fully developed flow.

Heat transfer per unit flow area

The heat transfer per unit flow area for a restricted-entry duct is given also by Eq. (3.22). It follows from Eq. (3.22) that, if the temperature excess of the heated surface and the lengths of the two sections of the duct are constant and the fluid properties do not

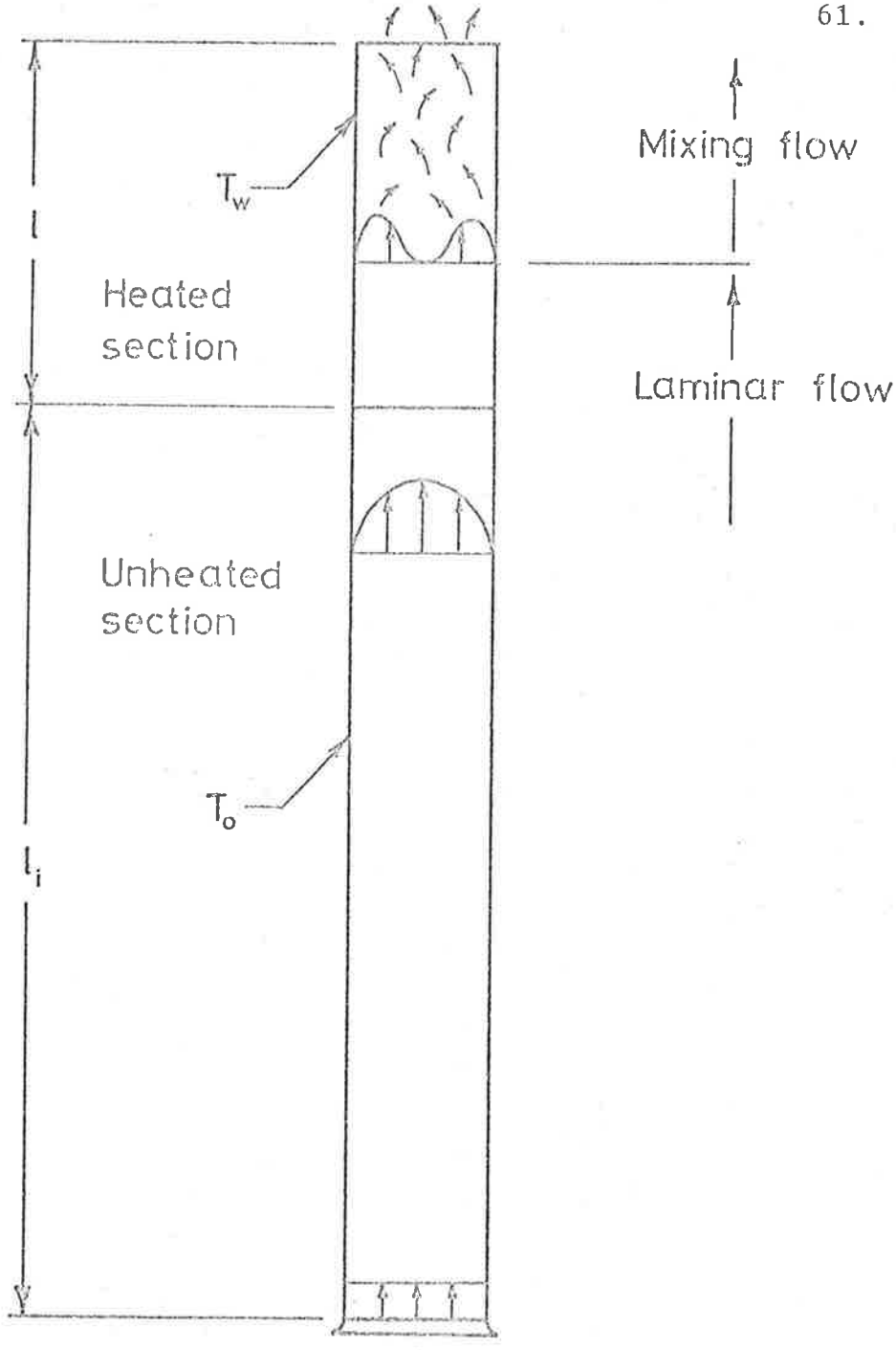

Fig. 4.7 Sketch showing the degeneration of laminar flow into mixing flow in a duct with a large entry restriction

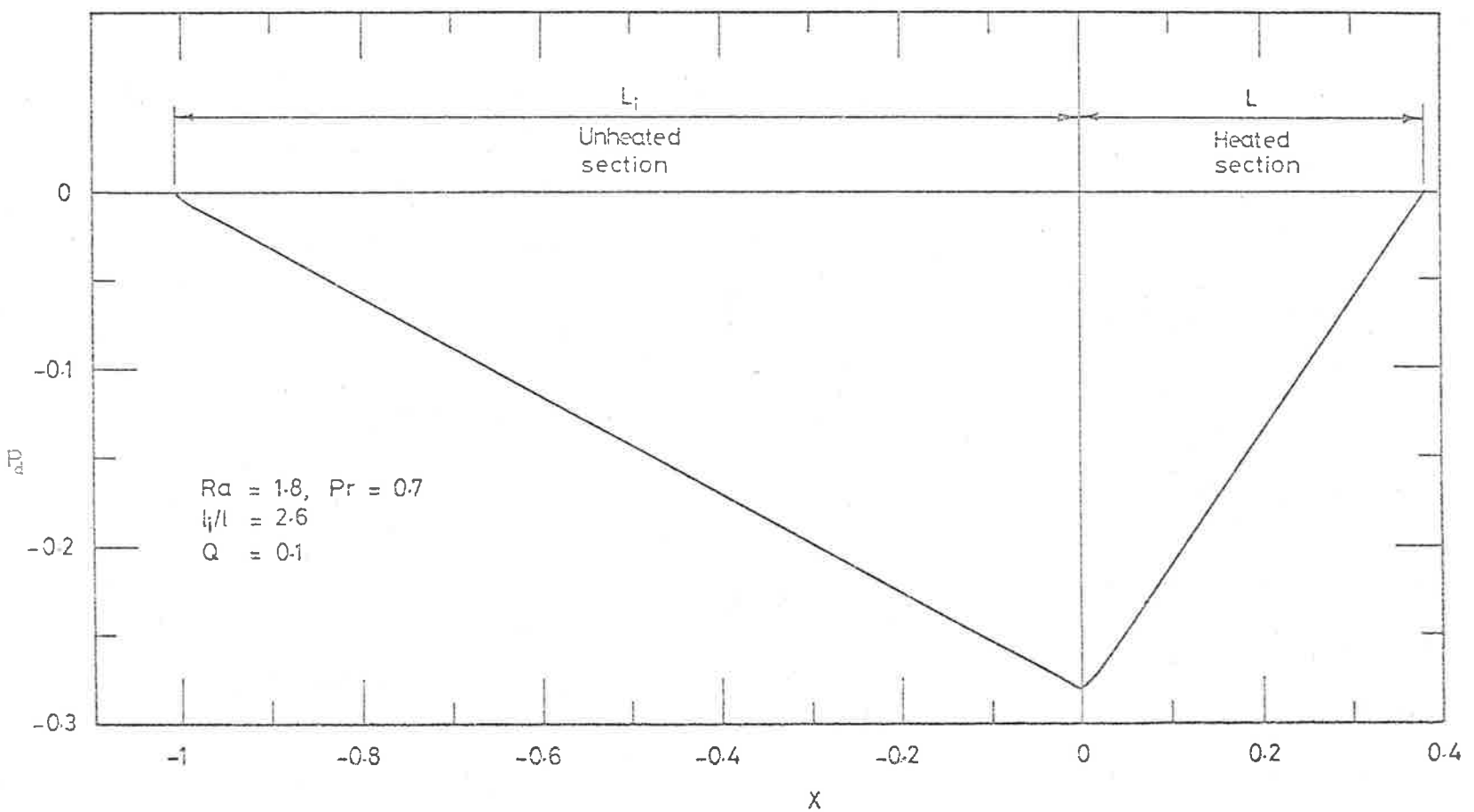

Fig. 4.8 Distribution of the pressure defect (P_d) in a restricted-entry duct in which the flow is laminar and fully developed in each section

vary, the heat transfer per unit flow area will be proportional to $Nu/\sqrt{Ra}$. In Fig. 4.9 it will be observed that the optimum value of Ra (Ra_{opt}) increases with the ratio ℓ_i/ℓ and coincides with the maximum values of Ra for $\ell_i/\ell > 6$.

Reynolds number

The relationship between Reynolds number (Re_r) and Ra is the same as that for plain-entry ducts and is given by Eq. (3.30). As shown in Fig. 4.10, Re_r decreases with increasing values of the ratio ℓ_i/ℓ. This is explained by the fact that an entry restriction reduces the flow rate.

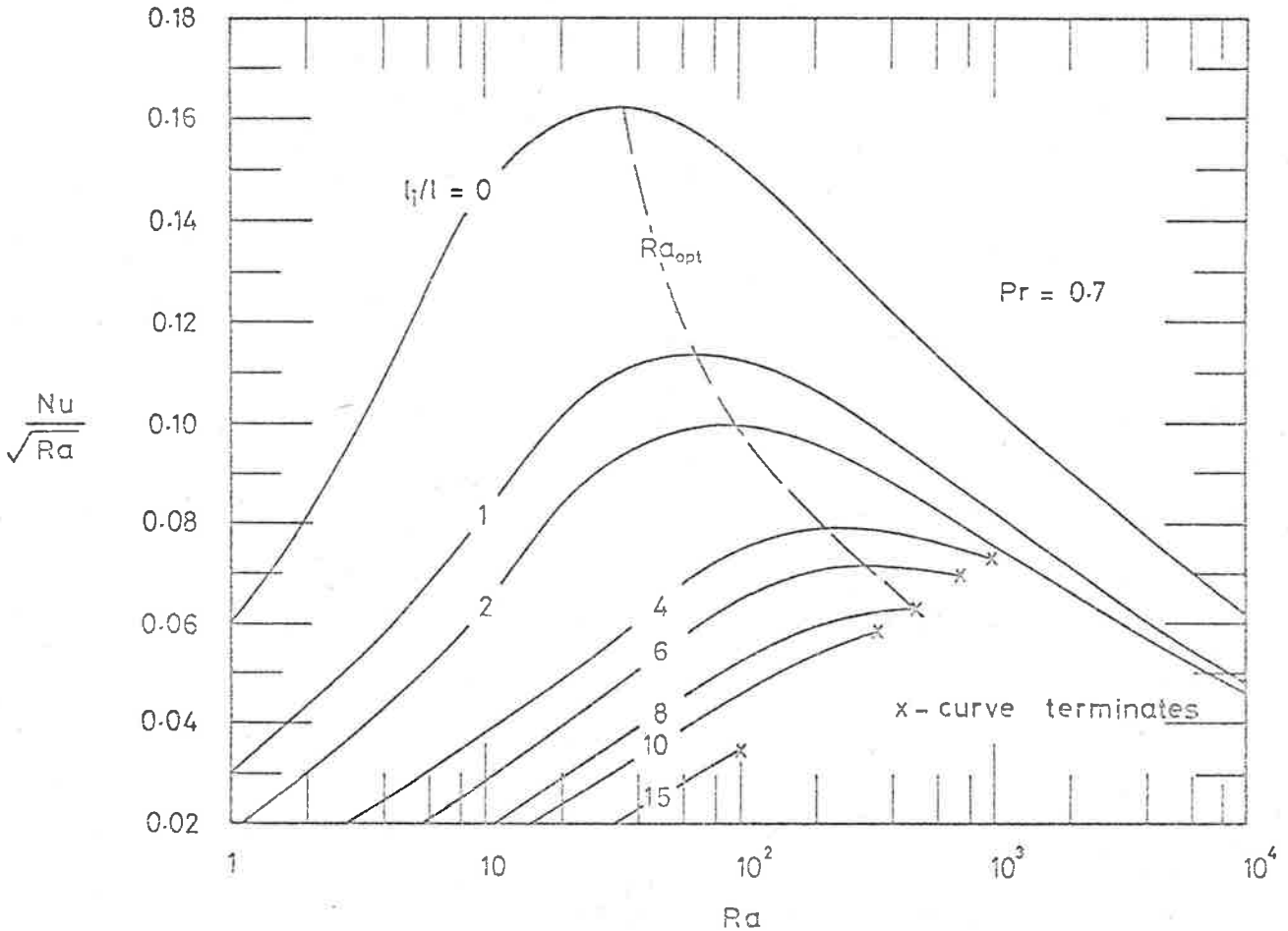

Fig. 4.9 Parameter $Nu/\sqrt{Ra}$, which is proportional to the rate of heat transfer per unit flow area, against Rayleigh number for restricted-entry ducts with uniform surface temperatures

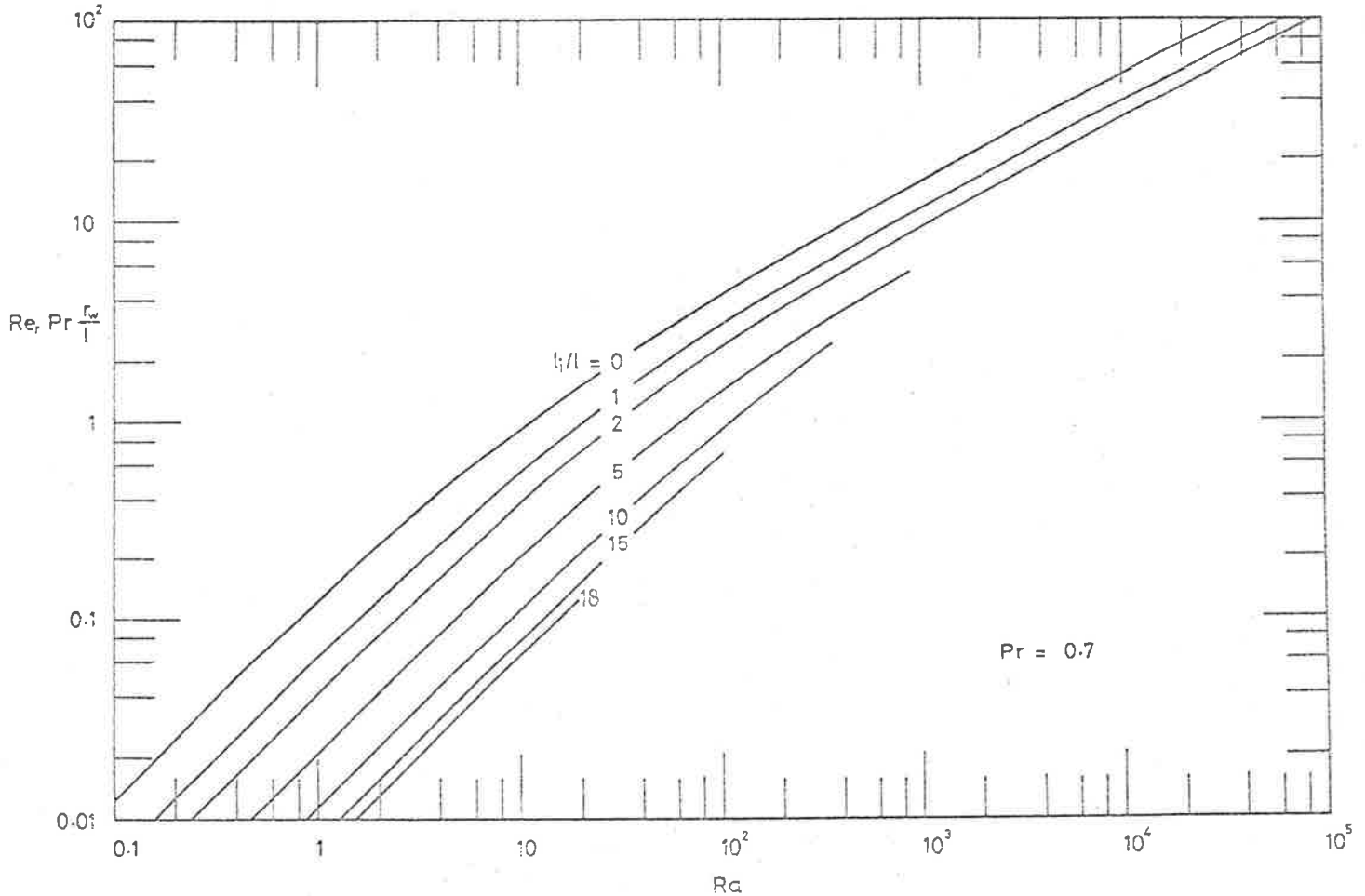

Fig. 4.10 Parameter $Re_r Pr\, r_w/\ell$ against Rayleigh number for constant values of ℓ_i/ℓ for laminar flow in restricted-entry ducts

5. UNIFORM SURFACE HEAT FLUX DUCTS

5.1 Introduction

In this section vertical ducts of circular cross-section with uniform heat fluxes will be considered. As shown in Fig. 1.1(c) it will be assumed that the fluid enters the duct with a uniform velocity and that the unknown temperature of the surface increases from ambient at the bottom of the duct.

5.2 General Nusselt relationship

In order to obtain the relationship between the Nusselt and Rayleigh numbers the following theoretical analysis is adopted.

The dimensionless volume flow (Q^*) and the rate of heat transfer (H_X^*) from the bottom of the duct to elevation X^* are given by

$$Q^* = 2\Pi \int_0^1 U^* R \, dR \qquad \ldots (5.1)$$

and

$$H_X^* = 2\Pi \int_0^1 U^* \theta^* R \, dR \qquad \ldots (5.2)$$

H_x^* can also be expressed in terms of the dimensionless uniform heat flux (F) as follows:

$$H_x^* = 2\Pi\ X^*\ F \qquad \ldots (5.3)$$

Since the surface temperature varies along the duct, a reference temperature has to be adopted. The mean surface temperature given by

$$T_{wm} = \frac{\int_o^{\ell} (T_{wx} - T_o)\,dx}{\ell} \qquad \ldots (5.4)$$

provides a suitable reference temperature (14).

The Nusselt number of the duct (Nu*) with the radius as the characteristic dimension is given by

$$Nu^* = \frac{Af}{A(T_{wm} - T_o)} \cdot \frac{r_w}{k} \qquad \ldots (5.5)$$

which reduces to

$$Nu^* = \frac{f\ r_w}{(T_{wm} - T_o)k} \qquad \ldots (5.6)$$

Multiplying Eq. (5.6) by the dimensionless mean surface temperature (θ^*_{wm}), which is given by

$$\theta^*_{wm} = \frac{(T_{wm} - T_o)k}{f\ r_w} \qquad \ldots (5.7)$$

yields

$$Nu^* = \frac{1}{\theta^*_{wm}} \qquad \ldots (5.8)$$

By definition, the overall dimensionless rate of heat transfer (H^*_t) is

$$H^*_t = \frac{h_t}{Gr^* \; Pr \; f \; \ell \; r_w} \qquad \ldots (5.9)$$

Substituting $2\Pi r_w \; \ell \; f$ for h_t in Eq. (5.9) yields

$$H^*_t = \frac{2\Pi}{Ra^*} \qquad \ldots (5.10)$$

where Ra* is equal to Gr* Pr.

It should be noted that dividing Eq. (5.10) by the dimensionless surface area ($2\Pi L^*$) and replacing L* by 1/Gr* yields the dimensionless heat flux (F). Thus

$$F = \frac{1}{Pr} \qquad \ldots (5.11)$$

Eq. (5.11) states that the dimensionless heat flux is simply the reciprocal of the Prandtl number.

From Eqs. (5.8) and (5.10) the general Nusselt relationship is obtained namely,

$$Nu^* = \frac{Ra^* \; H^*_t}{2\Pi \; \theta^*_{wm}} \qquad \ldots (5.12)$$

The strong similarity between Eq. (5.12) and Eq. (3.6) for UST ducts should be noted.

Although hitherto it has been implied that the uniform heat flux (f) is known, in practice only the temperatures along the surface may be available. Therefore, Nusselt number relationships will be derived for both a known uniform heat flux and a known surface temperature.

To corroborate the general solution, laminar flow Nusselt number relationships for extreme values of the Rayleigh number will be established in the sections that follow.

5.3 Nusselt relationship for small Rayleigh numbers based on the uniform heat flux

Small Rayleigh numbers are obtained by making the ratio ℓ/r_w sufficiently large. In contrast with UST ducts, fully developed flow cannot be achieved in USHF ducts. The mean temperature of the fluid will always lag behind that of the surface because the fluid is receiving heat along the entire length of the duct. However, to simplify the analysis, the velocity distribution will be assumed to be fully developed and the radial temperature gradients to be negligible. Thus the dimensionless

vertical component of the velocity at a radius R will be given by

$$U^* = \frac{2Q^*}{\Pi}(1 - R^2) \qquad \ldots (5.13)$$

and the dimensionless temperature of the fluid at elevation X^* and radius R by

$$\theta^* = \theta^*_X = \theta^*_{WX} \qquad \ldots (5.14)$$

For flow that is almost fully developed, the momentum equation, Eq. (2.15) reduces to

$$\frac{\partial P^*_d}{\partial X^*} = \frac{\partial^2 U^*}{\partial R^2} + \frac{1}{R}\frac{\partial U^*}{\partial R} + \theta^* \qquad \ldots (5.15)$$

Substituting Eqs. (5.13) and (5.14) into Eq. (5.15) yields

$$\frac{\partial P^*_d}{\partial X^*} = \theta^*_{WX} - \frac{8Q^*}{\Pi} \qquad \ldots (5.16)$$

For a uniform velocity profile, θ^*_{WX} will increase linearly along the length of the duct, and hence it follows from Eq. (5.16) that $\partial P^*_d/\partial X^*$ will also increase linearly. Furthermore, since P^*_d is zero at both the top and the bottom of the duct, $\partial P^*_d/\partial X^*$, as illustrated in Fig. 5.1, will change sign at mid-elevation ($X^* = L^*/2$).

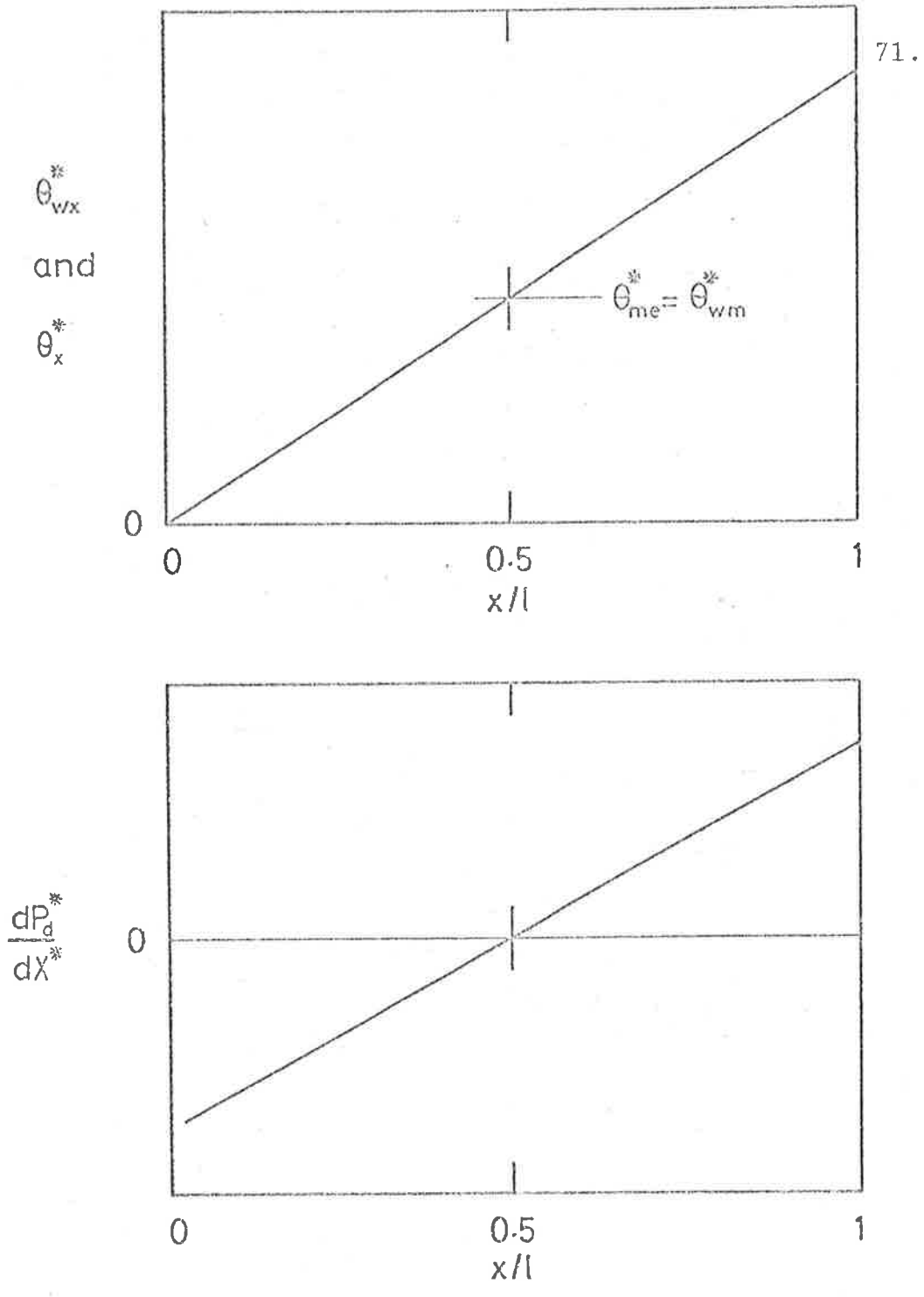

Fig. 5.1 Diagrammatic distribution of the surface temperature (θ^*_{wx}), the fluid temperature (θ^*_x), and the pressure gradient (dP^*_d/dX^*) in a uniform heat flux duct for a small Rayleigh number

Also at mid-elevation, since θ^*_{wx} increases linearly from the bottom to the top of the duct, the temperature of the surface will be equal to the mean surface temperature (θ^*_{wm}). Hence Eq. (5.16) at mid-elevation reduces to

$$\theta^*_{wm} = \frac{8Q^*}{\Pi} \qquad \ldots (5.17)$$

The rate at which the lower half of the surface dissipates heat (H^*_{me}) is given by

$$H^*_{me} = Q^*\theta^*_{wm} \qquad \ldots (5.18)$$

Using Eq. (5.18), Q^* in Eq. (5.17) can be replaced by H^*_{me}/θ^*_{wm} to yield

$$\theta^*_{wm} = \sqrt{\frac{8\ H^*_{me}}{\Pi}} \qquad \ldots (5.19)$$

Since the heat flux is uniform along the duct

$$H^*_{me} = \frac{H^*_t}{2} \qquad \ldots (5.20)$$

Using Eq. (5.10), Eq. (5.20) becomes

$$H^*_{me} = \frac{\Pi}{Ra^*} \qquad \ldots (5.21)$$

and substituting Eq. (5.21) into Eq. (5.19) gives

$$\theta^*_{wm} = \sqrt{\frac{8}{Ra^*}} \qquad \ldots (5.22)$$

Finally, substituting Eq. (5.22) into Eq. (5.8) yields the Nusselt relationship

$$Nu^* = \sqrt{\frac{Ra^*}{8}} \qquad \ldots (5.23)$$

Eq. (5.23) shows that, for small Ra*, Nu* is proportional to $\sqrt{Ra^*}$. In the case of the UST duct, it will be recalled that Nu is proportional to Ra for small Ra.

It is interesting to note that according to Eqs. (5.17) and (5.22) the relationship between Q* and small Ra* is given by

$$Q^* = \frac{\Pi}{\sqrt{8\ Ra^*}} \qquad \ldots (5.24)$$

5.4 Nusselt relationship for boundary layer flow based on the uniform heat flux

Boundary layer flow will occur if the ratio ℓ/r_w is made sufficiently small. Consequently, Ra* will be large. As in the case of the UST duct, it is reasonable to assume that the rate of heat transfer will be the same as that from an equivalent vertical flat surface. Therefore Nu* will be independent of the radius of the duct, and this requirement is achieved if

$$Nu^* = C_3 (Ra^*)^{\frac{1}{5}} \qquad \ldots (5.25)$$

where C_3 is a constant. Expanding both sides of Eq. (5.25) and multiplying through by ℓ yields

$$Nu^*_\ell = C_3(Ra^*_\ell)^{\frac{1}{5}} \qquad \ldots (5.26)$$

where the subscript ℓ indicates that the length of the duct is now the characteristic dimension. Sparrow and Gregg (14) derived the following relationship for a vertical flat surface dissipating a uniform heat flux for Pr = 0.7:

$$Nu^*_\ell = 0.62(Ra^*_\ell)^{\frac{1}{5}} \qquad \ldots (5.27)$$

Eq. (5.26) will be seen to have the same form as Eq. (5.27). Hence, if C_3 in Eq. (5.25) is assumed to be equal to the constant in Eq. (5.27), the relationship between Nu* and Ra* for laminar boundary layer flow in a vertical duct is given approximately by

$$Nu^* = 0.62(Ra^*)^{\frac{1}{5}} \qquad \ldots (5.28)$$

5.5 Nusselt relationship for small Rayleigh numbers based on the mean surface temperature

In order to obtain the Nusselt number relationship based on the mean surface temperature, it is necessary to establish a Grashof number based on the mean surface temperature (Gr^+). As shown by the following set of

equations, Gr^+ is obtained by dividing Gr* by Nu* (14).

$$\left.\begin{aligned} Gr^+ &= \frac{Gr^*}{Nu^*} \\ Gr^+ &= \frac{g\ \beta\ f\ r_w^5}{\nu^2\ \ell\ k} \cdot \frac{(T_{wm}-T_o)k}{f\ r_w} \\ Gr^+ &= \frac{g\ \beta(T_{wm}-T_o)r_w^4}{\nu^2\ \ell} \end{aligned}\right\} \quad \ldots (5.29)$$

Hence the Rayleigh number based on the mean surface temperature is

$$Ra^+ = \frac{Ra^*}{Nu^*} \quad \ldots (5.30)$$

Introducing Eq. (5.30) into Eq. (5.23) yields for small Ra^+

$$Nu^* = \frac{Ra^+}{8} \quad \ldots (5.31)$$

Comparing Eq. (5.31) with Eq. (3.10) will reveal that the Nusselt number of the USHF duct is twice that of the UST duct. The following analysis will explain the reason for this.

Multiplying θ^* by Nu* yields a dimensionless temperature (θ^+) which is based on the mean surface temperature of the duct as shown by the following set of equations.

$$\left.\begin{aligned} \theta^+ &= \theta^* \, Nu^* \\ \theta^+ &= \frac{(T-T_o)k}{f\, r_w} \cdot \frac{f\, r_w}{(T_{wm}-T_o)k} \\ \theta^+ &= \frac{T-T_o}{T_{wm}-T_o} \end{aligned}\right\} \quad \ldots (5.32)$$

It was shown in Section 5.3 that θ^*_{wm} for small Ra* is approximately equal to the temperature of the surface at mid-elevation, which in turn is approximately equal to the temperature of the fluid at the same elevation. Hence it follows from Eq. (5.32) that the dimensionless fluid temperature at mid-elevation is given approximately by

$$\theta^+_{me} = \theta^+_{wm} = 1 \qquad \ldots (5.33)$$

Since, as shown in Fig. 5.1, the temperatures of the surface and the fluid will increase linearly when the flow is approximately fully developed, the temperature of the fluid at the top of the duct is given by

$$\theta^+_t = 2\theta^+_{wm} = 2 \qquad \ldots (5.34)$$

From Eq. (5.17)

$$Q^* = \frac{\Pi}{8}\, \theta^*_{wm} \qquad \ldots (5.35)$$

and using Eq. (5.8) to replace θ^*_{wm} in Eq. (5.35) yields

$$Q^*Nu^* = \frac{\Pi}{8} \qquad \ldots (5.36)$$

However, the product of Q* and Nu* gives the dimensionless flow (Q^+) based on the mean surface temperature, as shown by the following set of equations.

$$\left.\begin{aligned} Q^+ &= Q^*\ Nu^* \\ Q^+ &= \frac{q}{\ell\ \nu\ Gr^*}\ .\ Nu^* \\ Q^+ &= \frac{q}{\ell\ \nu\ Gr^+} \end{aligned}\right\} \qquad \ldots (5.37)$$

Substituting Eq. (5.37) into Eq. (5.36) yields

$$Q^+ = \frac{\Pi}{8} \qquad \ldots (5.38)$$

The heat dissipated by the surface of the duct is

$$H_t^+ = Q^+\ \theta_t^+ \qquad \ldots (5.39)$$

Hence using Eqs. (5.34) and (5.38), Eq. (5.39) becomes

$$H_t^+ = \frac{\Pi}{4} \qquad \ldots (5.40)$$

In Section 3.2 it was shown that the heat dissipated by the surface of a UST duct in which the flow is fully

developed is

$$H_t = \frac{\Pi}{8} \qquad \ldots (5.41)$$

An inspection of Eqs. (5.40) and (5.41) will show that

$$H_t^+ = 2H_t \qquad \ldots (5.42)$$

Since $H_x^+ = H_x^*(Nu^*)^2$, Eq. (5.12) can be written

$$Nu^* = \frac{Ra^+ H_t^+}{2\Pi} \qquad \ldots (5.43)$$

Hence it follows from Eqs. (5.42), (5.43) and (3.6) that, for small values of Ra^+ and Ra, Nu* is twice Nu.

5.6 Nusselt relationship for boundary layer flow based on the mean surface temperature

To obtain the relationship between the Nusselt number and the Rayleigh number based on the mean surface temperature for boundary layer flow, Eq. (5.30) is introduced in Eq. (5.28). This yields

$$Nu^* = 0.55(Ra^+)^{\frac{1}{4}} \qquad \ldots (5.44)$$

An inspection of Eqs. (5.44) and (3.15) will show that for boundary layer flow the Nusselt numbers of a USHF

duct are about 7% less than those of a UST duct. This means that using the mean surface temperature in the UST duct relationship (Eq. (3.16)) will give a good estimate of the Nusselt number for a USHF duct for boundary layer flow. Sparrow and Gregg (14) reported the same finding for a vertical flat plate with a uniform heat flux.

5.7 Method of solving the flow equations

In order to obtain Nusselt numbers for all laminar flow values of Rayleigh numbers based on both the uniform heat flux and the mean surface temperature, Eqs. (2.14) to (2.17) were solved for the following boundary conditions.

Boundary conditions

$X^*=0$ and $R=1$; $U^*=0$, $V=0$, $\theta^*=0$, $P_d^*=0$. (a)

$X^*=0$ and $0 \leqslant R<1$; $U^*=\frac{Q^*}{\pi}$, $V=0$, $\theta^*=0$, $P_d^*=0$. (b)

$0<X^*<L^*$ and $R=1$; $U^*=0$, $V=0$, $P_d^*<0$. (c)

$0<X^*<L^*$ and $R=0$; $V=0$, $P_d^*<0$, $\frac{\partial U^*}{\partial R}=0$, $\frac{\partial \theta^*}{\partial R}=0$. (d)

$X^*=L^*$ and $R=1$; $U^*=0$, $V=0$, $P_d^*=0$. (e)

$X^*=L^*$ and $R=0$; $V=0$, $P_d^*=0$, $\frac{\partial U^*}{\partial R}=0$, $\frac{\partial \theta^*}{\partial R}=0$. (f)

$0 \leqslant X^* \leqslant L^*$; Q^* is constant. (g)

The finite difference forms of Eqs. (2.14), (2.15) and (2.17) are given in Appendix D, and the relaxation procedure is described in Appendix E.

5.8 Theoretical results

Relationships between the Nusselt number and the Rayleigh number for Rayleigh numbers based on both the uniform heat flux (Ra^*) and the mean surface temperature (Ra^+) are shown in Figs. 5.2 and 5.3 respectively. It will be seen that the curve based on the uniform heat flux agrees satisfactorily with Eqs. (5.23) and (5.28) for the extreme values of Ra^* and the curve based on the mean surface temperature with Eqs. (5.31) and (5.44) for extreme values of Ra^+. For boundary layer flow the general solution yielded the following relationships:

$$Nu^* = 0.67\ Ra^{*\frac{1}{5}} \qquad \ldots (5.45)$$

and

$$Nu^* = 0.61\ Ra^{+\frac{1}{4}} \qquad \ldots (5.46)$$

It is interesting to note that the relationships based on a vertical flat surface dissipating a uniform heat flux, Eqs. (5.27) and (5.44), have constants that are about 10% smaller than those in Eqs. (5.45) and (5.46).

The UST duct relationship is also plotted in Fig. 5.3 and it will be seen that for boundary layer flow the two curves are almost identical. This means, of course, that for boundary layer flow the Nusselt number relation-

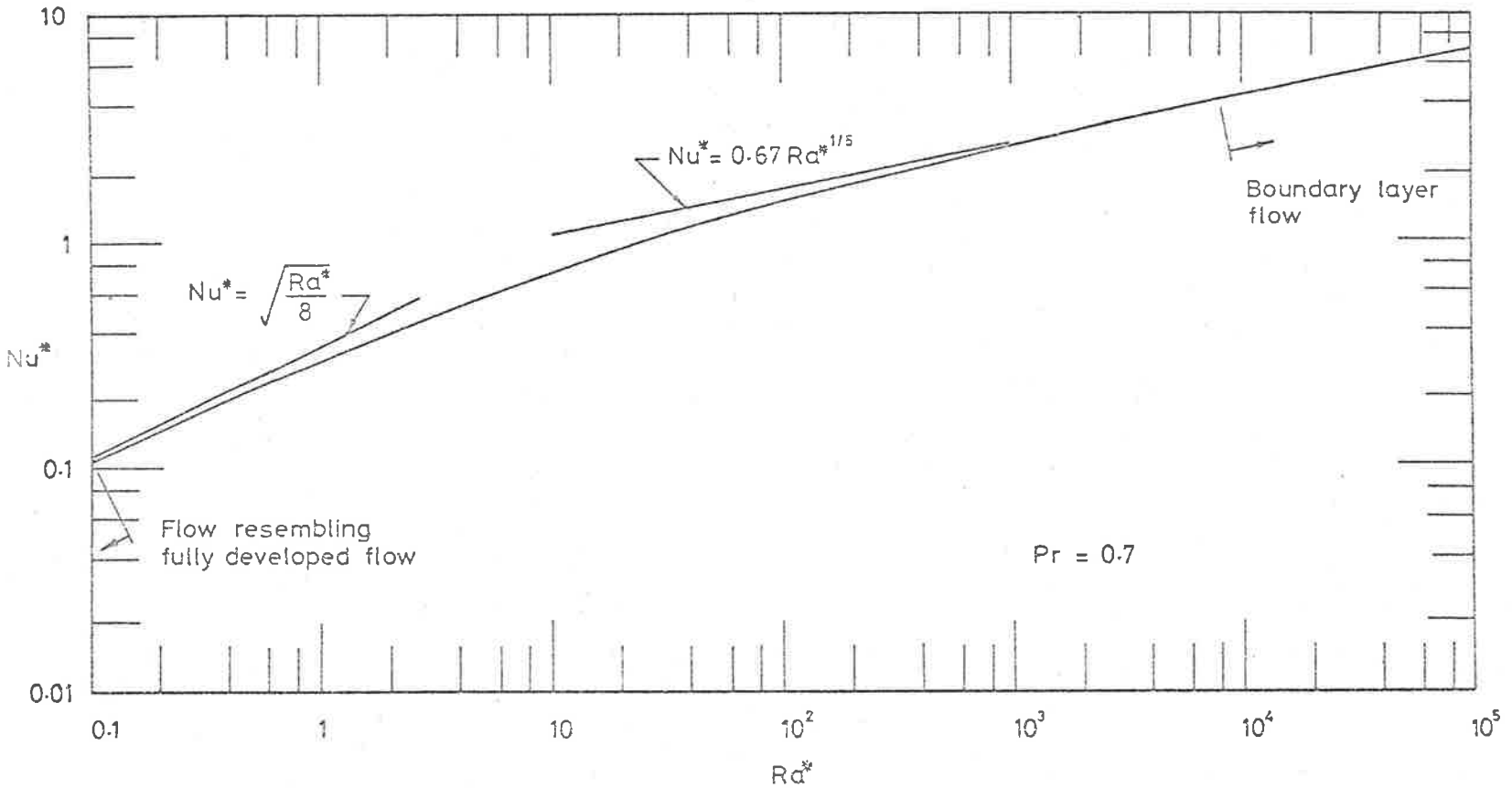

Fig. 5.2 Nusselt number (Nu*) against Rayleigh number (Ra*) for uniform surface heat flux ducts

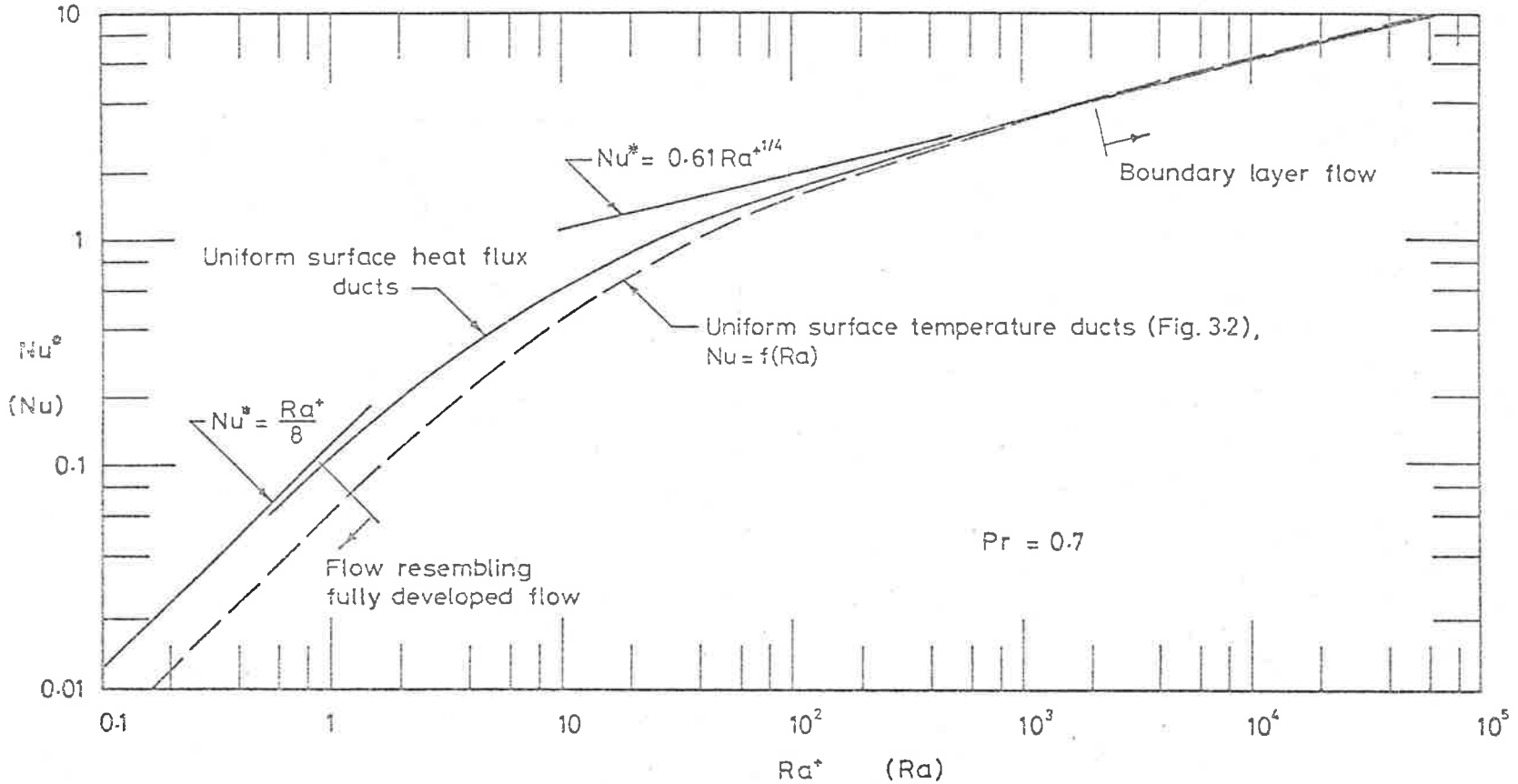

Fig. 5.3 Nusselt number (Nu*) against Rayleigh number based on the mean surface temperature (Ra^+) for uniform surface heat flux ducts

ship for UST ducts could be used if the entire surface were assumed to be at the mean surface temperature.

Fig. 5.4 compares the dimensionless temperatures along the surface (θ^*_{wx}) of the duct with those along the axis (θ^*_{cx}). It will be observed that for small Ra* these temperatures increase linearly as assumed in Section 5.3. However, for large Ra*, it is interesting to note that the temperature distribution on the surface approaches that of a USHF vertical flat surface (14). This finding is in accord with the assumption made in deriving the relationship between Nu* and large Ra* in Section 5.4.

In Fig. 5.5, Q^*, H^*_t, θ^*_{wt} and θ^*_{wm} are plotted against Ra*. Unlike Q and H_t for UST ducts, which are illustrated in Fig. 3.4, Q^* and H^*_t do not asymptotically approach a common value at small Ra*. In fact, Q^* for small Ra* will be seen to approach the relationship given by Eq. (5.24) namely, $Q^* = \Pi/\sqrt{8Ra^*}$, and H^*_t for all Ra* to be inversely proportional to Ra* in accordance with Eq. (5.10).

Figs. 5.6 and 5.7 show the stages of development of the temperature and velocity in ducts having a small and a large value of Ra* respectively. The shapes of

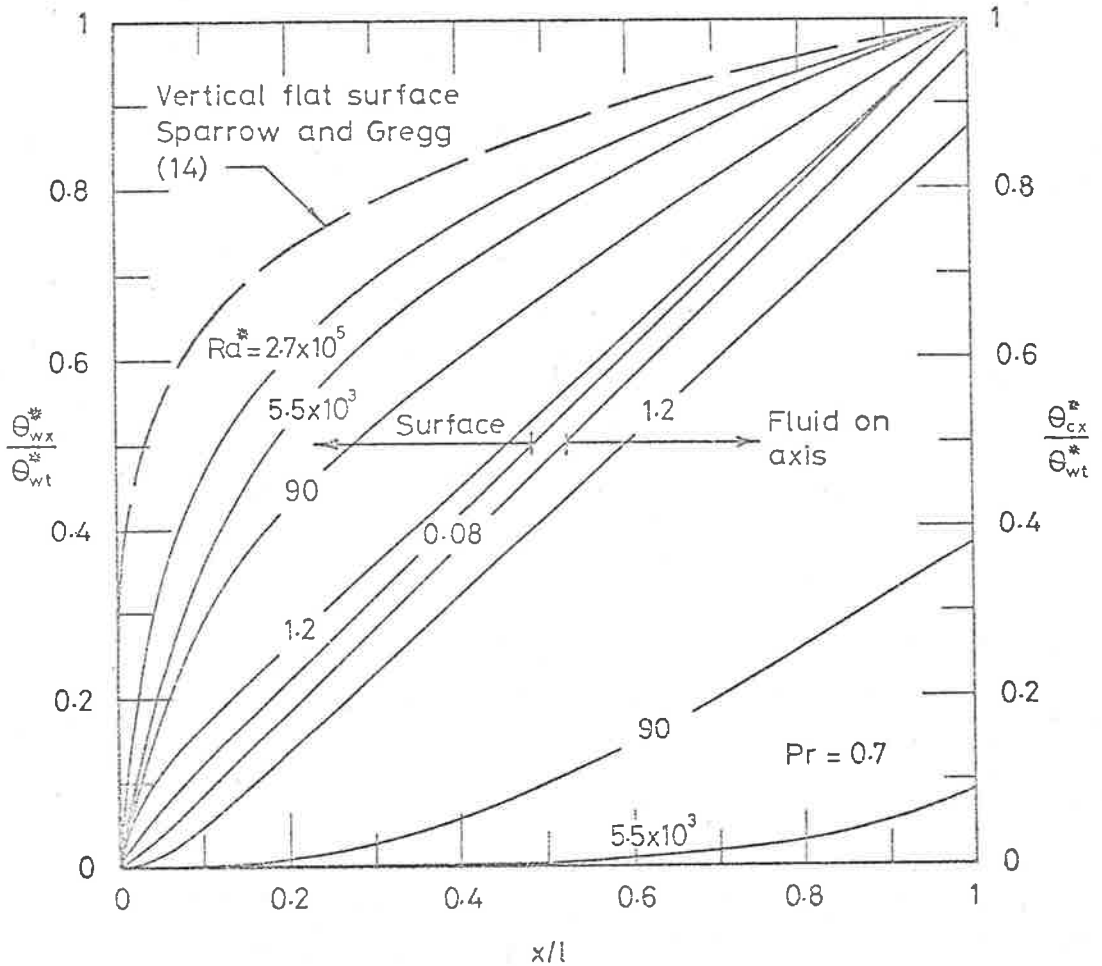

Fig. 5.4 Distributions of the dimensionless temperatures of the surface (θ^*_{WX}) and of the fluid on the axis (θ^*_{CX}) of uniform heat flux ducts; the distribution of temperature of the surface of a vertical flat surface (14) is shown for comparison

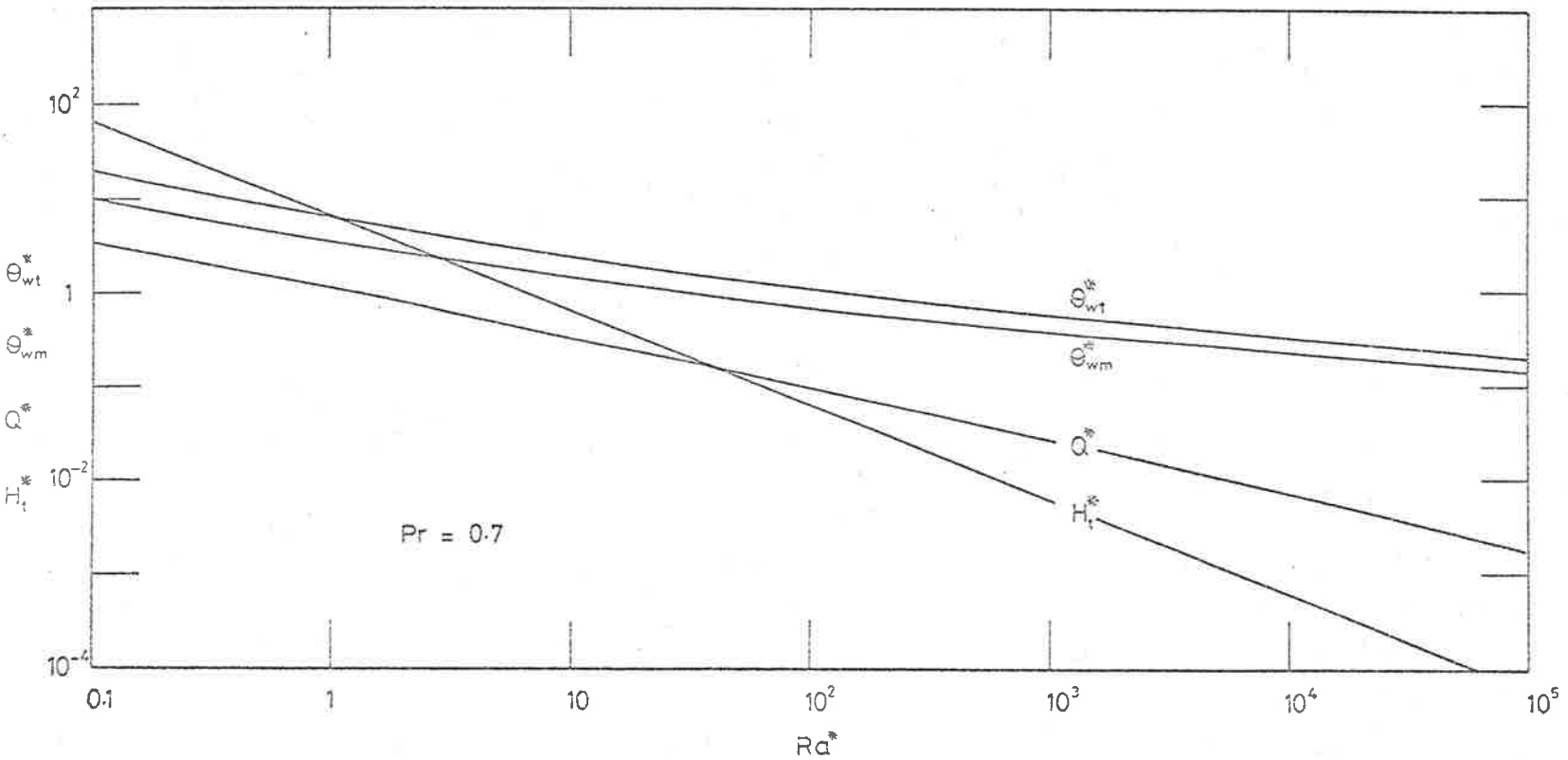

Fig. 5.5 Dimensionless flow (Q^*), total heat transfer (H_t^*), temperature of the surface at the top (θ^*_{wt}) and mean surface temperature (θ^*_{wm}) for uniform surface heat flux ducts against Ra*

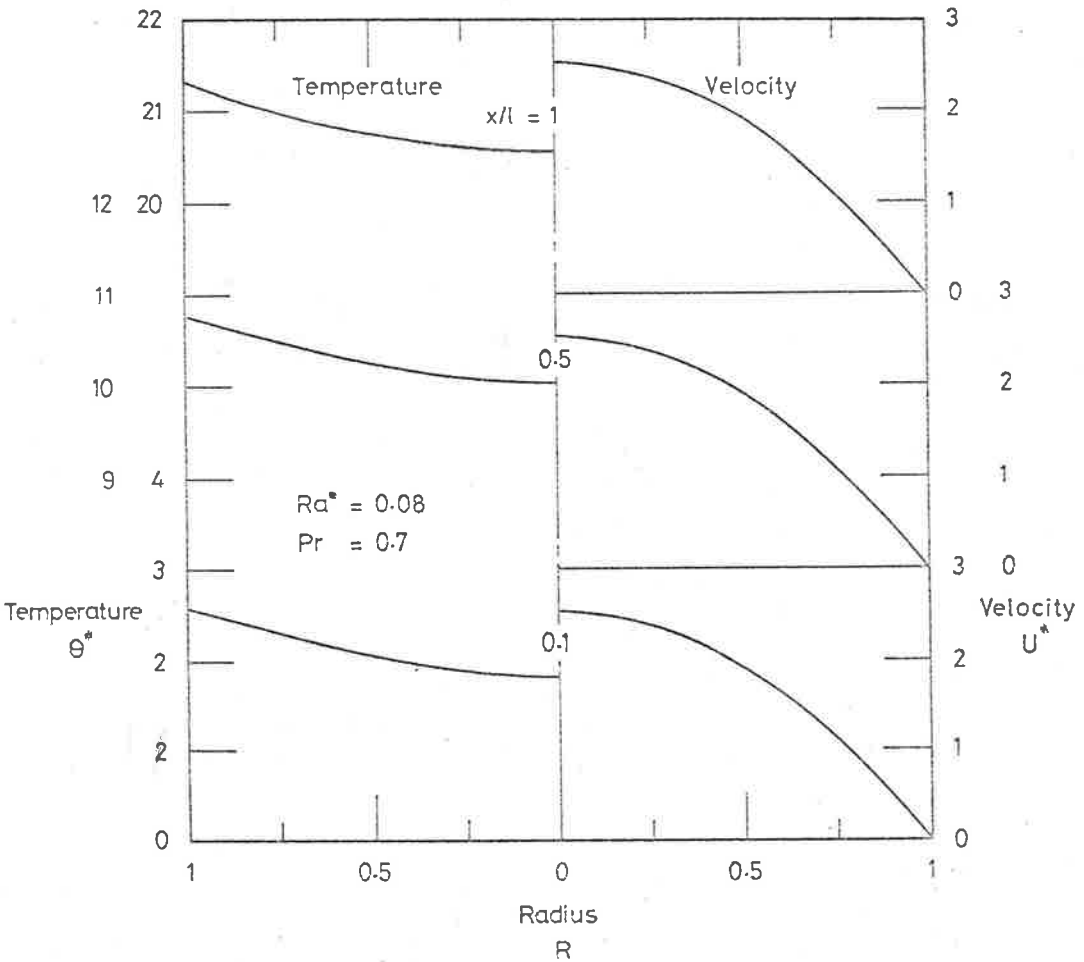

Fig. 5.6 Dimensionless temperature (θ*) and velocity (U*) profiles in a uniform surface heat flux duct for a small Rayleigh number

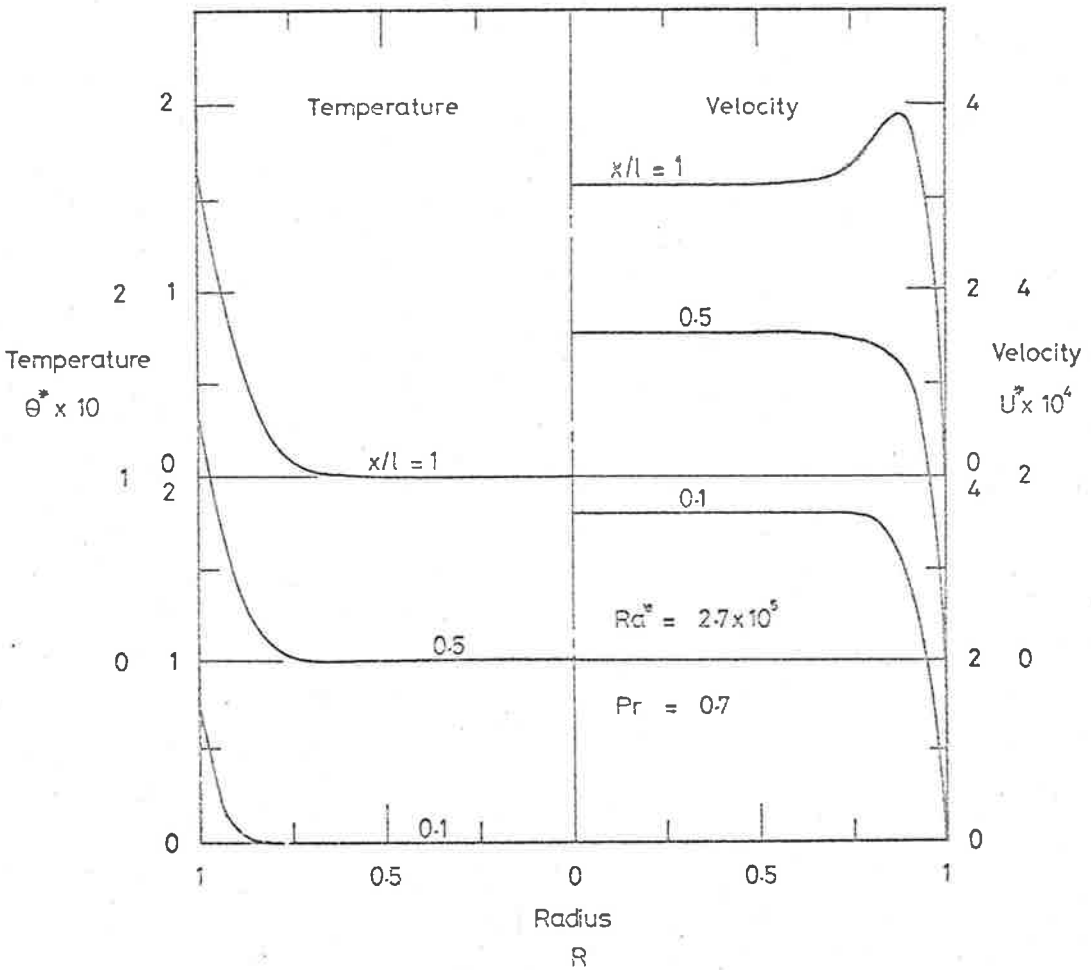

Fig. 5.7 Dimensionless temperature (θ*) and velocity (U*) profiles in a uniform surface heat flux duct for a large Rayleigh number

the temperature and velocity profiles will be seen to justify the assumptions made in Sections 5.3 and 5.4 to derive the Nu*-Ra* relationship for the extreme values of Ra*.

Fig. 5.8 shows the pressure defect along ducts having a small and a large Ra*. The zero pressure gradient which will be observed to occur half way along the duct with the small Ra* is in accord with the assumption made in Section 5.3.

Heat transfer per unit flow area

The USHF duct, unlike the UST duct, does not have a radius for which the heat dissipation per unit flow area is a maximum. This can be shown by the following analysis.

The heat dissipated per unit area is

$$\frac{h_t}{a} = \frac{h_t}{\pi r_w^2} \qquad \ldots (5.47)$$

and substituting $2\pi r_w \ell f$ for h_t on the right hand side of Eq. (5.47) yields

$$\frac{h_t}{a} = \frac{2\ell f}{r_w} \qquad \ldots (5.48)$$

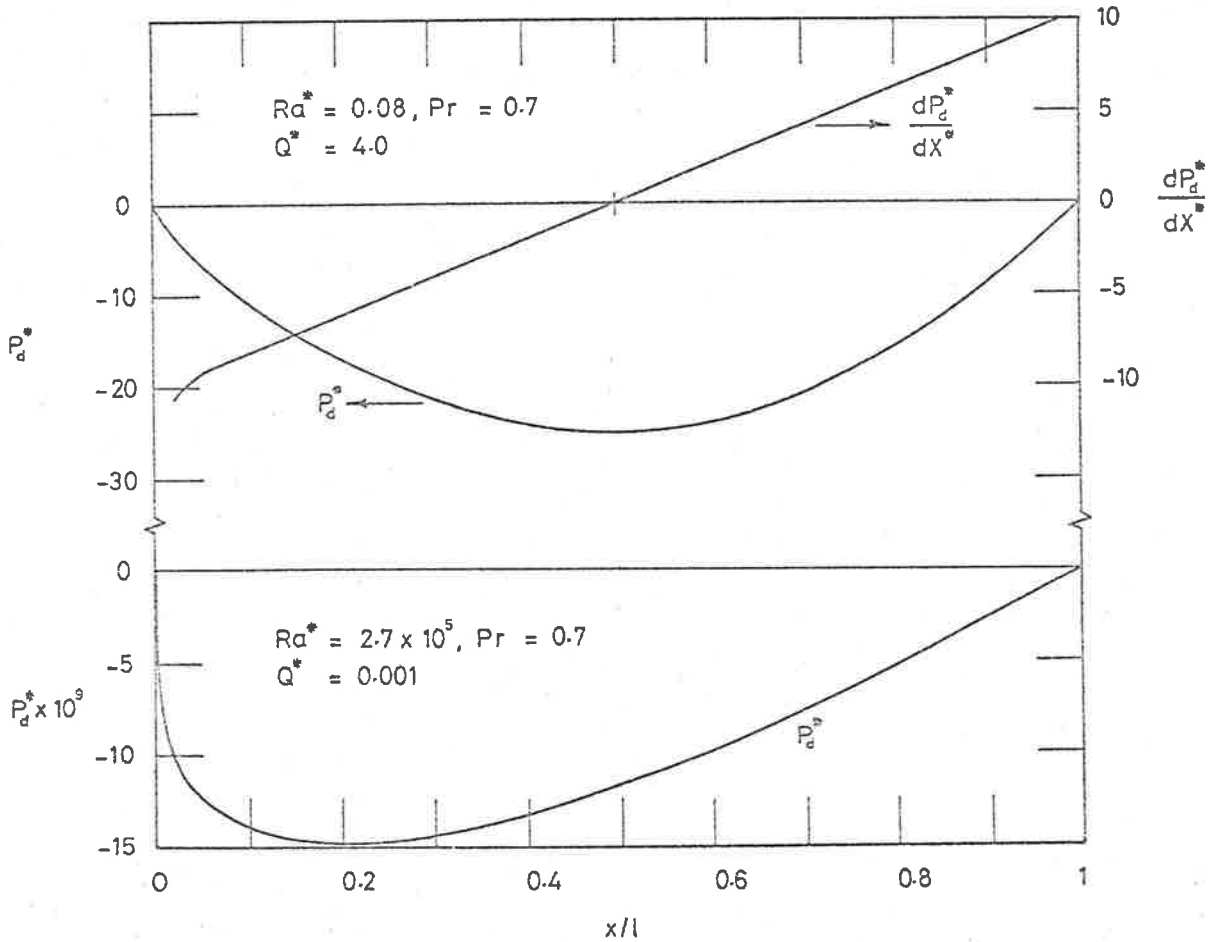

Fig. 5.8 Distribution of the dimensionless pressure defect (P_d^*) in uniform surface heat flux ducts for a small and a large Rayleigh number

From Eq. (5.48) it will be seen that, for given values of the length of the duct (ℓ) and the uniform heat flux (f), the heat transfer per unit flow area is simply inversely proportional to the radius of the duct.

Reynolds number

Based on the radius of the duct, Reynolds number of the uniform heat flux duct is given by

$$Re_r^* = \frac{u_m \, r_w}{\nu} \qquad \ldots (5.49)$$

Expressing u_m in terms of Q* yields

$$Re_r^* = \frac{Gr^* \, Q^*}{\Pi} \cdot \frac{\ell}{r_w} \qquad \ldots (5.50)$$

or

$$Re_r^* = \frac{Ra^* \, Q^*}{\Pi \, Pr} \cdot \frac{\ell}{r_w} \qquad \ldots (5.51)$$

Fig. 5.9 presents the relationship between (Re_r^* Pr r_w/ℓ) and Ra*.

Since for small Ra* Fig. 5.6 shows that the velocity profile is almost fully developed, it is reasonable to assume, as in the case of the UST duct, that the critical value of Reynolds number will be approximately the same as that for forced-convective flow in pipes.

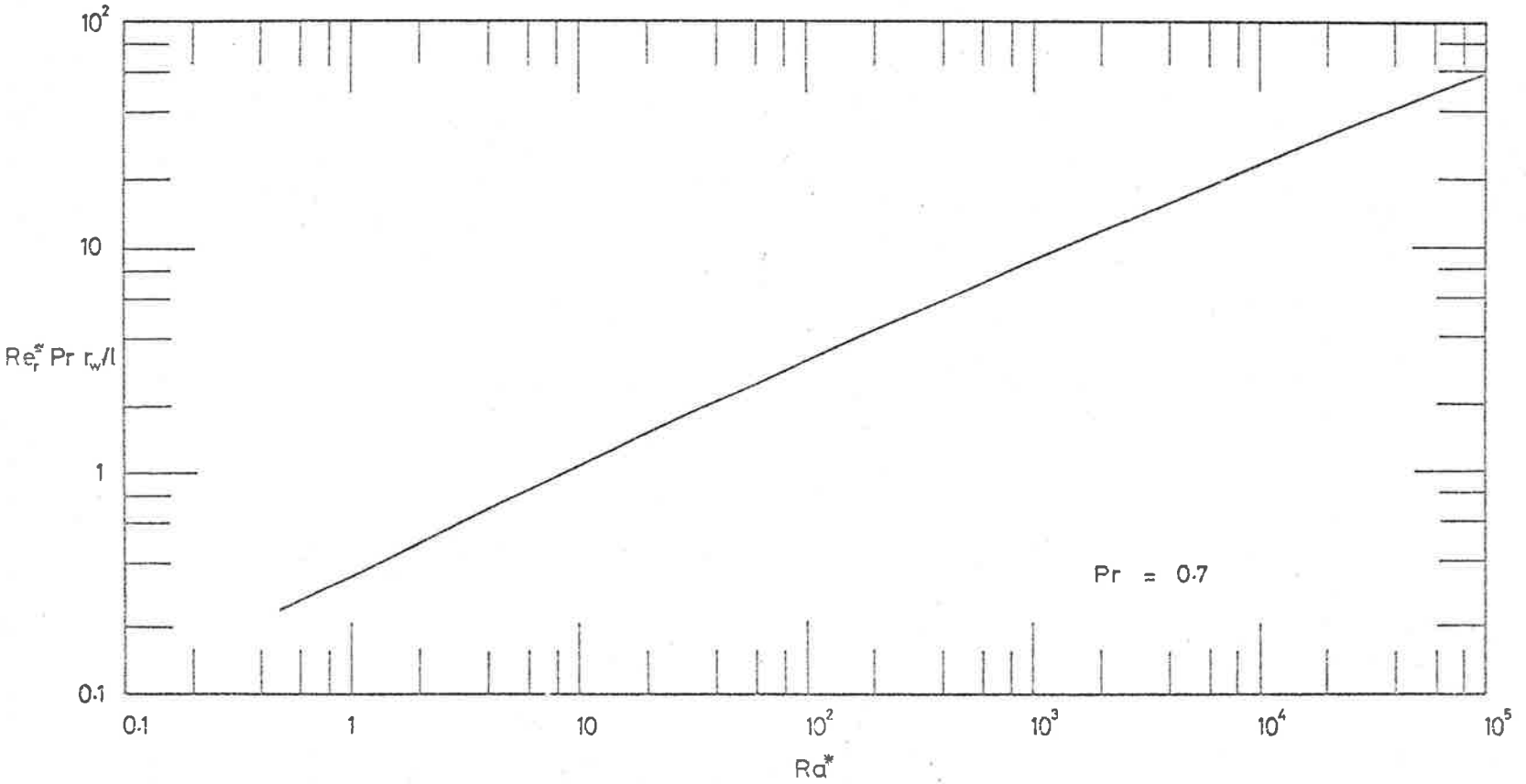

Fig. 5.9 Parameter $Re_r^* Pr\ r_w/\ell$ against Rayleigh number for laminar flow in uniform surface heat flux ducts

Thus for small Ra*, the critical Re_r^* will be approximately 1150 (9). However, for large Ra*, the critical value is likely to be smaller, because the velocity profile has a less stable shape as shown in Fig. 5.7.

6. EXPERIMENTAL STUDY

6.1 General

Experiments were conducted to confirm some of the theoretical findings. The tests were carried out on plain- and restricted-entry ducts with uniform surface temperatures.

With air as the working fluid, a range of Rayleigh numbers was studied which extended from the fully developed regime to the boundary layer regime. The study included tests with entry restrictions which were larger than the theoretical maxima for laminar flow shown in Fig. 4.4 and, for comparison, tests on open-thermosyphon ducts.

Gross heat transfer data were sought and also temperatures of the fluid along the axis. Owing to their smallness, no attempt was made to measure pressure defects and velocities.

6.2 Apparatus

Three ducts of different diameters, details of which are given in Table 6.1, were required to study a range of values of Ra from 10 to 10^4.

Table 6.1

Experimental ducts

Characteristic of the duct	Nominal internal diameter of the duct (in.)		
	1	2¼	3¾
Internal diameter (in.)	0.999	2.240	3.737
Heated length (in.)	48	48	48
Wall thickness (in.)	0.128	0.128	0.128
Material	Aluminium		
External surface finish	Hard anodised		

As illustrated in Fig. 6.1, the ducts were heated in three sections by independent electrical resistance elements and the external heat losses were reduced by surrounding the ducts with fibre-glass insulation. An insulation thickness of 6.5 in. was chosen as a suitable compromise between satisfactory insulation and the over-all size of the duct. Fig. 6.2 shows the lower heating

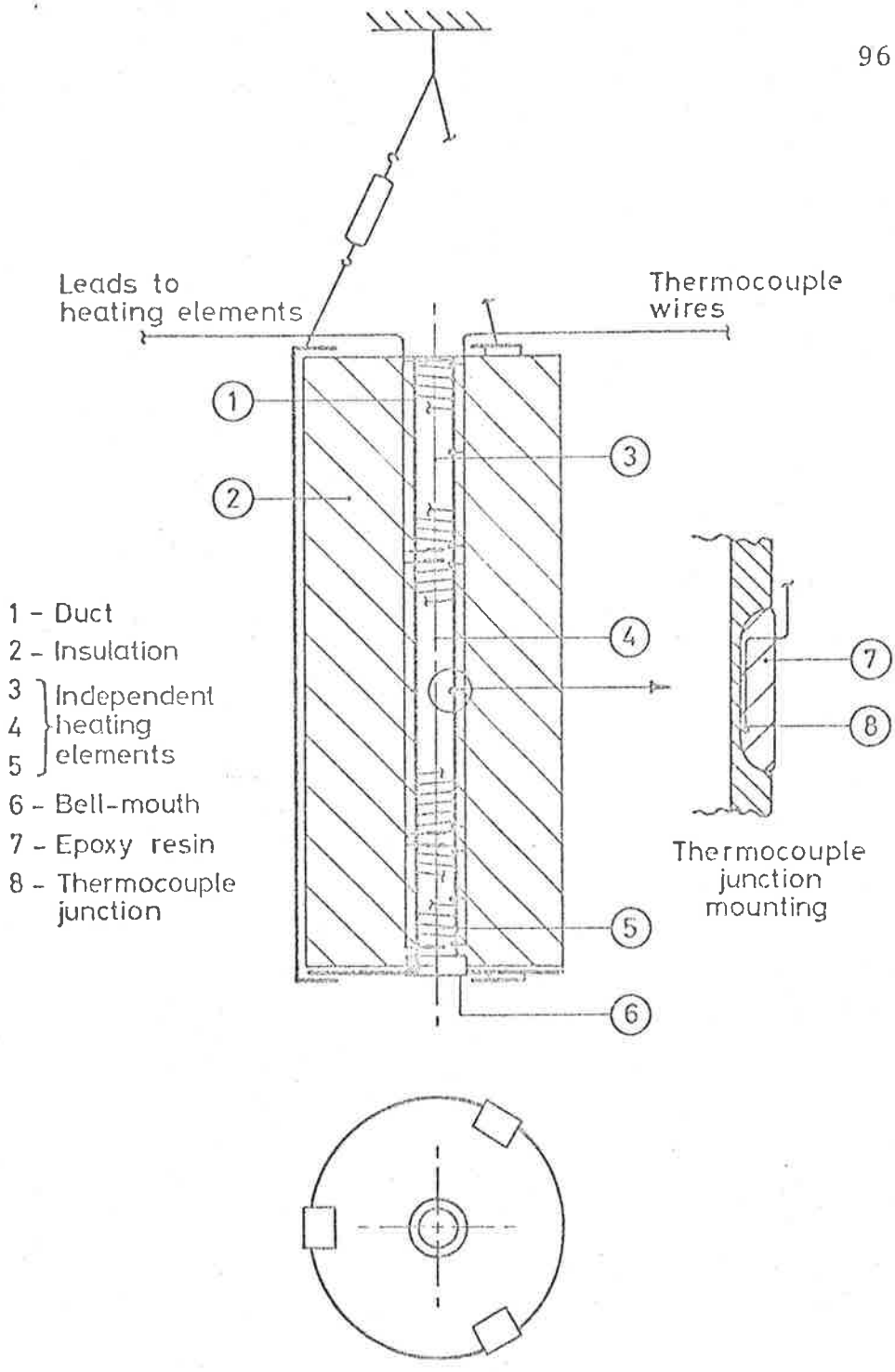

Fig. 6.1 Sketch of an experimental uniform surface temperature duct that is heated in three sections by independent resistance elements

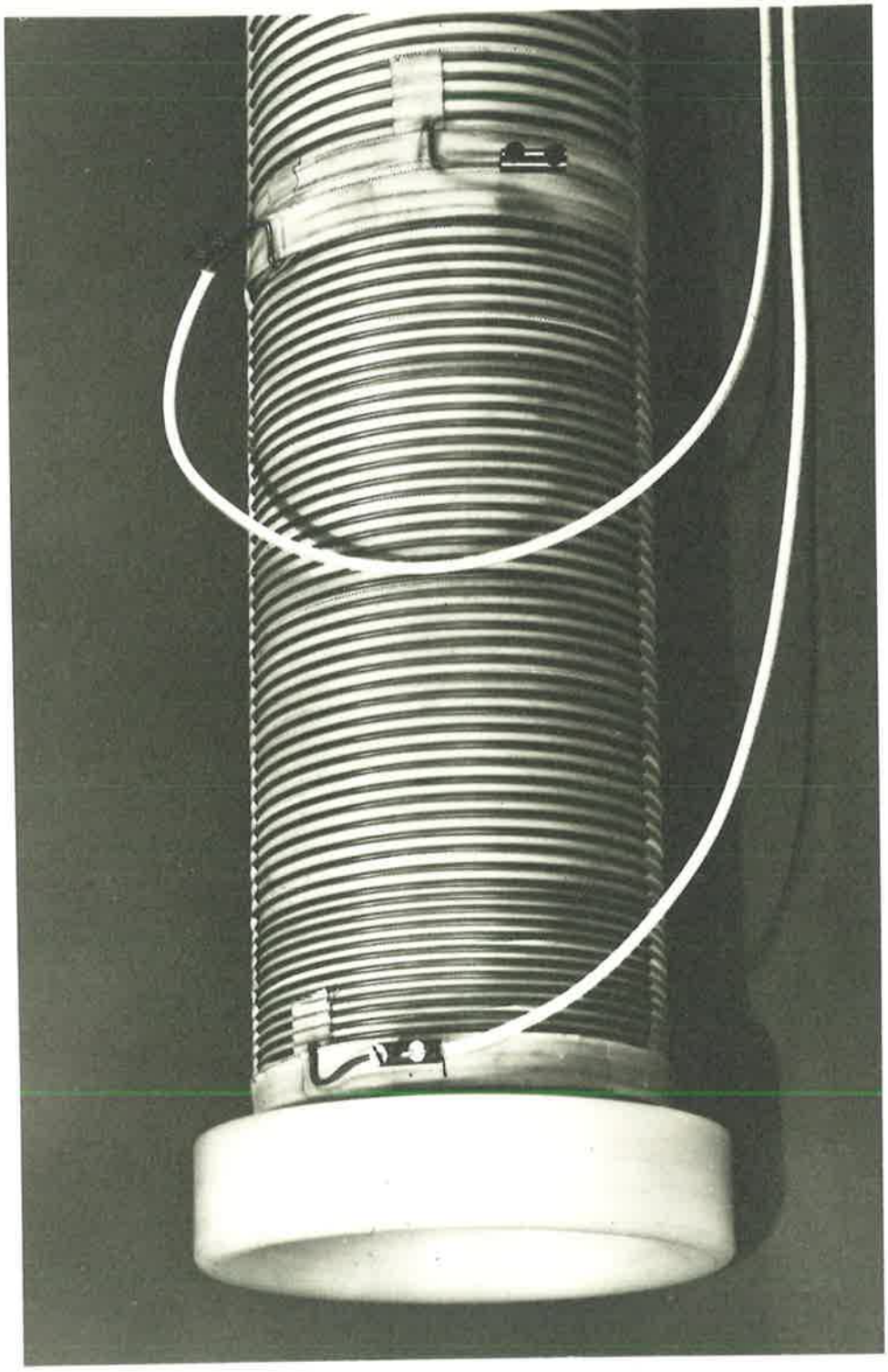

Fig. 6.2 Lower part of the $3\frac{3}{4}$ in. diameter duct without the insulation

element of the 3¾ in. diameter duct, and Fig. 6.3 the same duct after the addition of the insulation.

The design of the heating elements was based on calculated values of the local rates of heat dissipation and heat losses through the insulation. The details of the elements are given in Tables 6.2, 6.3 and 6.4. To form the elements, the bare resistance wire was wound directly on to the hard-anodised external surface of each of the two smaller diameter ducts. This was possible because the hard anodising provided a surface that was electrically non-conducting. After the turns of a coil were correctly positioned at the specified pitch, they were held in place by an epoxy resin adhesive. To position the coils more readily on the 3¾ in. diameter duct, shallow helical grooves were machined around the wall. Unfortunately, the edges of the grooves were inadequately radiused and consequently the anodised surface was damaged in several places when the elements were being wound. The problem was overcome, as shown in Fig. 6.2, by insulating the whole surface with fibre-glass tape before rewinding the elements.

The 240 volts, 50 cycles per second, A.C. mains provided the power supply, and, as shown in Fig. 6.4,

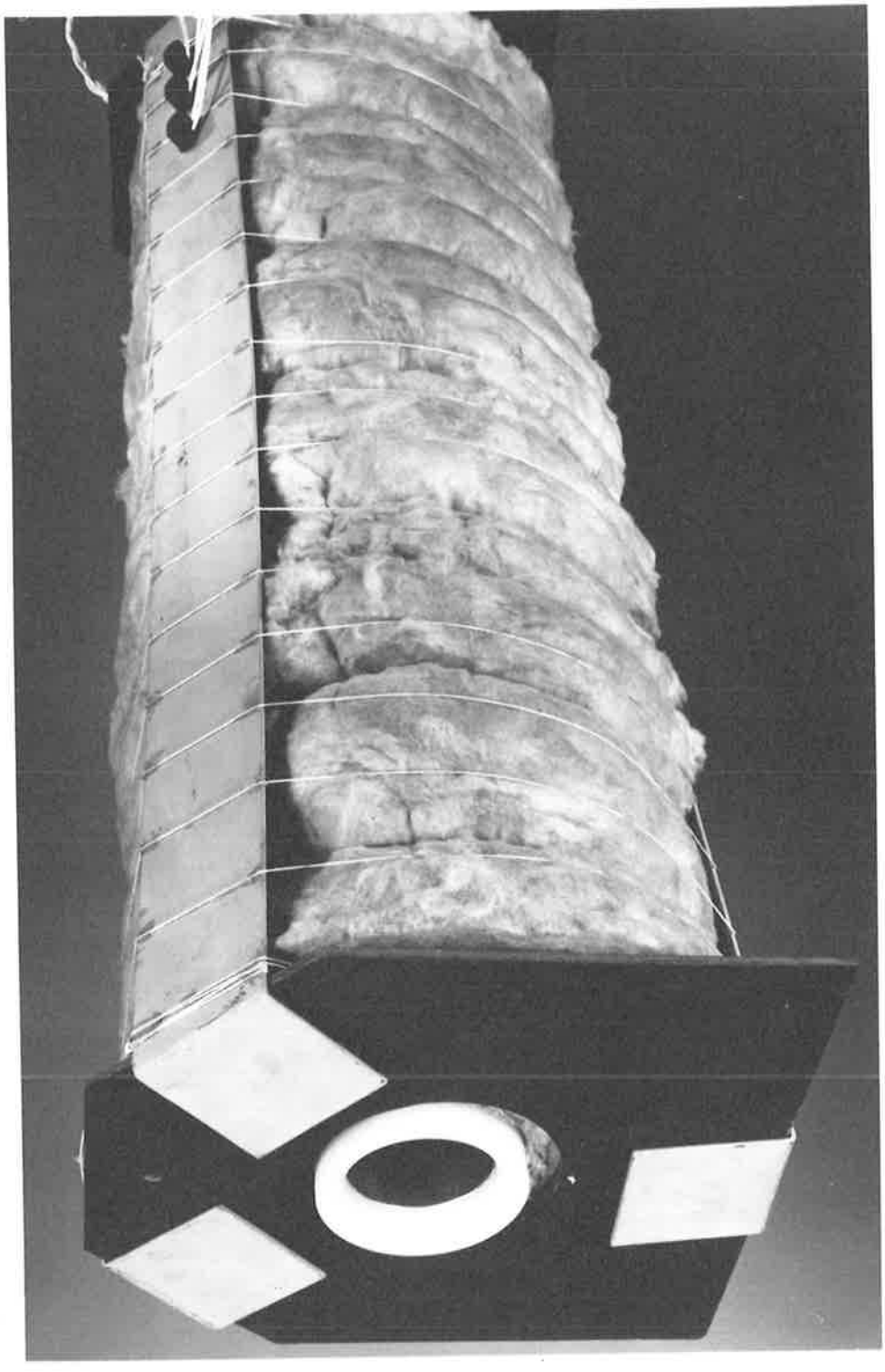

Fig. 6.3 $3\frac{3}{4}$ in. diameter duct surrounded by fibre glass insulation

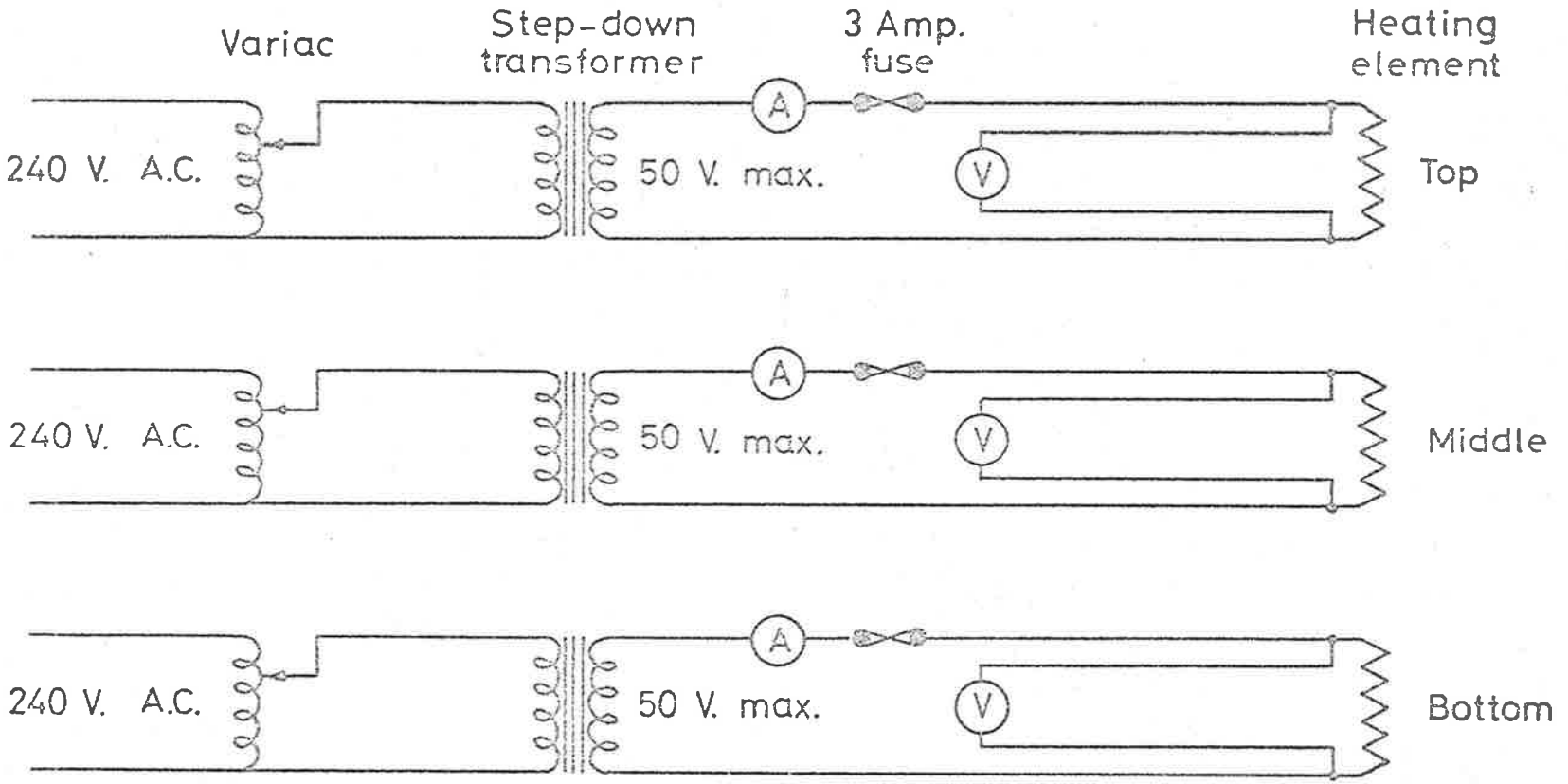

Fig. 6.4 Circuit for controlling the three independent heating elements

the voltage across each element was controlled by a variac. Since the breakdown voltage of the anodised surface of the ducts was between 200 and 300 volts, it was decided for safety reasons to limit the maximum voltage across each element to 50 volts. Calculations showed that the inductive reactance of the elements was negligible compared with the resistance, and therefore voltages and currents were in phase.

Three graded heating elements on each duct provided adequate flexibility for controlling the temperature of the surface; examples of the uniformity of the surface temperatures achieved are shown in Fig. 6.5.

Temperatures along the internal surface of each duct were measured by a number of 30-gauge copper-constantan thermocouples (Leeds & Northrup catalogue no. 30-5-1). The thermocouple junctions were cemented in grooves machined in the wall, as illustrated in Fig. 6.1; this method of mounting placed the junctions close to the internal surface and allowed the wires leaving each junction to be run along an isotherm for a short distance. The locations of the junctions are given in Table 6.5. It will be seen that five thermocouples were placed under each heating element on the 1 in. diameter duct, which was the first of the three ducts to be built. However,

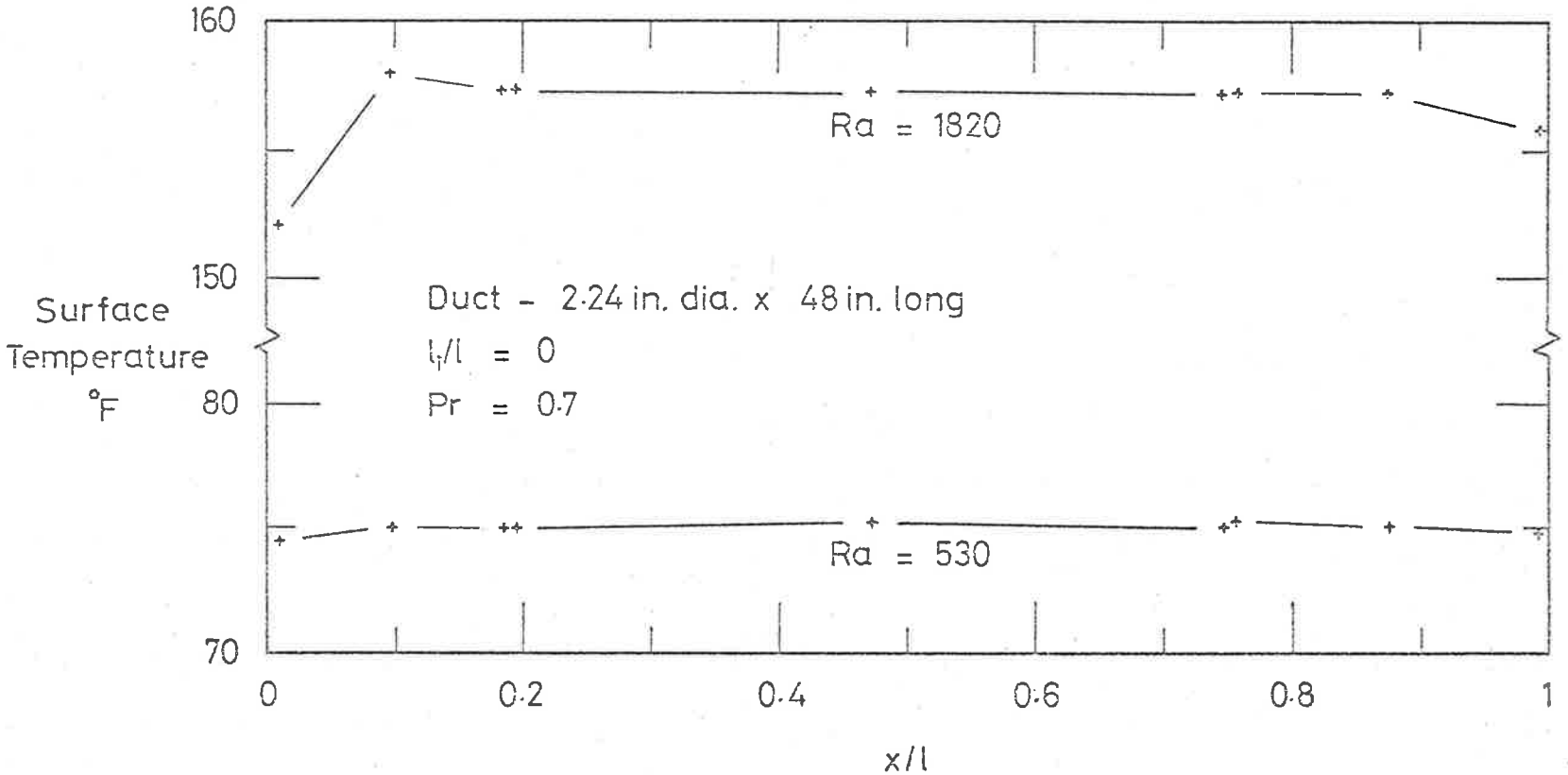

Fig. 6.5 Examples of the uniformity of the temperatures achieved along the surface of the 2¼ in. diameter duct; the temperatures were measured by thermocouples located in the wall at the ends and the middle of each heating element

Table 6.2

Heating elements for the 1 in. diameter duct

Heating element	Location from bottom of duct (in.)	Wire material	Wire diam. (in.)	Number of turns	Winding pitch (turns/in.)
Top	48.0 to 24.0	Eureka	0.036	213	13 to 3
Middle	24.0 to 4.8	Eureka	0.040	134	3 to 9
Bottom	4.8 to 0	Eureka	0.022	40	6 to 11

Table 6.3

Heating elements for the 2¼ in. diameter duct

Heating element	Location from bottom of duct (in.)	Wire material	Wire diam. (in.)	Number of turns	Winding pitch (turns/in.)
Top	48.0 to 36.0	Nichrome	0.028	120	14 to 10
Middle	36.0 to 9.0	Nichrome	0.064	270	9 to 12
Bottom	9.0 to 0	Nichrome	0.036	90	6 to 20

Table 6.4

Heating elements for the 3¾ in. diameter duct

Heating element	Location from bottom of duct (in.)	Wire material	Wire diam. (in.)	Number of turns	Winding pitch (turns/in.)
Top	48.0 to 36.0	Nichrome	0.036	102	10 to 8
Middle	36.0 to 9.0	Nichrome	0.056	135	5
Bottom	9.0 to 0	Nichrome	0.048	58	6 to 8

tests with the duct indicated that only three thermocouples under each element would have been quite satisfactory and therefore a total of nine thermocouples instead of fifteen was used on each of the two larger ducts.

Ambient air temperatures were obtained from two thermocouples located 20 in. from the axis of the duct and 10 in. above and below the heated section.

Temperatures along the axis of the duct were measured by a travelling thermocouple, which is illustrated in Fig. 6.6. It should be noted that the lower actuating cord of the travelling thermocouple was positioned to move along the surface of the duct so as not to disturb the flow approaching the junction.

The thermocouple E.M.F.'s were measured by a potentiometer, which was coupled to a null detector to give greater sensitivity. A recording potentiometer was used to observe the direction of surface temperature movements when equilibrium conditions were being established and to record the unsteady temperatures that were encountered within the duct.

In planning the tests on restricted-entry ducts, a serious problem concerning the overall lengths of the ducts was encountered. Ducts that were longer than

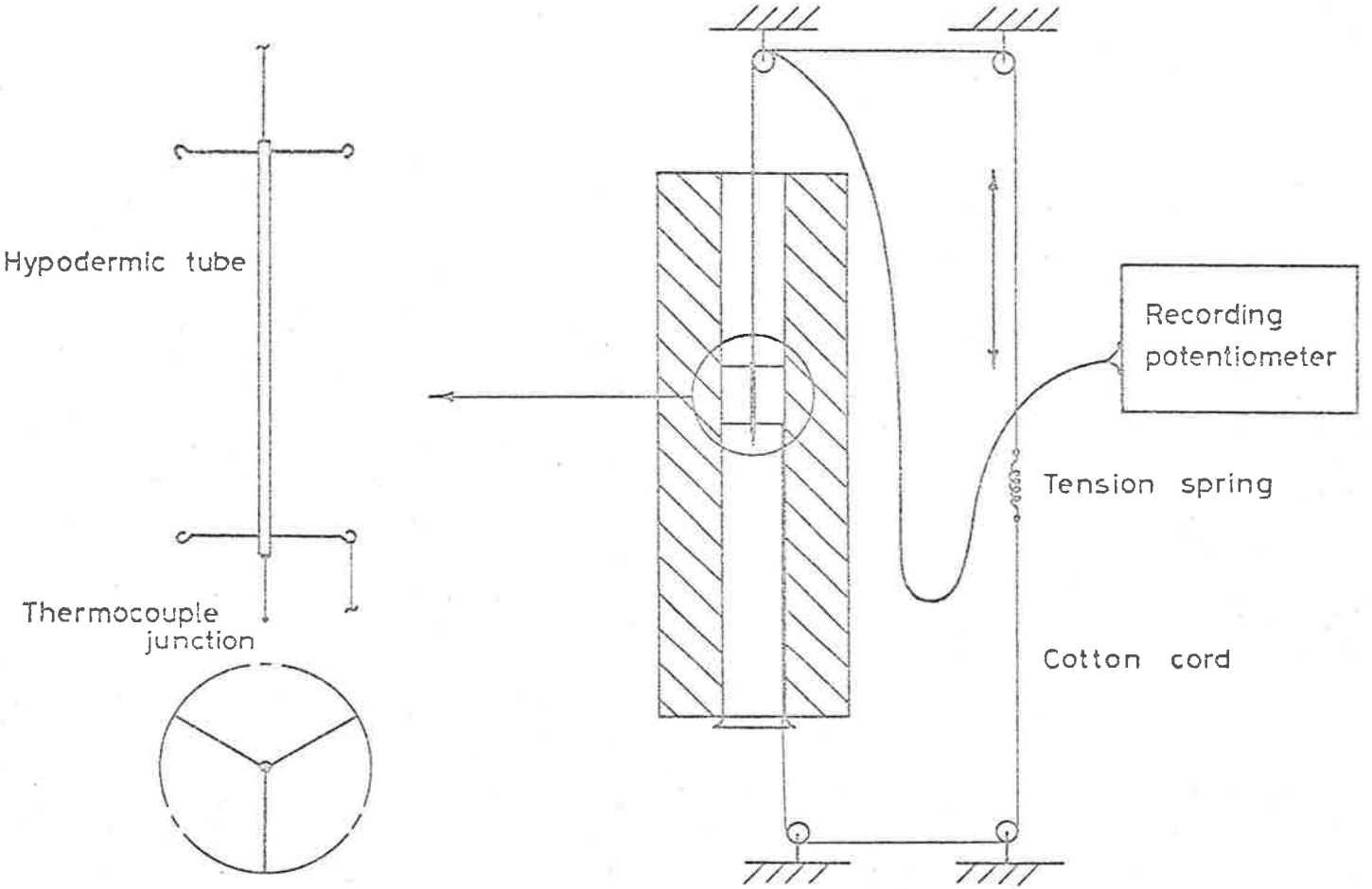

Fig. 6.6 Travelling thermocouple for measuring temperatures along the axis of a duct

Table 6.5

Locations of the thermocouple junctions along the ducts[1]

Thermocouple designation	Distances of junctions from bottom of duct (in.) 1 in. diameter duct	2¼ in. diameter duct	3¾ in. diameter duct
15	47.8		
14	41.4		
13	36.0		
12	29.7		
11	24.3		
10	24.0		
9	19.2	47.8	47.8
8	14.5	42.0	42.0
7	9.8	36.2	36.2
6	5.0	35.9	35.9
5	4.6	22.5	22.5
4	3.7	9.2	9.2
3	2.4	8.9	8.9
2	1.2	4.5	4.5
1	0.5	0.4	0.4

1 The junctions are grouped according to the heating elements under which they are located.

about 100 in. could not be accommodated in the laboratory and therefore, because 48 in. long unheated sections were to be used, the largest value of the ratio ℓ_i/ℓ that it was possible to obtain directly was about unity. To obtain the equivalent of a larger ℓ_i/ℓ, a smaller diameter restriction, as illustrated in Fig. 6.7, was fitted to the bottom of a 37 in. long unheated section. The equivalent length (ℓ_i) of the combined restriction was estimated by a procedure described in Appendix G. The heated and unheated sections of each duct were joined by a coupling made of nylon so that heat transfer to the unheated section was minimal.

To allow the air to enter the duct smoothly, a small bell-mouth, examples of which are shown in Figs. 6.2 and 6.8, was fitted. It was made of nylon to minimise heating the air before it reached the actual duct.

The ducts were suspended in a laboratory in which the diurnal temperature variations were relatively small. A large draught-shield protected the ducts from any abnormal air movements.

6.3 Procedure

To carry out a test, the heated surface of the

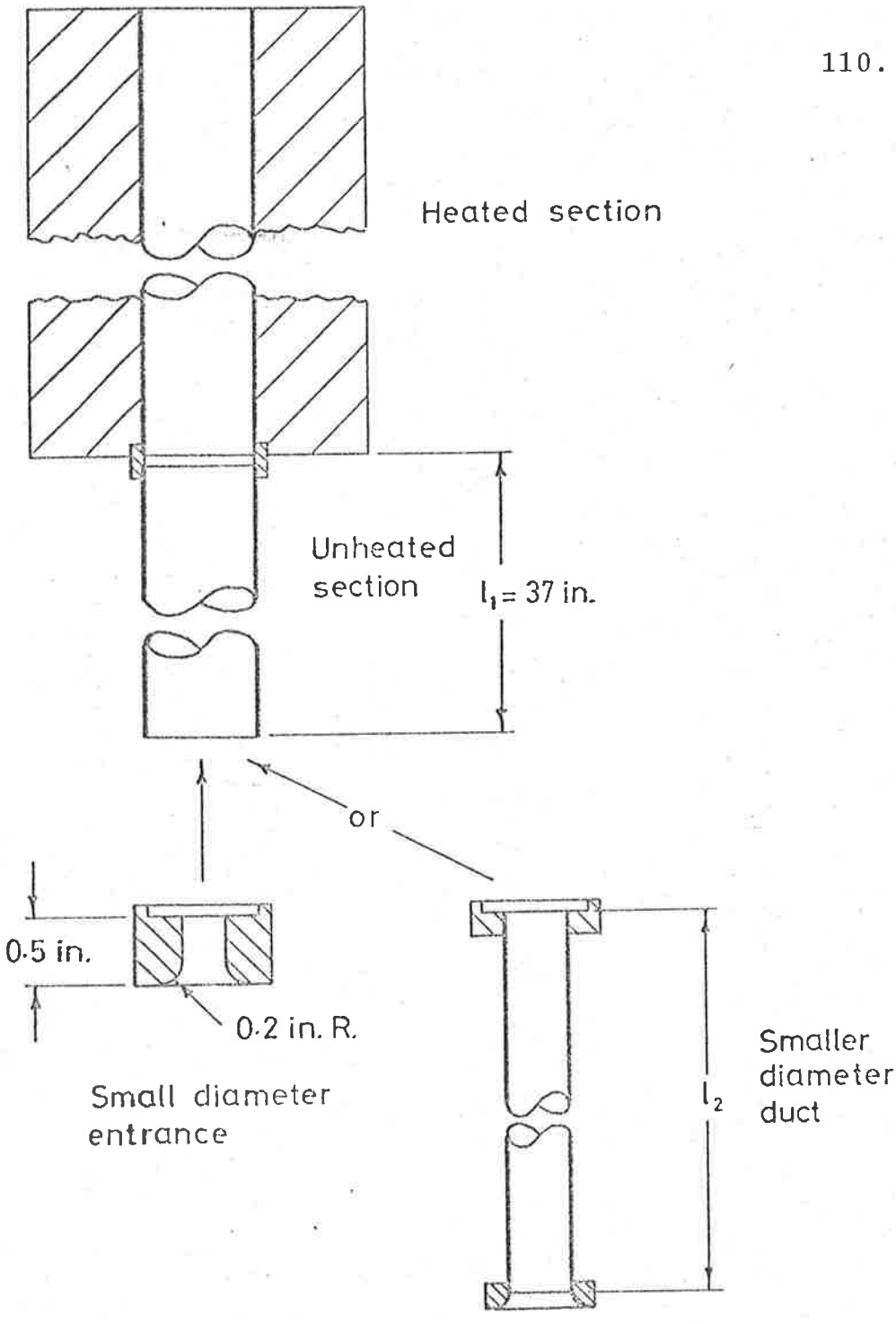

Fig. 6.7 Additional entry restrictions with smaller diameters than the duct to give values of ℓ_i/ℓ greater than 0.8

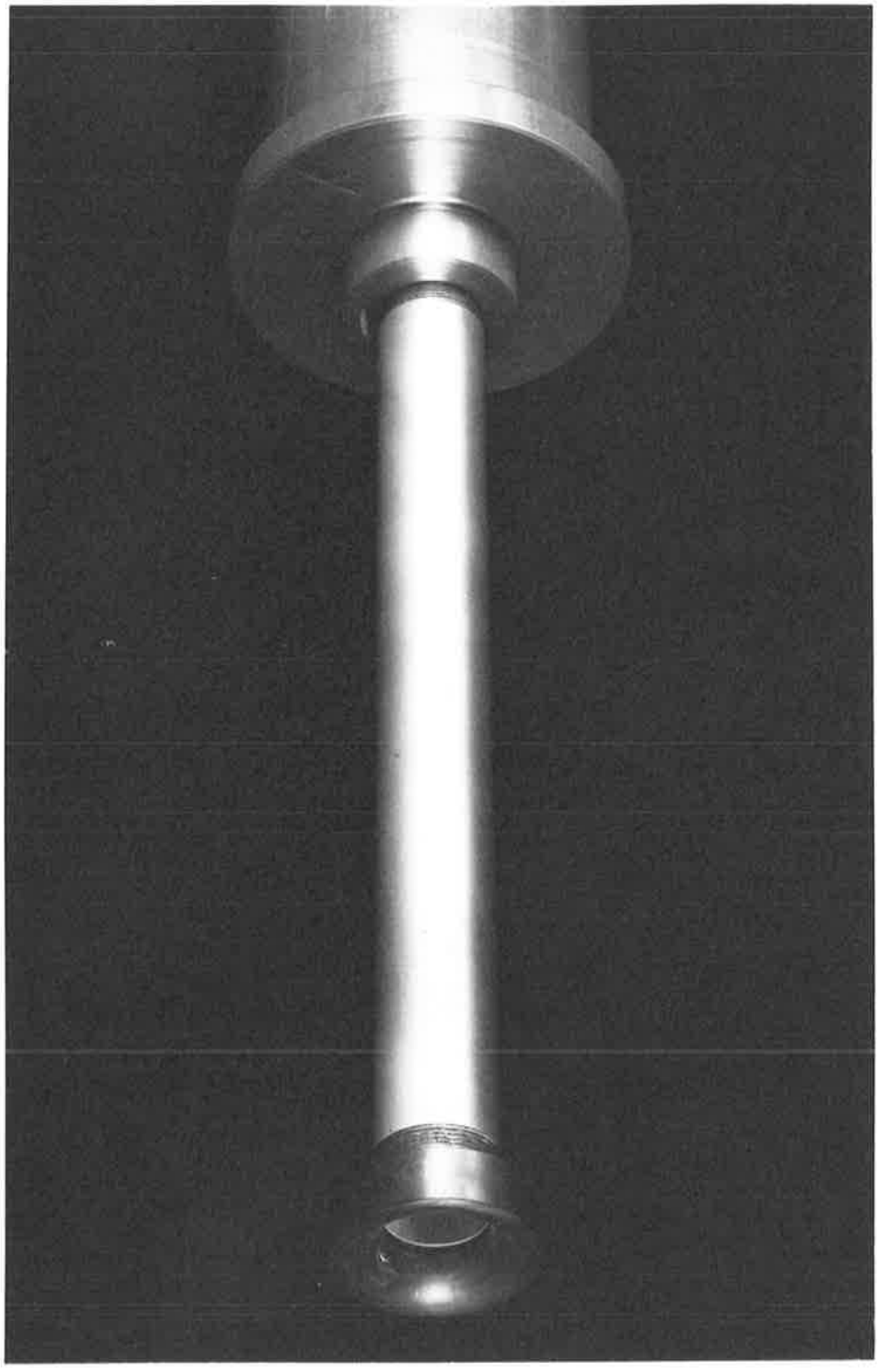

Fig. 6.8 Smaller diameter duct with bell-mouth entrance fitted to the 37 in. long unheated section; this combined entry restriction gave an equivalent ℓ_i/ℓ of about 48

duct had to be at a uniform temperature that was in equilibrium with its surroundings. Obtaining this condition was a tedious task, taking from 6 to 8 hours to achieve. It was expedient to raise the temperature of the surface quickly above that required, and then to reduce the voltages across the elements to the estimated values. Temperatures along the surface were monitored by a recording potentiometer to determine the direction of their movements and the voltages were adjusted accordingly. To ensure that the temperatures were in equilibrium, the readings for the test were not taken until 2 hours after the final voltages had been established. As voltage stabilisers were not available, very small adjustments to the variacs were occasionally necessary to keep the voltages constant.

The rate at which the internal surface of the duct dissipated heat was obtained indirectly by subtracting the heat losses through the insulation from the power input to the heating elements. The relationship between the heat losses and the surface temperature was obtained by operating the duct at various temperatures with the ends plugged and the bore filled with pieces of fibre-glass insulation to prevent internal air movements. Since

calculations showed that for the temperatures under consideration the heat losses from the exposed surfaces of the plugs were very approximately equal to the heat radiated by the internal surface through the ends when the duct was open, the heat dissipation of the duct was treated as purely convective.

The mean temperature of the surface of the duct was obtained by averaging the temperatures recorded under each heating element and then weighting these averages according to the lengths of the elements.

Axial temperature measurements were not made until after the surface temperatures had been measured because the travelling thermocouple slightly impeded the flow and thereby brought about a small increase in the surface temperature.

For most tests, the temperature difference between the surface of the duct and the ambient air was kept within the range from 10 to 120F°[1]. Temperature differences less than 10F° could not be obtained with sufficient accuracy because the subtraction involved magnified small errors in the measured temperatures. On the other hand, neither were large temperature differences suitable

---

[1] Temperature differences are shown thus, F°.

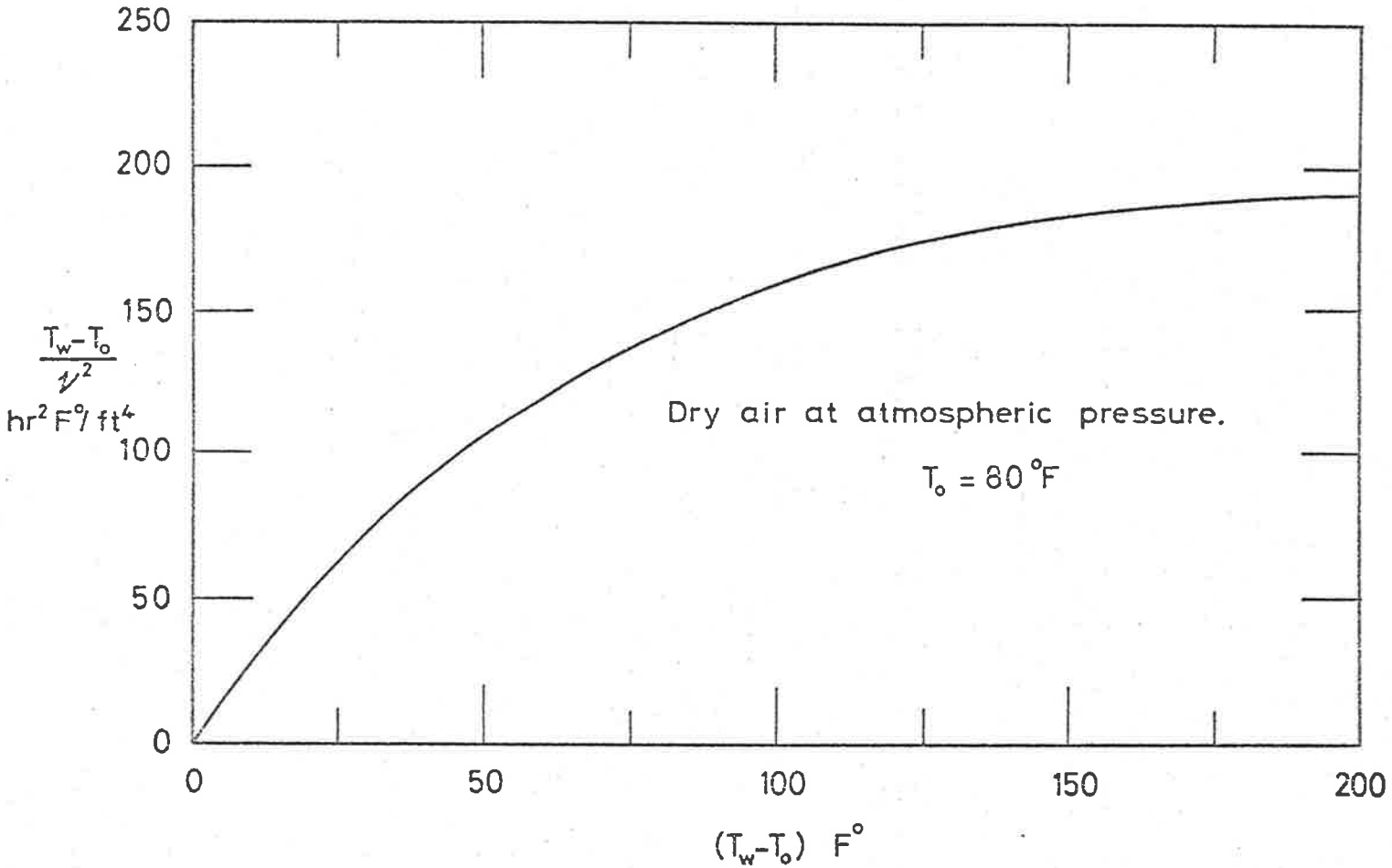

Fig. 6.9 Parameter $(T_w-T_o)/\nu^2$, which is contained in the Rayleigh number, against the difference in temperature between the surface and the ambient air (T_w-T_o)

because, as shown in Fig. 6.9, $(T_w-T_o)/\nu^2$ and consequently Ra increase at a diminishing rate with temperature difference. Furthermore, large temperature differences would violate the condition on Page 12 that the density variations should be small.

For evaluating Nu and Ra, the air properties, except the coefficient of thermal buoyancy, were based on the temperature of the surface of the duct (9). The coefficient of thermal buoyancy (β) of the air was obtained from the following relationship, which was derived for a perfect gas (9).

$$\beta = \frac{1}{\text{Absolute temperature of the air entering the duct}} \qquad \ldots (6.1)$$

Inspection of Fig. 6.10 will show that the properties of dry air at atmospheric pressure, unlike those of the ideal fluid considered in the theory, vary significantly with temperature.

To study the behaviour of the flow into and out of the duct, smoke was carefully injected into the air. The smoke was produced by passing air through a smoke generating tube[1].

---

1 The smoke generating kit was manufactured by Drägerwerk of Lübeck, West Germany.

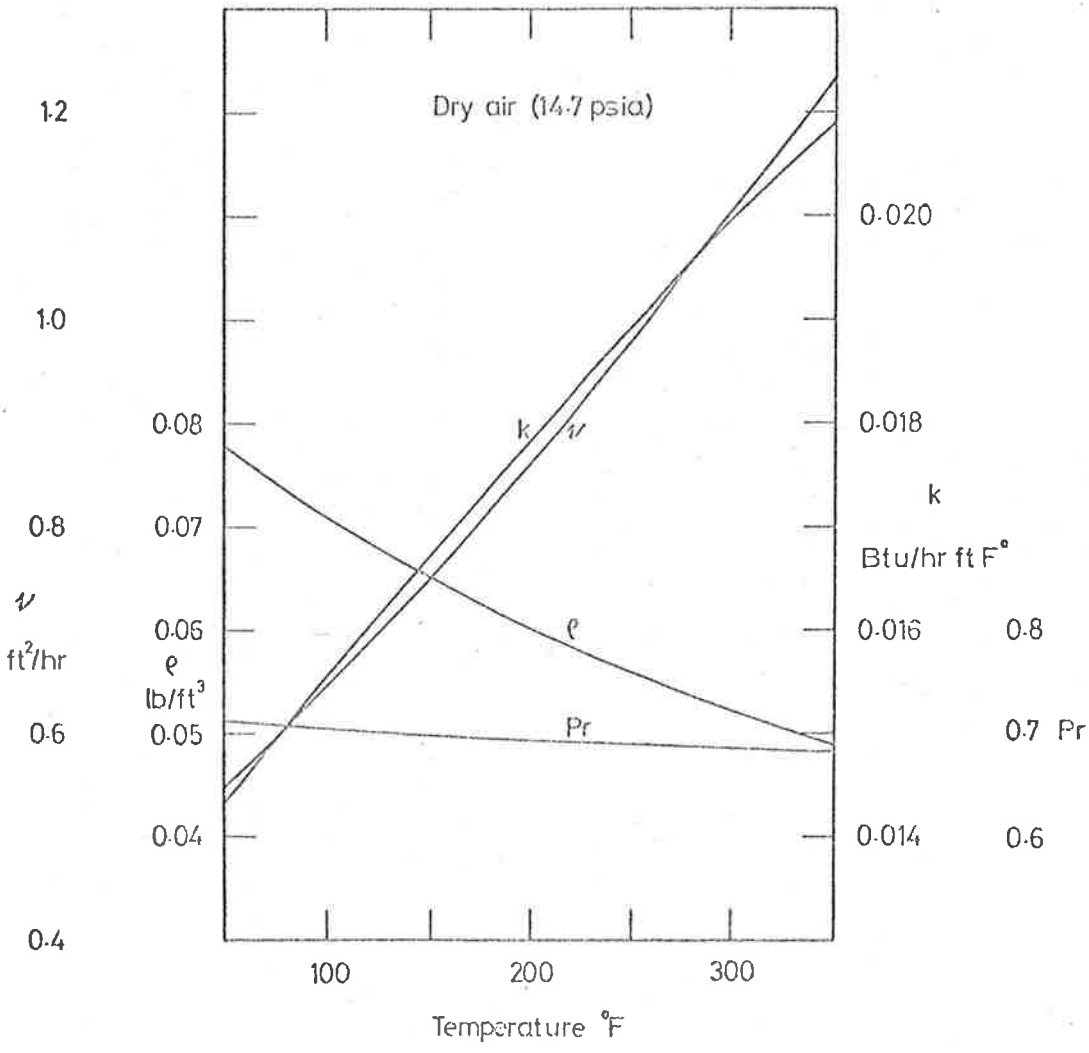

Fig. 6.10 Properties of dry air at atmospheric pressure. (Thermal conductivity (k), kinematic viscosity (ν) and density (ρ) were taken from M. Jakob and G.A. Hawkins, Elements of Heat Transfer, 3rd Ed., John Wiley and Sons Inc., New York, 1959 and Prandtl number (Pr) from A.J. Chapman, Heat Transfer, 2nd Ed., the Macmillan Company, New York, 1967)

7. EXPERIMENTAL RESULTS

7.1 Plain-entry ducts with uniform surface temperatures

Experimental values of Nu for plain-entry ducts with uniform surface temperatures are presented in Fig. 7.1. Air was the convective fluid. It will be seen that these results compare satisfactorily with the theoretical laminar flow relationship reproduced from Fig. 3.2 and also with the experimental results of Elenbaas (4).

Smoke studies revealed that for Ra in excess of about 10^3 the out-flowing plume became less laminar in appearance. Hence, an inspection of Fig. 7.1 will show that for some of the tests on the 2¼ in. diameter duct and for all of the tests on the 3¾ in. diameter duct the flow was transitional. These findings are in accord with the following critical values of Ra obtained from the theoretical analysis: using 1150 as the critical value of Re_r (see Section 3.5), Fig. 3.10 yields critical Ra of 3×10^2, 2×10^3 and 4×10^3 for the 1 in., 2¼ in. and 3¾ in. diameter ducts respectively.

In Fig. 7.1, it is interesting to observe that for large Ra the experimental values of Nu are smaller than those given by the theoretical curve. This is attributed to the mixing which took place in the transitional flow bringing about a reduction in the flow rate and, conse-

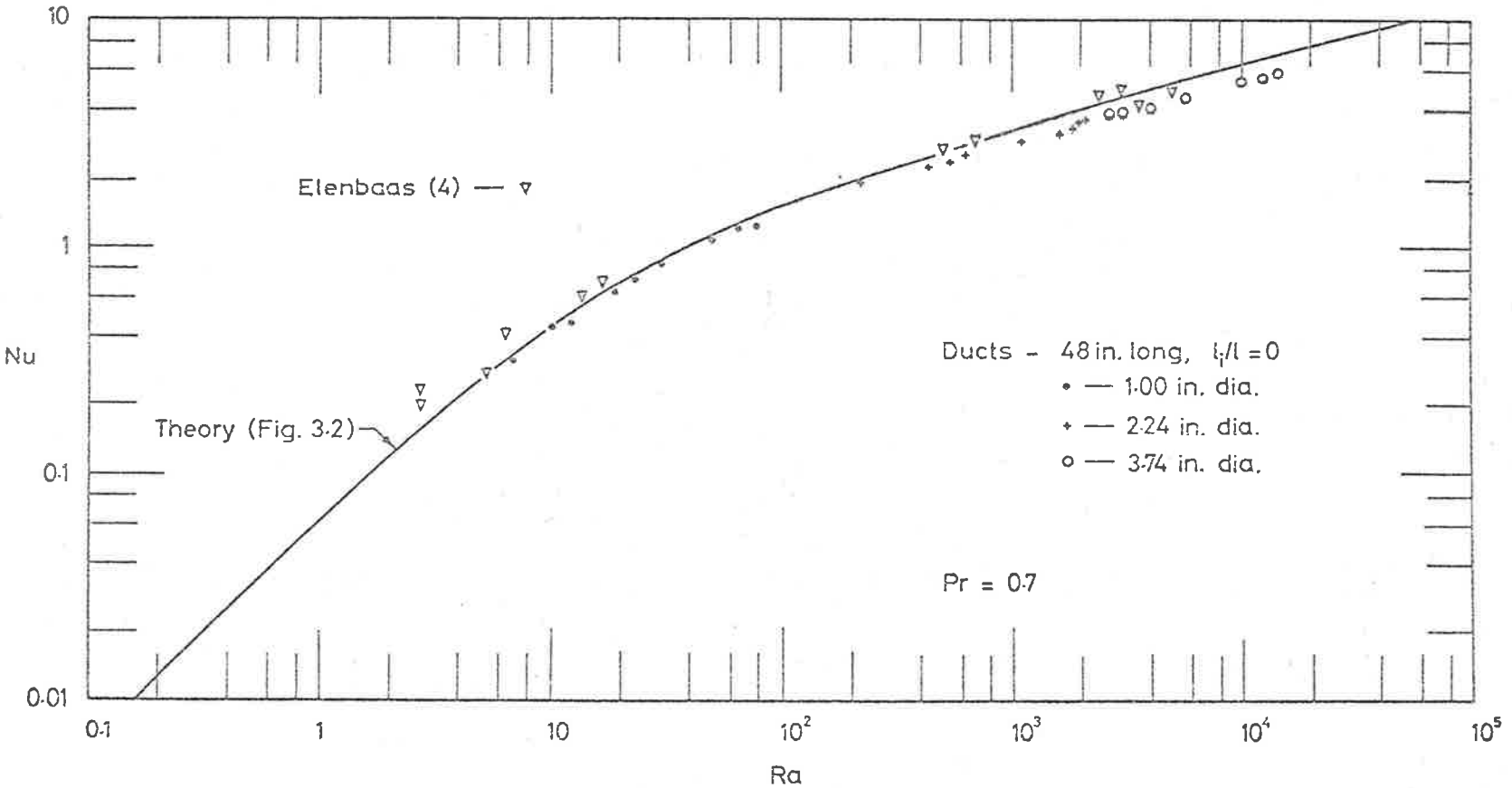

Fig. 7.1 Nusselt number against Rayleigh number for the 1 in., $2\frac{1}{4}$ in. and $3\frac{3}{4}$ in. diameter plain-entry ducts with uniform surface temperatures

quently, the rate of heat transfer. The validity of this deduction is strengthened by the fact that for the same range of Ra there was less mixing in the air emerging from restricted-entry ducts with $\ell_i/\ell = 0.8$ and, as will be seen later, there was better agreement between the experimental and theoretical values of Nu.

Fig. 7.2 shows temperatures measured along the axis of the 1 in. diameter duct for Ra = 11 and 69. As the air approaching the entrance of the duct was heated by the underside of the insulation and by the bell-mouth, temperatures obtained from the theoretical analysis for comparison were based on the slightly higher entry temperatures. Although their trends were similar, the experimental temperatures will be seen to be still higher than the theoretical for a number of reasons. First, the travelling thermocouple slightly impeded the flow and therefore, as the heat input remained constant, the surface temperature and temperatures in the air stream were raised. Secondly, although the values of Ra were well below the critical Ra of 3×10^2, some mixing did occur in the air stream. This mixing would have reduced the radial temperature gradients in the centre part of the duct and thereby would have raised the temperatures along the axis. Thirdly, the increasing temperature in the

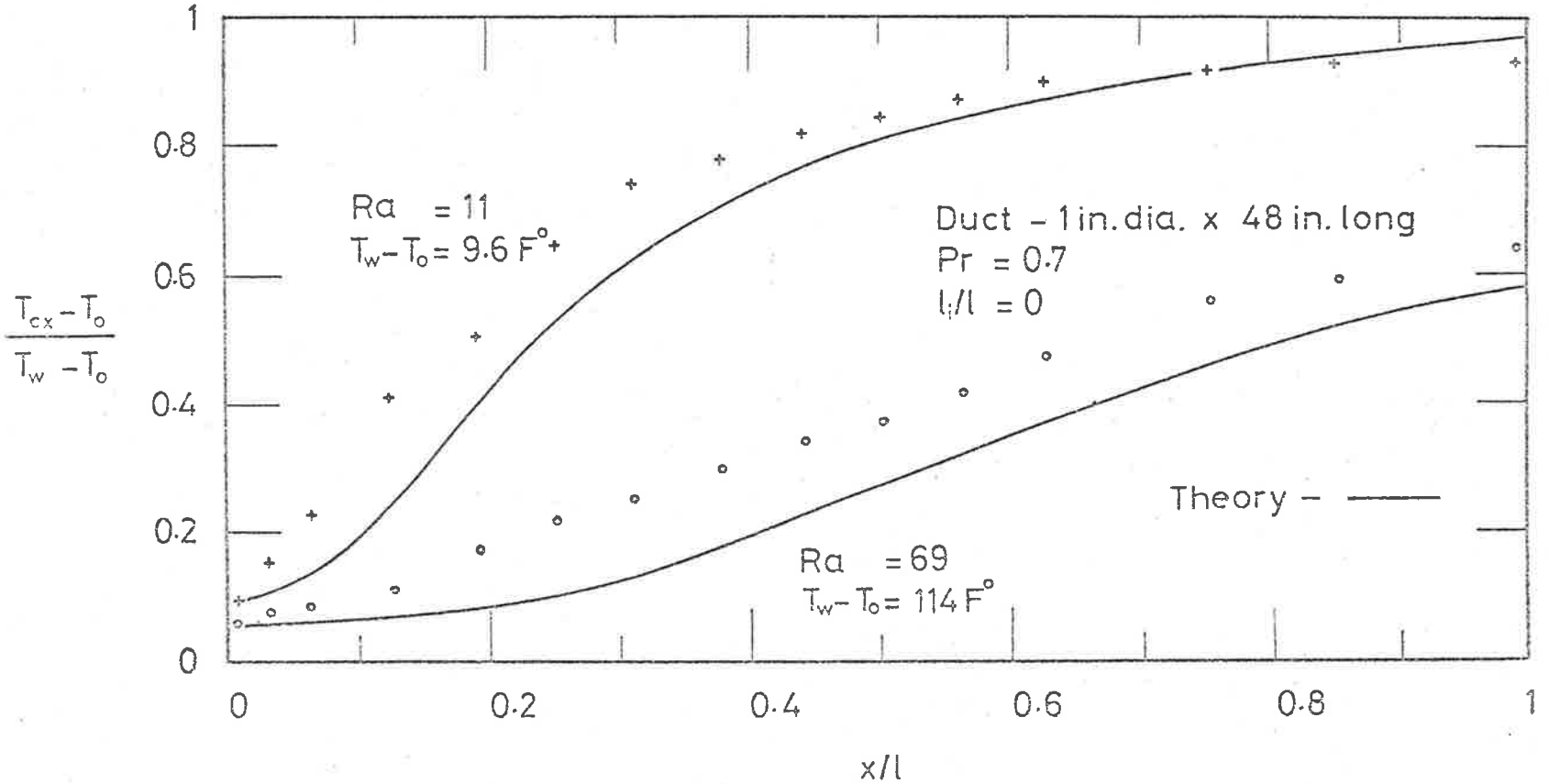

Fig. 7.2 Temperatures along the axis of the 1 in. diameter plain-entry duct with uniform surface temperatures; the theoretical curves were based on the actual entry temperatures

thermocouple wires directly above the junction would have produced a temperature reading that was too high.

Although all the tests conducted on the 1 in. diameter duct yielded Ra below the critical value of 3×10^2, it was surprising to find that temperatures along the axis fluctuated at random as shown in Fig. 7.3. Turning to Fig. 7.4, it will be seen that the maximum variation in temperature recorded over 10 minutes was as large as 11% of $(T_w - T_o)$ and that this occurred at $x/\ell = 0.3$. In actual fact, the temperature variations would have been in excess of 11% of $(T_w - T_o)$ if the thermocouple junction had had a sufficiently large frequency response to enable it to follow the temperature changes accurately. Since smoke studies revealed that the flow pattern at entry was axisymmetric and also varied with time, it was decided to shield the entrance from the influence of stray air movements in the room. Hence a cylindrical shield, 7 in. in diameter and 8 in. long, was concentrically attached to the bottom of the duct. As a result, it was found that the amplitudes of the fluctuations were reduced by about 50%. This modification to the duct clearly showed that the temperature fluctuations were brought about by flow irregularities in the air as

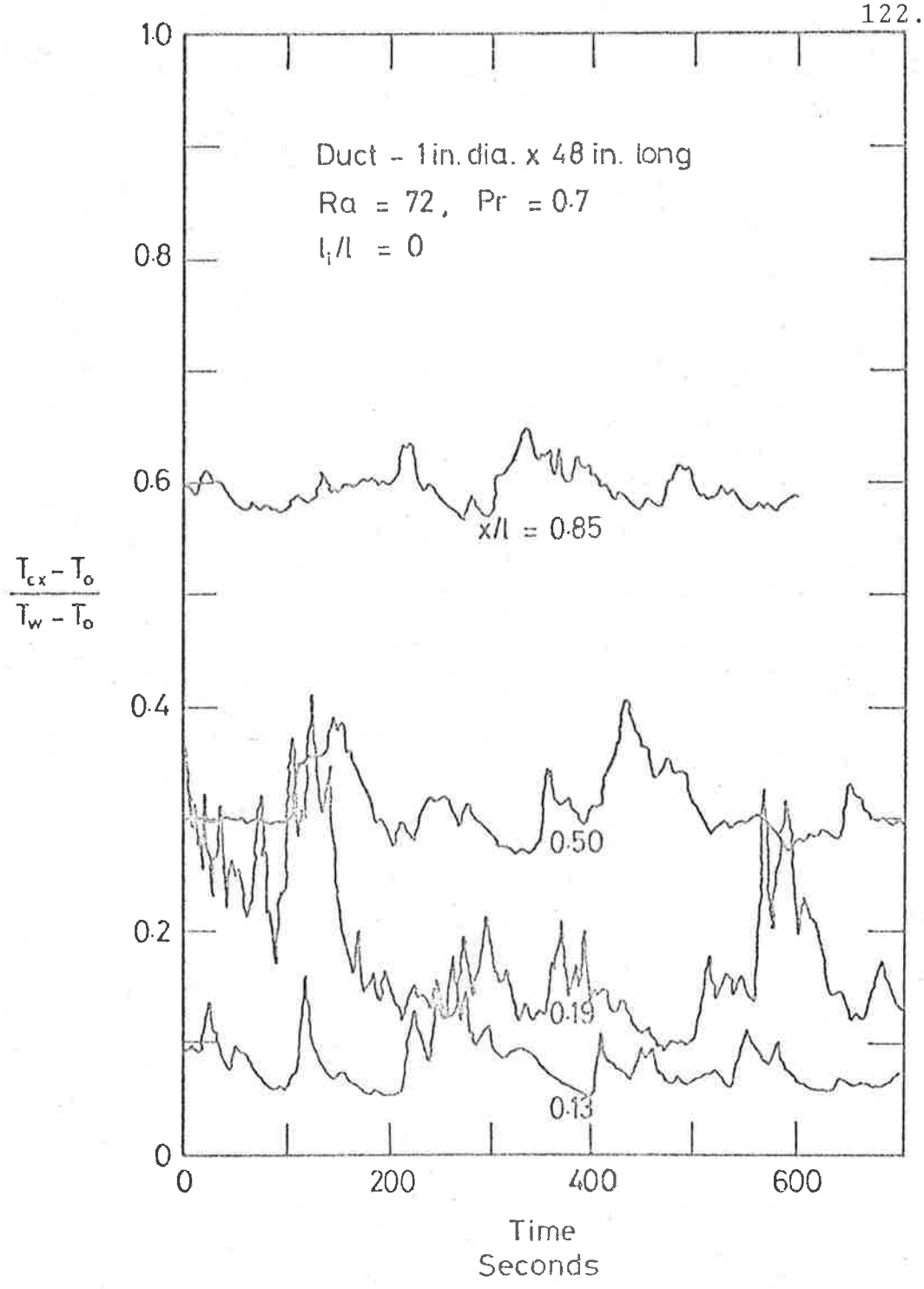

Fig. 7.3 Temperature fluctuations on the axis of the 1 in. diameter plain-entry duct with a uniform surface temperature. (The temperatures at each elevation were not recorded simultaneously). The Rayleigh number was smaller than the transitional value of 300

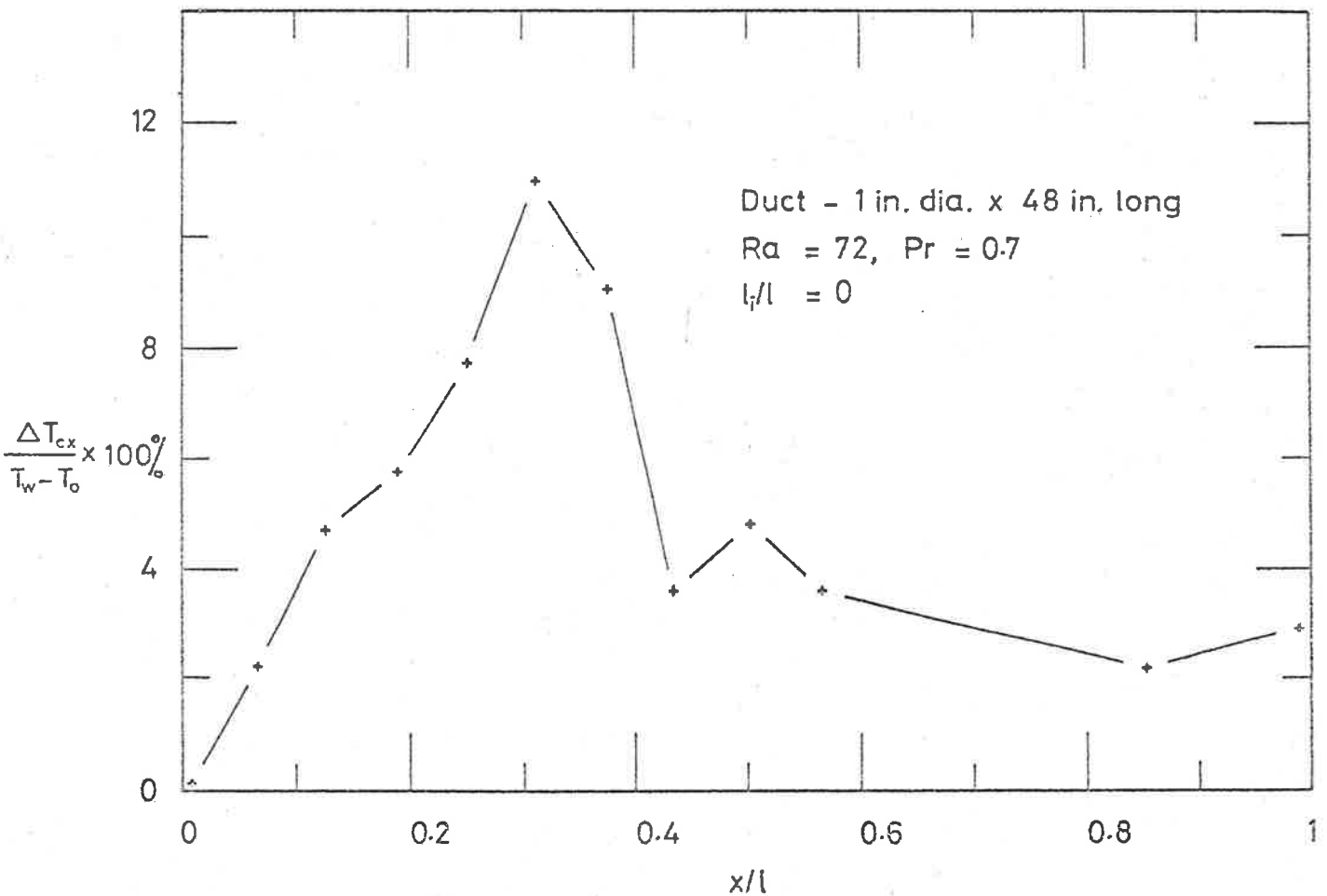

Fig. 7.4 Distribution of the largest temperature variations in Fig. 7.3

it entered the duct. More evidence will be presented in a later section, where it will be shown that the temperature fluctuations in the 1 in. diameter restricted-entry duct with $\ell_i/\ell = 0.8$ were quite insignificant.

It is interesting to note that temperature fluctuations along the axis of the duct were simulated by solving the flow equations for two different velocity profiles at entry which yielded the same value of Ra. The difference between the axial temperatures obtained at each elevation simulated the amplitude of the temperature fluctuations. An example of simulated temperature fluctuations is presented in Fig. 7.5. Comparing Fig. 7.4 with Fig. 7.5, it will be seen that the simulated temperature variations along the axis are remarkably similar to those which were measured. In each case, the largest variation occurred at approximately $x/\ell = 0.3$.

7.2 Restricted-entry ducts with uniform surface temperatures

The heat dissipating characteristics of the restricted-entry ducts are presented in Figs. 7.6 and 7.7 for the 1 in. diameter duct and the 2½ in. and 3¾ in. diameter ducts respectively. Also shown in these figures

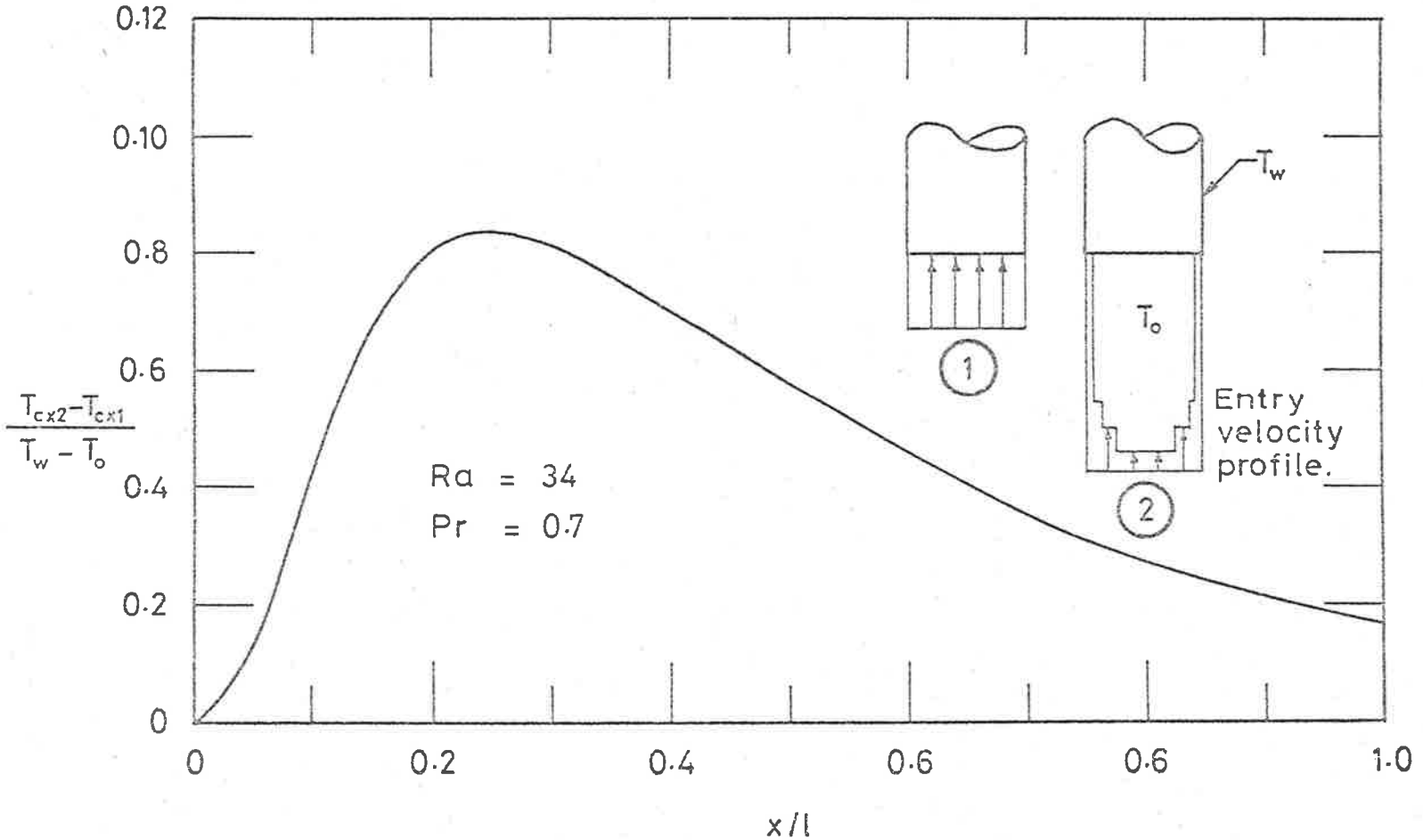

Fig. 7.5 Simulated distribution of the largest temperature variations on the axis; T_{cx1} and T_{cx2} are the temperatures on the axis for entry velocity profiles 1 and 2 respectively

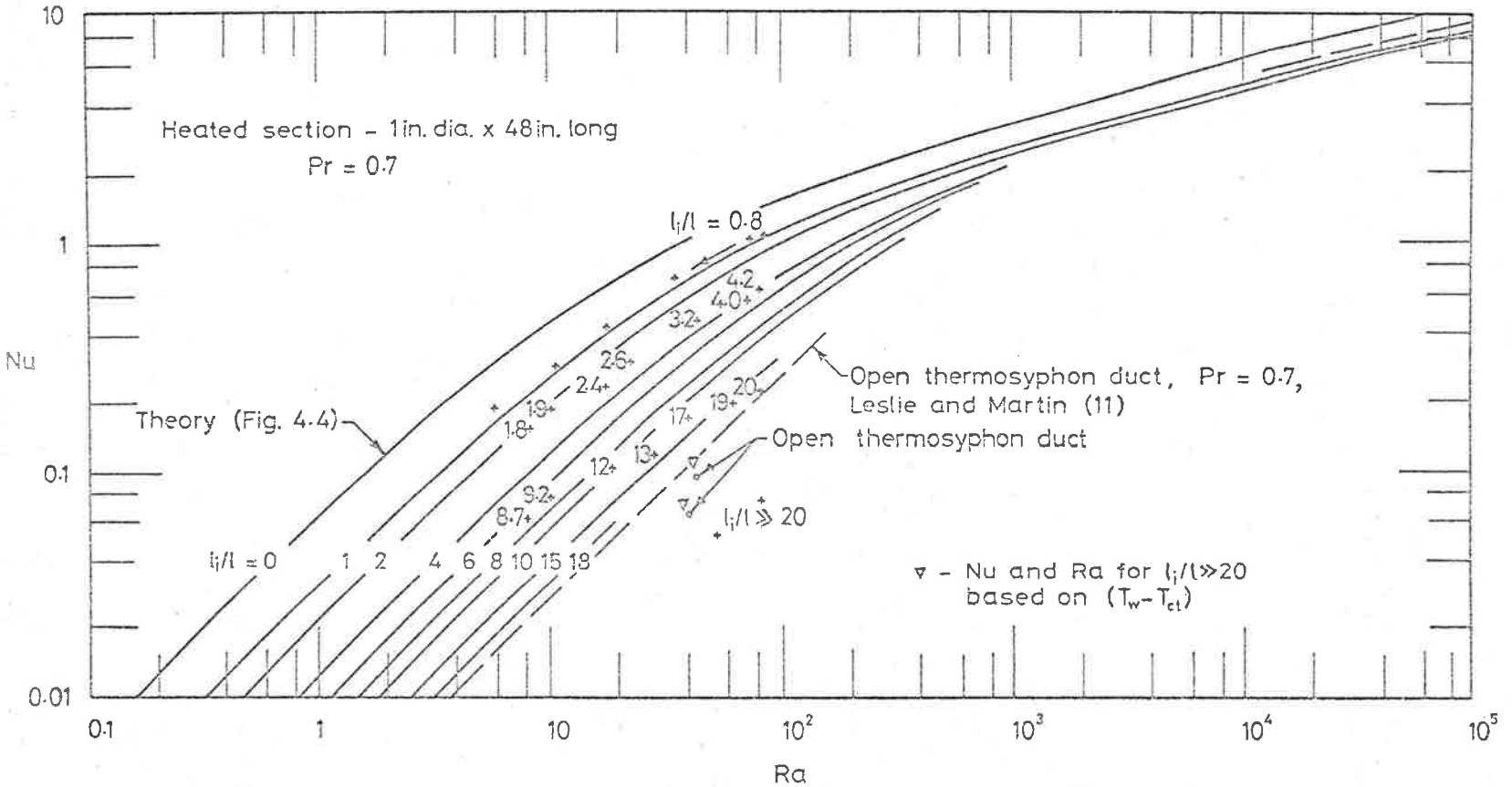

Fig. 7.6 Nusselt number against Rayleigh number for the 1 in. diameter restricted-entry duct with uniform surface temperatures

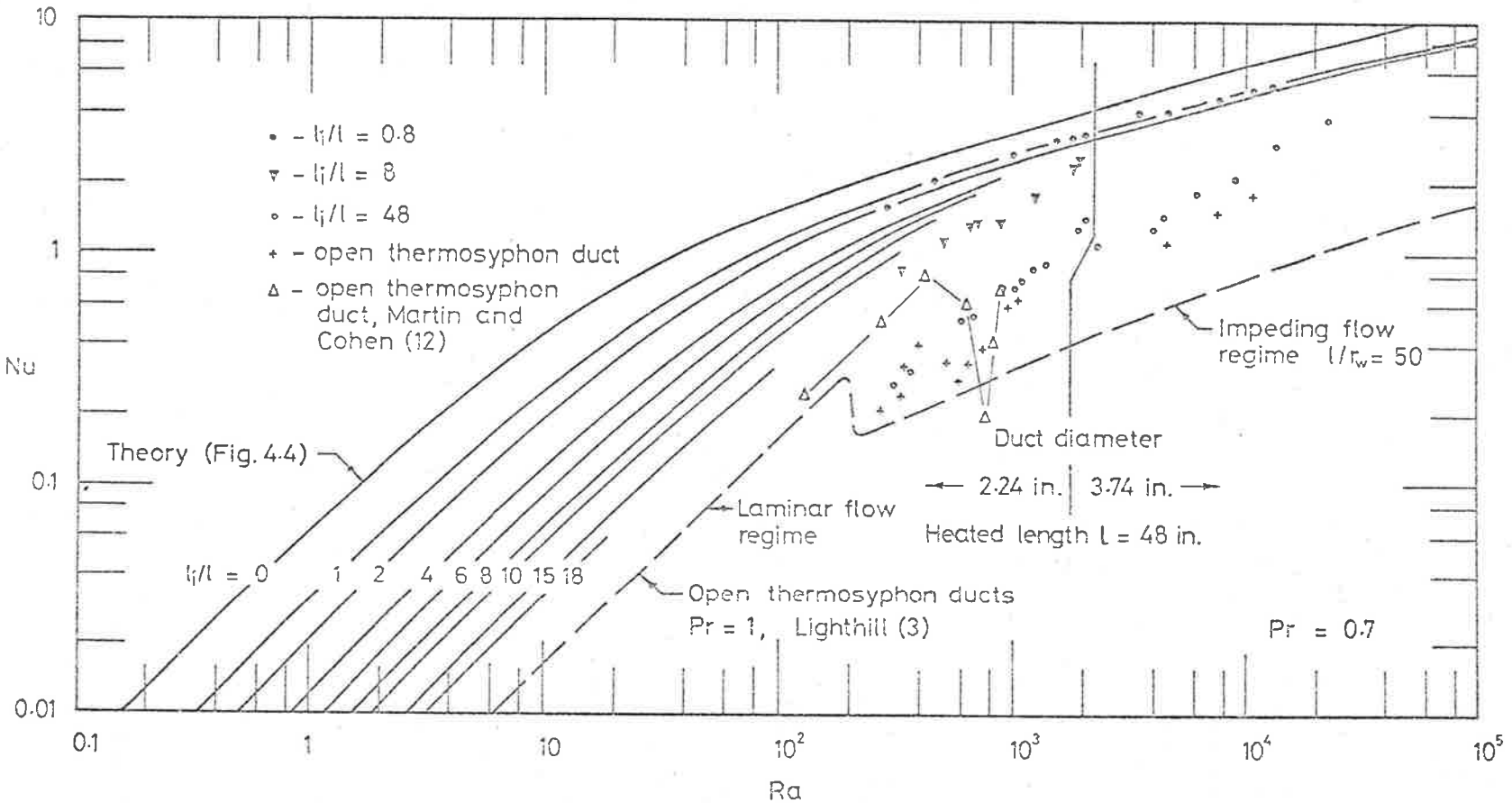

Fig. 7.7 Experimental Nusselt numbers against Rayleigh numbers for the $2\frac{1}{4}$ and $3\frac{3}{4}$ in. diameter restricted-entry ducts with uniform surface temperatures

for comparison is the theoretical Nu-Ra relationship in Fig. 4.4.

In the following discussions on the results, it should be noted that the values of ℓ_i/ℓ exceeding 0.8 are only approximate because unfortunately, for the reason explained in Section 6.2, it was necessary to use a smaller diameter restriction at the bottom of the 37 in. long unheated section.

Laminar flow

Smoke studies showed that the flow in restricted-entry ducts was laminar for those tests that yielded values of Nu within the theoretical laminar flow regime. Referring to Figs. 7.6 and 7.7, it will be seen that the results of these tests compare satisfactorily with the theoretical relationship.

Fig. 7.8 compares for two values of Ra the temperatures measured along the axis of the 1 in. diameter duct having $\ell_i/\ell = 0.8$ with those obtained from the theoretical analysis. In each case the experimental and theoretical temperatures will be observed to display similar growth patterns. It should be noted that near the top of the duct the temperature of the surface was slightly

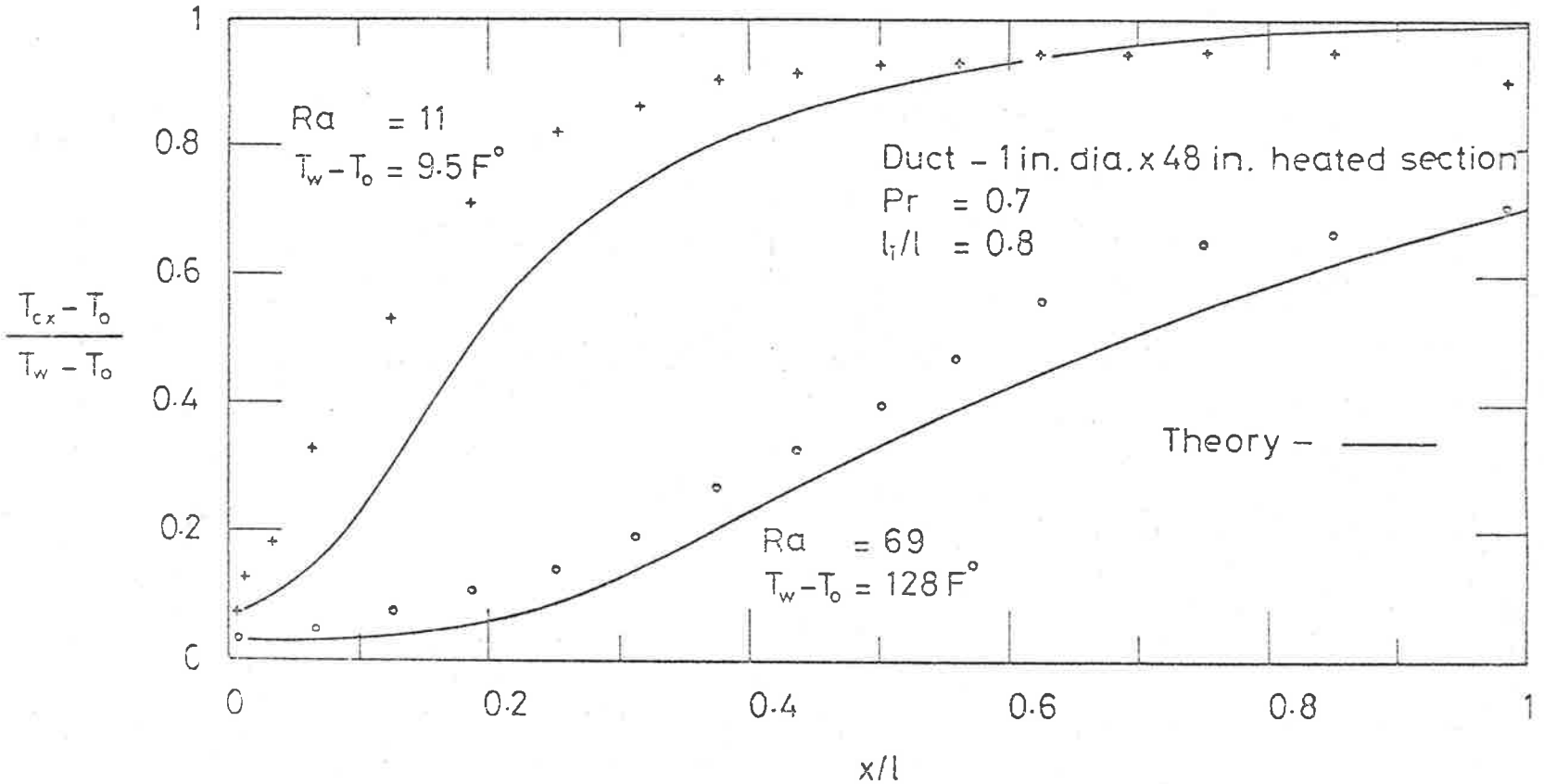

Fig. 7.8 Temperatures along the axis of the 1 in. diameter restricted-entry duct; the theoretical curves were based on the actual entry temperatures

lower owing to the heating element not fully compensating for the external heat loss. A comparison of Fig. 7.2 with Fig. 7.8 will show that the restricted-entry duct for the same value of Ra produced higher temperatures along the axis than the plain-entry duct. The explanation for this is that the entry restriction reduced the flow rate which, in turn, led to greater flow development.

The amplitudes of the axial temperature fluctuations shown in Fig. 7.9 will be seen to be considerably less than those in Fig. 7.3 for a plain-entry duct. The smaller temperature variations were brought about by the 37 in. long unheated section smoothing the flow before it reached the heated section.

Open-thermosyphon ducts

Some tests were carried out with the ducts closed at the bottom to yield $\ell_i/\ell = \infty$. The results of these tests on open-thermosyphon flow are presented in Figs. 7.6 and 7.7 and will be seen to agree satisfactorily with the experimental work of Martin and Cohen (12) and with the theory of Lighthill (3) and of Leslie and Martin (11).

Smoke studies revealed that when Ra was below 4×10^2 the open-thermosyphon flow was laminar. However,

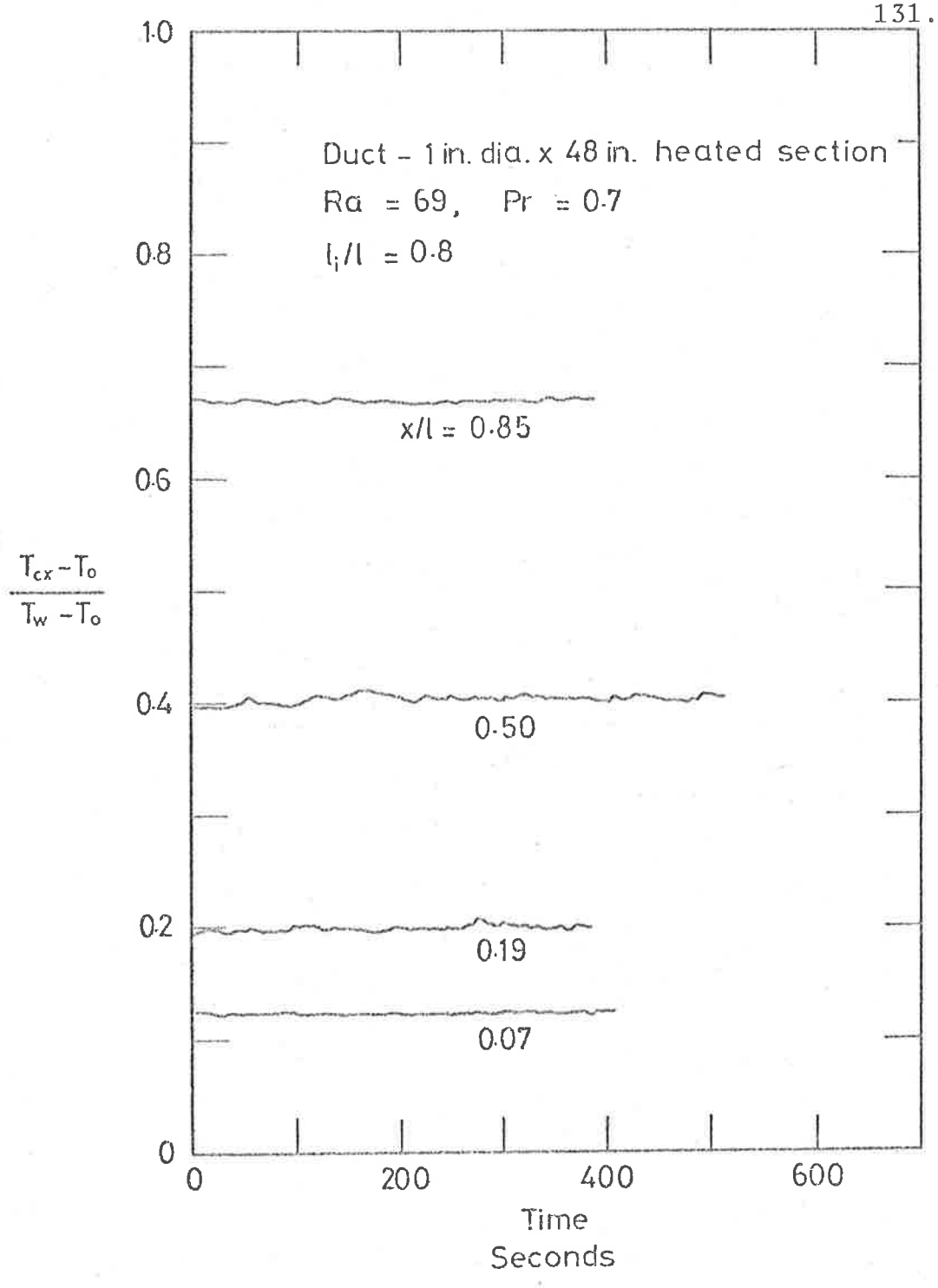

Fig. 7.9 Temperature fluctuations on the axis of the 1 in. diameter restricted-entry duct. (The temperatures at each elevation were not recorded simultaneously). Comparison of this figure with Fig. 7.3 will show that the entry restriction smoothed the flow in the heated section

for Ra > 4×10^2 the down- and up-flowing streams were observed to mix with each other. This interaction between the streams produced the impeding flow regime which gave lower values of Nu (3, 12, 13).

It should be noted that, as in other work on open-thermosyphon ducts (3, 11, 12, 13), Nu and Ra have been based not on (T_w-T_o), which was used in the case of plain- and restricted-entry ducts, but on (T_w-T_{ct}). Since the temperature on the axis at the top of the duct (T_{ct}) was higher than that of the ambient air (T_o), (T_w-T_{ct}) was less than (T_w-T_o).

Combined upward and open-thermosyphon flow

When the entry restriction was very large, it was found that an open-thermosyphon flow occurred in the upper part of the heated section of the duct. Smoke studies revealed that air still entered the bottom of the duct. Thus heat was dissipated by a restricted-entry flow in the lower part of the heated section and by an open-thermosyphon flow in the upper part.

In Fig. 7.6 it will be seen that a 1 in. diameter duct with $\ell_i/\ell >> 20$ yielded smaller values of Nu than the same duct operating as an open-thermosyphon duct.

It should be noted that since a smaller diameter entrance was used (see Fig. 6.7) a more accurate value could not be given to ℓ_i/ℓ for reasons stated in Appendix G.

In comparing the values of Nu for $\ell_i/\ell >> 20$ with those for the open-thermosyphon duct in Fig. 7.6, it is important to realise that the temperature of the air entering the top of the restricted-entry duct was higher than ambient. This was brought about by the hot outflowing air heating the air space above the duct. Thus the problem involved not one, but two temperature differences. To be consistent with the other tests on restricted-entry ducts, the temperature difference for calculating Nu and Ra was based on the temperature of the ambient air (T_o). On the other hand, basing the temperature difference on the temperature of the air entering at the top (T_{ct}), the results for $\ell_i/\ell >> 20$ will be seen in Fig. 7.6 to be similar to those for the open-thermosyphon duct. This was because the open-thermosyphon flow was the predominant heat transfer mechanism.

In Fig. 7.10, showing temperatures along the axis of the heated section of the 1 in. diameter duct with $\ell_i/\ell >> 20$, it will be observed that from $x/\ell = 0.15$ to 0.8 the air stream was at the same temperature as the

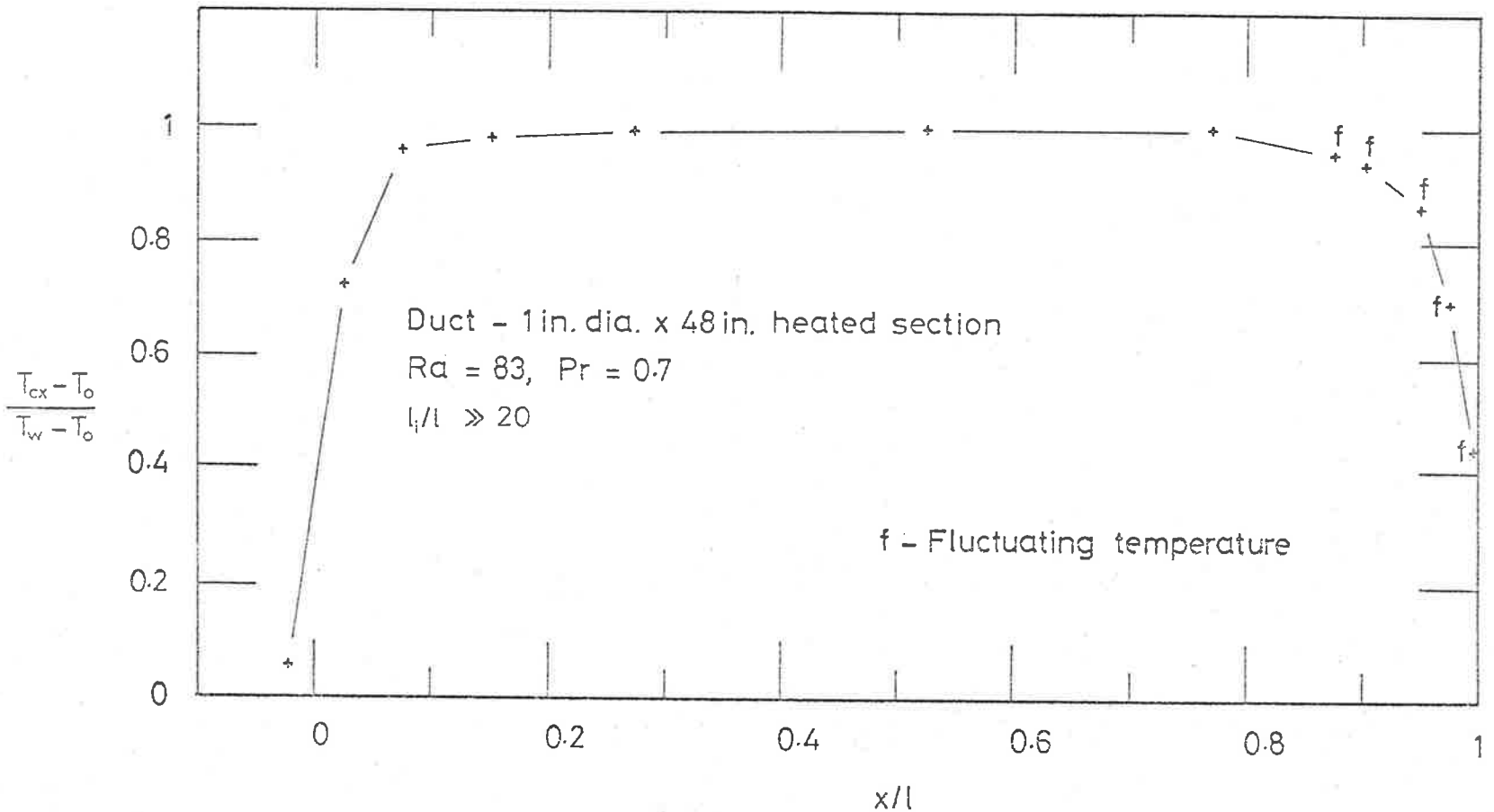

Fig. 7.10 Temperatures along the axis of the 1 in. diameter restricted-entry duct; the entry restriction was sufficiently large for air to enter the duct at the top

surface. Hence it follows that heat dissipation took place only near the two ends of the heated section.

Turning to Fig. 7.7, tests on the 2¼ and 3¾ in. diameter ducts with ℓ_i/ℓ = 48 also produced a combined upward and open-thermosyphon flow. Although most of the values of Nu for ℓ_i/ℓ = 48 will be seen to be only slightly larger than those obtained for the open-thermosyphon ducts, the rates of heat transfer were not similar. The reasons for this are as follows. First, higher temperatures were experienced in the open-thermosyphon ducts and therefore the properties of the air in these tests were quite different. Secondly, Nu and Ra for the open-thermosyphon ducts were based on a different temperature difference namely, $(T_w - T_{ct})$. An inspection of Table 7.1 will show that for approximately the same value of Ra, the open-thermosyphon duct dissipated 110% more heat than the restricted-entry duct with ℓ_i/ℓ = 48. Furthermore, it is interesting to observe in Table 7.2 that, despite the open-thermosyphon flow, the lower part of the heated section of the restricted-entry duct with ℓ_i/ℓ = 48 was responsible for the greater part of the heat dissipation. Of course, if the entry restriction had been increased, the open-thermosyphon flow would have assumed greater significance.

Table 7.1

Comparison between the heat dissipated by a restricted-entry duct with ℓ_i/ℓ = 48 and by an open-thermosyphon duct; the ducts were 2¼ in. in diameter and the heated sections were 48 in. long

Heat transfer data	Restricted-entry duct ℓ_i/ℓ = 48	Open-thermosyphon duct
Ra[1]	1040	1060
Nu[1]	0.71	0.66
T_w (°F)	112	216
T_o (°F)	68	75
T_{ct} (°F)	98 (av.)	126
Temperature difference (F°)	(T_w-T_o) = 44	(T_w-T_{ct}) = 90
Heat dissipated (Btu/hr)	12.7	26.5

1 The fluid properties for calculating Nu and Ra were evaluated at the temperature of the surface.

Table 7.2

Percentage of the total heat that was dissipated by each heating element; the ducts were 2¼ in. in diameter and the heated sections were 48 in. long.

Distance above the bottom of the heated section (in.)	Percentage of the total rate of heat transfer	
	Restricted-entry duct with $\ell_i/\ell = 48$	Open-thermo-syphon duct
	Ra=1040	Ra=1060
36 to 48	7	95
9 to 36	27	5
0 to 9	66	0
Total	100	100

Temperatures along the axis of the heated section of the 2¼ in. diameter duct with $\ell_i/\ell = 48$ for Ra = 1040 are presented in Fig. 7.11. It will be observed that the temperatures were unsteady with the largest fluctuations occurring near the bottom of the heated section and at the top of the duct. At $x/\ell = 0.04$ and 0.12 the fluctuating temperatures were caused by the laminar flow degenerating into a mixing flow as illustrated in Fig. 4.7.

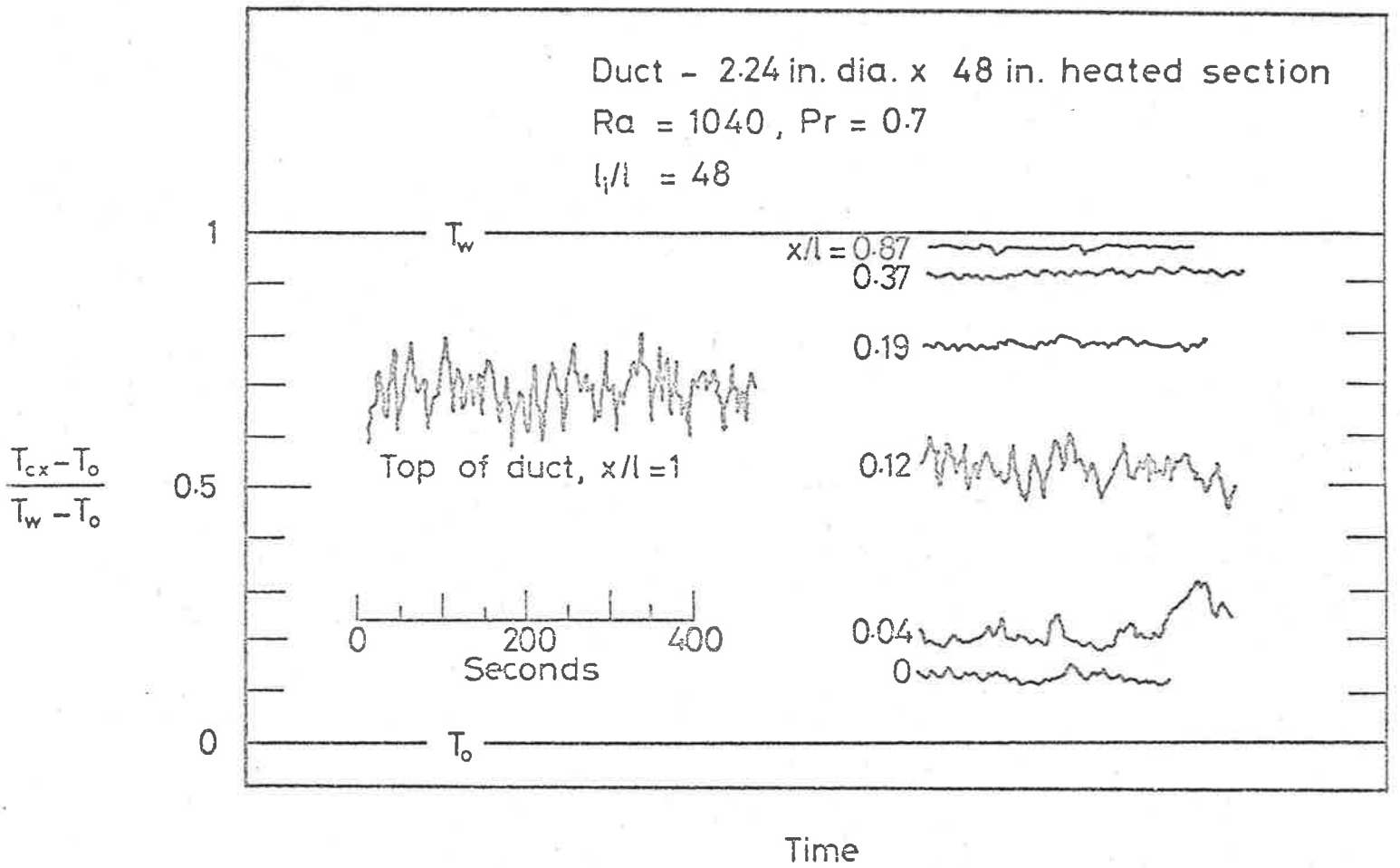

Fig. 7.11 Temperature fluctuations on the axis of the 2¼ in. diameter restricted-entry duct. (The temperatures at each elevation were not recorded simultaneously). The temperature at the top of the duct was reduced by the unsteady open-thermosyphon flow

At $x/\ell = 1$ the entering air in the open-thermosyphon flow was responsible for the lower mean temperature, and flow visualisation studies revealed that the large temperature fluctuations were caused by the air being alternately drawn in and pushed out.

For the test on the restricted-entry duct described in Table 7.1, Reynolds number (Re_r) of the upward flow in the lower part of the heated section can be obtained as follows. In Fig. 7.11 it will be seen that between $x/\ell = 0.37$ and 0.87 the air had almost reached the temperature of the surface. In addition, the heat dissipated up to $x/\ell = 0.75$ was 3.47 watts. A heat balance yielded the following equation.

$$h_{x/\ell=0.75} = \Pi r_w^2 \, u_m \, \rho \, c_p (T_w - T_o) \qquad \ldots (7.1)$$

Solving Eq. (7.1) gave a mean flow velocity (u_m) of 570 ft/hr. and from Eq. (3.26) Re_r was found to be 80. Re_r being very much smaller than the critical value of 1150 supports the explanation given in the previous paragraph for the temperature fluctuations in the lower part of the heated section.

Mixing flow

If the entry restriction were too large for laminar flow to be sustained yet not large enough for an open-thermosyphon flow to develop at the top, a mixing flow occurred above the degeneration of the laminar flow, as illustrated in Fig. 4.7. The 2¼ in. diameter duct with ℓ_i/ℓ = 8 produced such a mixing flow. Flow visualisation studies for these tests showed that considerable mixing took place in the air stream as it emerged from the top of the duct with the intensity of mixing increasing with Ra. In Fig. 7.7 the experimental values of Nu for the 2¼ in. diameter duct with ℓ_i/ℓ = 8 will be seen to approach the theoretical laminar flow regime just below the curve derived for the same value of ℓ_i/ℓ. This discrepancy could have resulted from errors inherent in the method of estimating ℓ_i/ℓ (see Appendix G) and from errors arising out of the use of small temperature differences in order to obtain values of Ra less than 6×10^2.

It is considered that ducts with values of ℓ_i/ℓ just larger than those allowed by the laminar flow regime merit further investigation to obtain a better understanding of the heat transfer mechanism in the mixing flow regime.

8. CONCLUSIONS

From the theoretical investigations into laminar natural-convective flow in vertical ducts described in this thesis, the following conclusions were drawn.

Plain-entry ducts with uniform surface temperatures

For $Ra < 1$ and $Pr = 0.7$, the flow was fully developed and

$$Nu = \frac{Ra}{16} \qquad \ldots (8.1)$$

At the other extreme, for $Ra > 3 \times 10^3$ and $Pr = 0.7$, boundary layer flow occurred and

$$Nu = 0.63\ Ra^{\frac{1}{4}} \qquad \ldots (8.2)$$

For intermediate values of Ra, Nu can be obtained from Fig. 3.2.

The Prandtl number of the fluid was found to have only a small influence on the Nu-Ra relationship for $Pr \geqslant 0.7$ but an increasingly significant influence as Pr decreased below 0.7 as shown in Fig. 3.3.

The heat transfer per unit flow area was found to be a maximum when $Ra = 32$ for $Pr = 0.7$. Fig. 3.9 shows that as Pr decreased below 0.7 the optimum value of Ra increased.

Restricted-entry ducts with uniform surface temperatures

An entry restriction in the form of an unheated section of the duct reduced the flow rate and consequently Nu was dependent upon both Ra and the ratio of the lengths of the unheated and heated sections (ℓ_i/ℓ). The largest value of ℓ_i/ℓ yielding laminar flow was shown to decrease from 18 in the fully developed flow regime to about 2 in the boundary layer regime.

For Ra < 20, Pr = 0.7, and ℓ_i/ℓ = 18 (the largest value of the ratio yielding fully developed flow)

$$Nu = \frac{Ra}{304} \qquad \ldots (8.3)$$

At the other extreme, for Ra > 3×10^3, Pr = 0.7 and ℓ_i/ℓ = 2 (the largest value of the ratio yielding boundary layer flow)

$$Nu = 0.48\ Ra^{\frac{1}{4}} \qquad \ldots (8.4)$$

For intermediate values of Ra and other laminar flow values of ℓ_i/ℓ, Nu can be obtained from Fig. 4.4.

Uniform heat flux ducts

The relationships between Nusselt and Rayleigh numbers for uniform surface heat flux ducts were derived

in terms of both a known heat flux and a known mean surface temperature.

In terms of the uniform heat flux, the relationships obtained for laminar flow are:

For $Ra^* < 0.1$ and $Pr = 0.7$, a flow resembling fully developed flow occurred and

$$Nu^* = \sqrt{\frac{Ra^*}{8}} \qquad \ldots (8.5)$$

At the other extreme, for $Ra^* > 8 \times 10^3$ and $Pr = 0.7$, boundary layer flow occurred and

$$Nu^* = 0.67\ (Ra^*)^{\frac{1}{5}} \qquad \ldots (8.6)$$

In terms of the mean surface temperature, the corresponding relationships are:

For $Ra^+ < 0.9$ and $Pr = 0.7$,

$$Nu^* = \frac{Ra^+}{8} \qquad \ldots (8.7)$$

and for $Ra^+ > 2 \times 10^3$ and $Pr = 0.7$,

$$Nu^* = 0.61(Ra^+)^{\frac{1}{4}} \qquad \ldots (8.8)$$

It is interesting to note the similarity between Eqs. (8.2) and (8.8). Nu^* for intermediate values of Ra^* and Ra^+ can be obtained from Figs. 5.2 and 5.3 respectively.

The experimental investigation yielded results that agreed satisfactorily with those obtained theoretically for laminar flow. Although air was the only fluid used in the experiments, it is reasonable to infer from these results and from those of other studies in natural-convective heat transfer that the theory is also valid for Prandtl numbers in excess of 0.7 (9).

An interesting experimental finding was that the temperature of the air in plain-entry ducts fluctuated even though the flow was nominally laminar. Since the fluctuations were caused by flow irregularities as the air entered the duct, they were much less apparent in restricted-entry ducts owing to the smoothing effect produced by the unheated section.

The experimental work was carried beyond the laminar flow regime. Tests revealed that if the ratio of the unheated to the heated length of a restricted-entry duct (ℓ_i/ℓ) were greater than that allowed by the laminar flow theory, laminar flow entering the heated section degenerated into a mixing flow, as illustrated in Fig. 4.7. Furthermore, if the restriction were very large, an unsteady open-thermosyphon flow was found to occur in the top part of the duct. As a result, heat

was dissipated in the lower part of the heated section by the upward flow through the restriction, and by the open-thermosyphon flow near the top of the duct. Unfortunately, it was not possible to carry out a sufficient number of tests to establish the values of ℓ_i/ℓ at which open-thermosyphon flow began.

As large entry restrictions are of some practical interest, it would be profitable in future work to study the behaviour of mixing flow and of combined upward and open-thermosyphon flow in transparent ducts (15).

Although the only entry restrictions considered in this work were unheated sections of the duct, it would be permissible, in the absence of any other information, to transform other entry restrictions into an unheated section of the duct and use the Nu-Ra relationships presented in this thesis.

APPENDIX A

Finite difference equations for uniform surface temperature ducts

Since the flow is assumed to be axisymmetrical, the relaxation can be performed on a two-dimensional grid passing through the vertical axis of the duct as shown in Fig. A.1.

In the finite difference forms of Eqs. (2.10), (2.11) and (2.13) which follow, it will be seen that separate equations have been written for points on the axis of the duct. To write these equations, terms containing $\frac{1}{R}\frac{\partial}{\partial R}$, which in finite difference form cannot be directly evaluated at R = 0, were reduced to $\frac{\partial^2}{\partial R^2}$ by L'Hospital's rule.

Continuity equation

When $0 < R < 1$:

$$\frac{2}{R_k + R_{k+1}} \left(\frac{V_{j,k+1} R_{k+1} - V_{j,k} R_k}{\Delta R} \right) + \frac{(U_{j,k+1} + U_{j,k}) - (U_{j-1,k+1} + U_{j-1,k})}{2 \Delta X} = 0 \qquad \ldots \text{(A.1)}$$

The continuity equation in finite difference form for R = 0 was not required to solve the flow equations. However, it should be noted that when R = 0

$$V_{j,k} = 0 \qquad \ldots (A.2)$$

Momentum equation

When 0 < R < 1:

$$U_{j-1,k}\left(\frac{U_{j,k}-U_{j-1,k}}{\Delta X}\right) + \left(V_{j-1,k}-\frac{1}{R_k}\right)\left(\frac{U_{j,k+1}-U_{j,k-1}}{2\ \Delta R}\right)$$

$$= \left(\frac{U_{j,k+1}-2\ U_{j,k}+U_{j,k-1}}{\Delta R^2}\right) - \left(\frac{P_{dj}-P_{dj-1}}{\Delta X}\right) + \theta_{j,k} \qquad \ldots (A.3)$$

When R = 0:

$$U_{j-1,k}\left(\frac{U_{j,k}-U_{j-1,k}}{\Delta X}\right) + V_{j-1,k}\left(\frac{U_{j,k+1}-U_{j,k-1}}{2\ \Delta R}\right)$$

$$= 2\left(\frac{U_{j,k}-2\ U_{j,k}+U_{j,k-1}}{\Delta R^2}\right) - \left(\frac{P_{dj}-P_{dj-1}}{\Delta X}\right) + \theta_{j,k} \qquad \ldots (A.4)$$

Energy equation

When $0 < R < 1$:

$$U_{j-1,k}\left[\frac{\theta_{j,k}-\theta_{j-1,k}}{\Delta X}\right] + \left[V_{j-1,k} - \frac{1}{Pr\ R_k}\right]\left[\frac{\theta_{j,k+1}-\theta_{j,k-1}}{2\ \Delta R}\right]$$

$$= \frac{1}{Pr}\left[\frac{\theta_{j,k+1}-2\ \theta_{j,k}+\theta_{j,k-1}}{\Delta R^2}\right] \qquad \ldots (A.5)$$

When $R = 0$:

$$U_{j-1,k}\left[\frac{\theta_{j,k}-\theta_{j-1,k}}{\Delta X}\right] + V_{j-1,k}\left[\frac{\theta_{j,k+1}-\theta_{j,k-1}}{2\ \Delta R}\right]$$

$$= \frac{2}{Pr}\left[\frac{\theta_{j,k+1}-2\ \theta_{j,k}+\theta_{j,k-1}}{\Delta R^2}\right] \qquad \ldots (A.6)$$

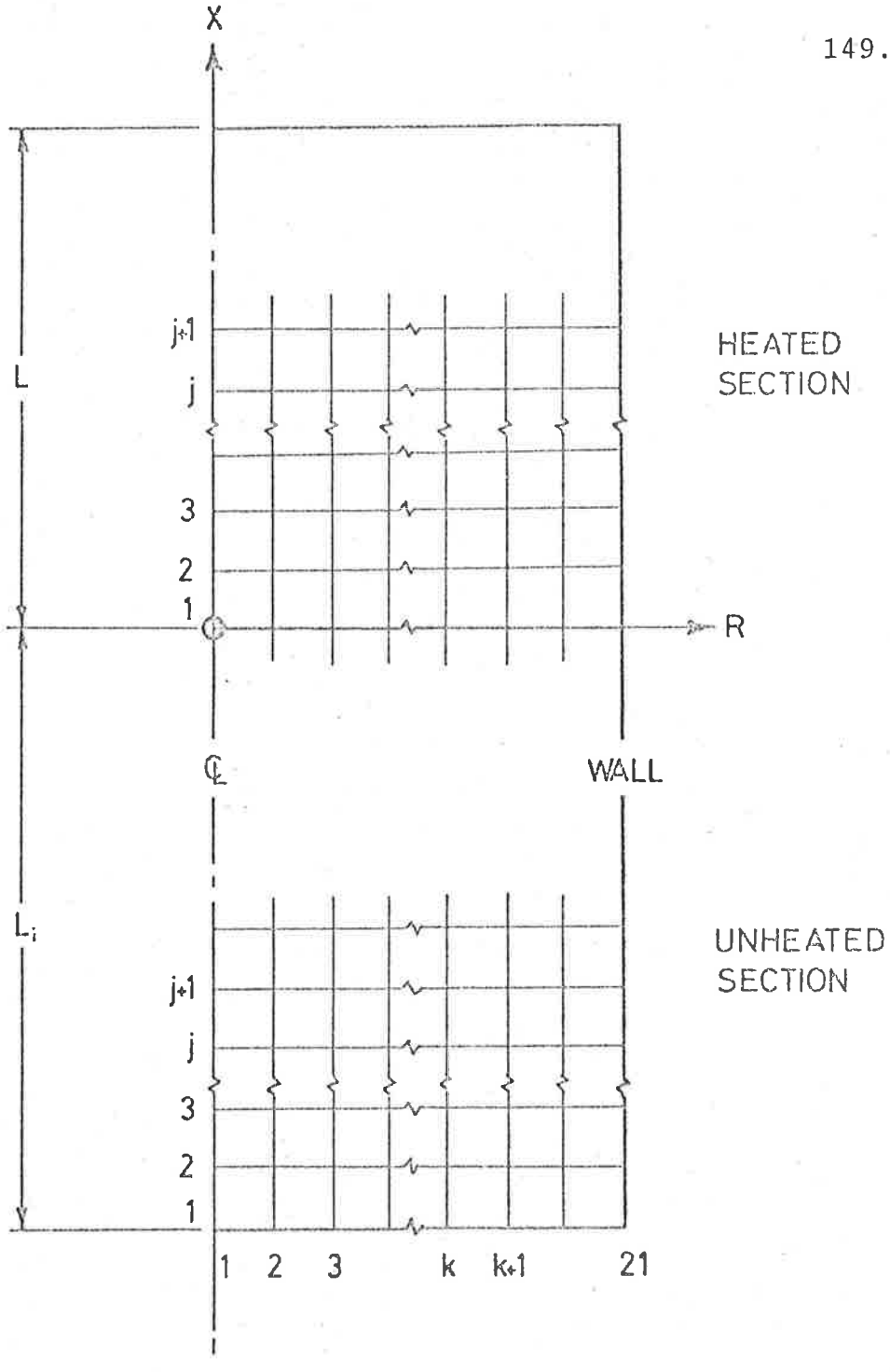

Fig. A.1 Relaxation grid

APPENDIX B

Relaxation solution for uniform surface temperature ducts

Since laminar flow in a duct is unidirectional, the governing equations were solved by a step-by-step relaxation (6, 16). With this method, each row of the grid shown in Fig. A.1 was relaxed in turn, beginning at the bottom of the duct.

For the boundary conditions in Section 3.1 for plain-entry ducts and in Section 4.4 for restricted-entry ducts, the procedure is as follows:

1. Values are chosen for Pr, the volume flow (Q) ($0<Q<\Pi/8$) and the length of the unheated section (L_i) ($L_i=0$ for plain-entry ducts).
2. On the bottom row of the grid the pressure defect (P_{d1}) is set equal to zero, the temperature of the fluid ($\theta_{1,k}$) to zero, the flow velocity ($U_{1,k}$) to Q/Π, and the radial velocity ($V_{1,k}$) to zero.

3a. Plain-entry ducts:

For initial values of the temperatures on Row 2, $\theta_{2,k}$ is set equal to $\theta_{1,k}$. The energy equation in Appendix A is relaxed until satisfactory values of $\theta_{2,k}$ are obtained. An over-relaxation

factor of about 1.2 was found to be advantageous in reducing the number of iterations.

3b. Restricted-entry ducts:

Throughout the unheated section $\theta_{j,k}$ is zero.

4. The momentum equation in Appendix A is relaxed for the grid points on Row 2. Both $U_{2,k}$ and P_{d2} are unknown and therefore the equation is solved for

$$U_{2,k} + \left[\frac{P_{d2}-P_{d1}}{\Delta X}\right] \Big/ \left[\frac{U_{1,k}}{\Delta X} + \frac{C}{\Delta R^2}\right]$$

where $C = 2$ for $0 < R < 1$ and $C = 4$ for $R = 0$. Since P_{d2} has the same value for each grid point on Row 2 and Q is constant throughout the duct, Eq. (3.1) in finite difference form is used to separate the two unknown variables.

5. The continuity equation in Appendix A is solved directly for each point on Row 2 to give $V_{2,k}$.

6. The procedure is repeated for Row 3 and subsequent rows until P_d ceases to be negative. Linear interpolation yields the elevation at which $P_d=0$; this elevation gives the top of the duct.

7. The rate at which the fluid transports heat across each row is obtained from Eq. (3.2) in finite difference form.

8. The reciprocal of the dimensionless length of the heated section of the duct (L) yields the Grashof number, and the Nusselt number is obtained from Eq. (3.6).

9. Restricted-entry ducts:

   The Nu-Ra relationship for restricted-entry ducts is obtained by successive solutions of the equations for constant values of Q and increasing values of L_i.

The computer programme, which will be presented in Appendix C, was designed to place the top of the duct between Rows 40 and 100. Since the changes in temperature and velocity near the bottom of each section were relatively large, a smaller row spacing was used between Rows 1 and 21.

Twenty-one grid points per row were found to be satisfactory for all calculations. However, it is interesting to note that trial computations using 41 grid points per row yielded almost identical data.

APPENDIX C

Computer programme for uniform surface temperature ducts

The programme for uniform surface temperature ducts given in Fig.C.1 was originally written for a CDC 3200 digital computer and later modified to run on a faster CDC 6400 computer. The actual computing time for a solution on the CDC 6400 computer was usually between 5 and 60 seconds.

Information that is required on the data cards will be found in Statement No. 100 of the programme. The symbols used in this statement are defined as follows:

Data Card Symbols

Q	Dimensionless flow volume; $0<Q<\Pi/8$
PR	Prandtl number
DX	Dimensionless spacing of the rows from the first to the LLL^{th} row in each section
DCX	Dimensionless spacing of the rows above the LLL^{th} row in each section
WT	Over-relaxation factor for temperatures; WT is usually 1.2
LLL	Row at which the grid spacing changes from DX to DCX; LLL is usually 21

III Number of rows that are relaxed beyond the highest row having a negative P_d; III is usually 1

PHI Angle of the duct to the vertical; PHI should not exceed 0.2 and is zero for a vertical duct

XP Dimensionless length of the unheated section

LX Number of rows in the unheated section

TA Constant in the expression for the temperature of the heated surface; TA=1 for a uniform surface temperature duct

TB Constant in the expression for the temperature of the heated surface; TB=0 for a uniform surface temperature duct

LCO Controls the amount of data printed; LCO=1 gives Nu and Ra, and temperatures, velocities and the pressure defect for each of the top three or four rows, and LCO=0 gives, in addition, temperatures, velocities and the pressure defect for each tenth row

```
      PROGRAM JRD031U (INPUT,TAPE60=INPUT,OUTPUT,TAPE61=OUTPUT)
C     DYER MECH ENG DEPT U OF A TEL X2439
C     NATURAL CONVECTION THROUGH A CYLINDER
C     WITH FLAT VELOCITY PROFILE AT INLET
C     VARIABLE WALL TEMP OR UNIFORM WALL TEMP
C     JRD/031U
      DIMENSIONU(2,22),T(3,22),V(22),SU(22),TU(22),UU(22),WU(22),XU(22)
      DIMENSIONZU(22),AU(22),BU(22),CU(22),YU(22),DU(22,
    1 FORMAT(4E10.3,F5.2,2I4,F9.6,E9.2,I4/2E10.3,I2)
    5 FORMAT(/1H1,5X,13HJRD/031U      I3)
   10 FORMAT(1H ,5X,37HNATURAL CONVECTION THROUGH A CYLINDER)
   15 FORMAT(1H ,5X,35HWITH FLAT VELOCITY PROFILE AT INLET)
   20 FORMAT(1H ,5X,26H21 EQUALLY SPACED STATIONS)
   25 FORMAT(1H ,5X,17HSTATION 22 = WALL)
   30 FORMAT(1H ,5X,24HSTATION  2 = CENTRE-LINE)
   32 FORMAT(1H ,5X,17HWALL TEMP = A+B*X)
   35 FORMAT(1H ,5X,10HDATA CARD 4E10.3,F5.2,2I4,F9.6,E9.2,I4,2E10.3,I2)
   40 FORMAT(1H ,5X,4HQ  =F7.4,7X,18HUNHEATED LENGTH  =E9.2)
   45 FORMAT(1H ,5X,4HPR =F7.3,7X,5HPHI =F7.3,7X)
   47 FORMAT(1H ,5X,13HWALL  TEMP = E10.3,2H +E10.3,4H * X/)
   50 FORMAT(1H ,7X,47HX          DP/DX      P DIFF     HT/TRANS  FLOW UP,
     136X,7HD2U/DR2)
   55 FORMAT(/1H ,5X,5E10.3,I6,9X,I5,5X,I5,E10.3)
   60 FORMAT(/1H ,5X,1E10.3,10X,3E10.3,I6,9X,I5,5X,I5,E10.3)
   65 FORMAT(1H ,5X,5E10.3,10X,5E10.3)
   70 FORMAT(/1H ,7X,44HL            GR*       GRPR*       NU          PI,
     117X,47HL/L       PR         Q          H          TW OUT)
   75 FORMAT(/1H ,5X,5E10.3,10X,5E10.3)
   80 FORMAT(/1H ,7X,26HTW MEAN   GRPR TWM  NU TWM)
   85 FORMAT(/1H ,5X,3E10.3/)
  100 READ(60,1)Q,PR,DX,DCX,WT,LLL,III,PHI,XP,LX,TA,TB,LCO
      LLLL=1
      IF(Q.EQ.0.)GOTO360
  105 WRITE(61,5)LLLL
      WRITE(61,10)
      WRITE(61,15)
      WRITE(61,20)
      WRITE(61,25)
      WRITE(61,30)
      WRITE(61,32)
      WRITE(61,35)Q,PR,DX,DCX,WT,LLL,III,PHI,XP,LX,TA,TB,LCO
      WRITE(61,40)Q,XP
      WRITE(61,45)PR,PHI
      WRITE(61,47)TA,TB
      WRITE(61,50)
      DO120K=2,22
      Y=K-2
      YU(K)=Y*.05
      V(K)=0.
      U(1,K)=U(2,K)=Q/3.141592654
  120 T(1,K)=T(2,K)=.0
      P1=0.
      IF(LX.NE.0)GOTO122
      T(1,22)=TA
  122 X=P=H=D2U=0.
      DBX=DX
      AA=.0125/DX
```

Fig. C.1-1 Sheet 1 of 4 of the computer programme for plain- and restricted-entry ducts with uniform surface temperatures

```
      PRA=400./PR
      PRB=PRA*2.
      II=L=0
      LC=20
      LXL=LX
      LL=1
      WRITE(61,60)X,P,H,Q,LL,L,L,D2U
      WRITE(61,65)(T(1,K),K=2,22)
      WRITE(61,65)(U(1,K),K=2,22)
      U(1,22)=U(2,22)=0.
      CU(22)=.00125
      UU(2)=WU(2)=PRB
      AU(2)=BU(2)=800.
      DO126K=2,21
  126 DU(K)=(YU(K+1)*YU(K+1)-YU(K)*YU(K))*1.570796327
  128 LL=LL+1
      X=X+DX
      IF(LL.LT.LX.OR.LL.EQ.LX)GOTO130
      T(2,22)=TA+TB*X
      IF(T(2,22).LT.0.)GOTO100
  130 DO135K=3,21
      ZU(K)=(V(K)-1./(PR*YU(K)))/.1
      UU(K)=PRA+ZU(K)
      WU(K)=PRA-ZU(K)
      TU(K)=U(1,K)/DX
      XU(K)=TU(K)*U(1,K)
      BU(K)=(V(K)-1./YU(K))/.1
      AU(K)=400.-BU(K)
      BU(K)=400.+BU(K)
      CU(K)=1./(TU(K)+800.)
      SU(K)=TU(K)*T(1,K)
  135 TU(K)=TU(K)+PRB
      SU(2)=U(1,2)*T(1,2)/DX
      TU(2)=U(1,2)/DX+PRB*2.
      CU(2)=1./(U(1,2)/DX+1600.)
      XU(2)=U(1,2)*U(1,2)/DX
      IF(LL-LX)170,136,138
  136 LL=1
      LC=20
      LX=0
      GOTO170
  138 L=0
      N=3
      FT=1.
  140 DO150M=1,N
      L=L+1
      SUM=0.
      T(2,1)=T(2,3)
      DO150KK=1,20
      K=22-KK
      TEMP=(T(2,K+1)*WU(K)+T(2,K-1)*UU(K)+SU(K))/TU(K)
      TEMP=FT*(TEMP-T(2,K))
      SUM=SUM+TEMP*TEMP
      T(2,K)=T(2,K)+TEMP
  150 CONTINUE
      IF(LL.GT.1000.AND.LX.EQ.0)WRITE(61,65)(T(2,K),K=2,22)
      IF(SUM.LT.1.E-14)GOTO170
      FT=WT
```

Fig. C.1-2 Sheet 2 of 4 of the computer programme for plain- and restricted-entry ducts with uniform surface temperatures

```
    N=1
    GOTO140
170 R=0.
    DO190K=2,21
    T(3,K)=T(2,K)*COSF(PHI)
    T(3,K)=T(2,K)
190 R=R+DU(K)*(CU(K+1)+CU(K))
    SU(22)=0.
    I=0
200 I=I+1
    SUM=A=0.
    U(2,1)=U(2,3)
    DO210KK=1,20
    K=22-KK
210 SU(K)=(XU(K)+U(2,K+1)*AU(K)+U(2,K-1)*BU(K)+T(3,K))*CU(K)
    DO220K=2,21
220 A=A+DU(K)*(SU(K+1)+SU(K))
    DPDX=(A-Q)/R
    SU(22)=DPDX/800.
    DO230K=2,21
    TEMP=SU(K)-DPDX*CU(K)
    TEMP=TEMP-U(2,K)
    U(2,K)=U(2,K)+TEMP
230 SUM=SUM+TEMP*TEMP
    IF(LL.GT.1000.AND.LX.EQ.0)WRITE(61,65)(U(2,K),K=2,22)
    IF(SUM.GT.1.E-14)GOTO200
    DO260K=2,20
    V(K+1)=(U(2,K+1)+U(2,K)-(U(1,K+1)+U(1,K)))*(YU(K)+YU(K+1)))*AA
260 V(K+1)=(V(K)*YU(K)-V(K+1))/YU(K+1)
    P=DPDX*DX+P
    IF(LL.NE.1)GOTO282
    DX=DBX
    AA=.0125/DX
    X=0.
    T(1,22)=T(2,22)=1.
    PI=P
    GOTO290
282 IF(LL.GT.999.AND.LX.EQ.0.AND.(P+4.0*DPDX*DX).LT.0.)GOTO290
    IF(LCO.EQ.1.AND.LL.GT.4)GOTO286
    IF(LL.LT.20)GOTO290
    IF(LL.EQ.LC.AND.LX.EQ.0)284,286
284 LC=LC+10
    GOTO290
286 IF(P+4.0*DPDX*DX.GT.0..OR.LL.EQ.999.OR.LL.EQ.(LX-1))290,300
290 R=H=0.
    DO292K=2,21
    H=H+DU(K)*(U(2,K+1)*T(2,K+1)+U(2,K)*T(2,K))
292 R=R+DU(K)*(U(2,K+1)+U(2,K))
    D2U=(U(2,3)-U(2,2))*800.
    WRITE(61,55)X,DPDX,P,H,R,LL,L,I,D2U
    WRITE(61,65)(T(2,K),K=2,22)
    WRITE(61,65)(U(2,K),K=2,22)
    WRITE(61,65)(V(K),K=2,22)
300 IF(P.GT.0.)305,310
305 II=II+1
    IF(II-III)310,350
310 DO320K=2,22
    T(1,K)=T(2,K)
```

Fig. C.1-3 Sheet 3 of 4 of the computer programme for plain- and restricted-entry ducts with uniform surface temperatures

```
320 U(1,K)=U(2,K)
    PP=-P
    QP=Q
    HP=H
    IF(LL.NE.LLL)GOTO128
    DX=DCX
    AA=.0125/DX
    GOTO128
350 X=X-P*DX/(PP+P)
    GR=1./X
    GRPR=GR*PR
    Q=QP+(Q-QP)*PP/(PP+P)
    H=HP+(H-HP)*PP/(PP+P)
    TO=T(1,22)+(T(2,22)-T(1,22))*PP/(PP+P)
    FU=H*GRPR/6.2831853
    R=XP/X
    WRITE(61,70)
    WRITE(61,75)X,GR,GRPR,FU,PI,R,PR,Q,H,TO
    TM=(TA+TO)/2.
    GRPR=GRPR*TM
    FU=FU/TM
    WRITE(61,80)
    WRITE(61,85)TM,GRPR,FU
    WRITE(61,47)TA,TB
    IF((1.-TO)**2.LT.2.E-07.AND.LL.GT.39)GOTO100
    TI=(1.-TA)/X
    TB=(TB*30.+TI)/31.
    DX=DBX
    LX=LXL
    LLLL=LLLL+1
    IF(LL.LT.94)GOTO354
    DX=DBX*2.
    DCX=DCX*2.
    GO TO 105
354 IF(LL.GT.40)GOTO105
    DX=DBX/2.
    DCX=DCX/2.
    GO TO 105
360 STOP
    END
```

Fig. C.1-4 Sheet 4 of 4 of the computer programme for plain- and restricted-entry ducts with uniform surface temperatures

APPENDIX D

Finite difference equations for uniform surface temperature ducts

The finite difference forms of Eq. (2.14), (2.15) and (2.17) become identical to those in Appendix A for ducts with uniform surface temperatures after replacing

P_d	by	P_d^*
U	by	U*
X	by	X*
θ	by	θ^*

and substituting $V_{j,k}$ for $V_{j-1,k}$ in Eqs. (A.5) and (A.6).

APPENDIX E

Relaxation solution for uniform surface heat flux ducts

Again a step-by-step relaxation was used but the procedure differed slightly from that described in Appendix B because the local surface temperature of the uniform heat flux duct had to be determined concurrently with the other temperatures on each row.

An expression will now be derived which was used to obtain the surface temperature of a row. From Eq. (5.10) it follows that

$$H_x^* = \frac{2\Pi}{Pr} \cdot X^* \qquad \ldots (E.1)$$

and according to Eq. (5.2)

$$H_x^* = 2\Pi \int_0^1 U^* \, \theta^* \, R \, dR \qquad \ldots (E.2)$$

Combining Eqs. (E.1) and (E.2) yields

$$\frac{X^*}{Pr} = \int_0^1 U^* \, \theta^* \, R \, dR \qquad \ldots (E.3)$$

For the boundary conditions in Section 5.7, the relaxation procedure is as follows:

1. Values are chosen for Pr and the volume flow (Q).
2. On the bottom row of the grid shown in Fig. A.1 the pressure defect (P^*_{d1}) is set equal to zero, the temperatures of the surface ($\theta^*_{1,21}$) and the fluid ($\theta^*_{1,k}$) to zero, the flow velocity ($U^*_{1,k}$) to Q/Π and the radial velocity ($V_{1,k}$) to zero.
3. On the second row:

   $U^*_{2,k}$ is initially made equal to $U^*_{1,k}$

   and

   $\theta^*_{2,k}$ is initially made equal to $\theta^*_{1,k}$.

4. The momentum equation (see Appendix D) is relaxed for all fluid points on Row 2. Since both $U^*_{2,k}$ and P^*_{d2} are unknown at each point, the equation is relaxed for the variable

$$U^*_{2,k} + \left[\frac{P^*_{d2}-P^*_{d1}}{\Delta X^*}\right] \Bigg/ \left[\frac{U^*_{1,k}}{\Delta X^*} + \frac{C}{\Delta R^2}\right]$$

where C=2 for 0<R<1 and C=4 for R=0.

As each point on Row 2 has the same value of P^*_{d2},

the variables are separated by using Eq. (5.1) in finite difference form.

5. The continuity equation (see Appendix D) is solved for each point on Row 2 to give $V_{2,k}$.

6. The energy equation (see Appendix D) is solved for all the points in the fluid on Row 2. Eq. (E.3) is then solved to obtain a new estimate of the surface temperature $\theta^*_{2,21}$. This procedure is repeated until all temperatures on the row are satisfactorily relaxed.

7. The procedure is repeated for Row 3 and subsequent rows until P_d ceases to be negative. Linear interpolation yields the elevation at which $P^*_d=0$; this elevation gives the top of the duct.

8. The reciprocal of the dimensionless length of the duct yields the Grashof number. The Nusselt number is obtained from Eq. (5.8).

The computer programme will be presented in Appendix F. As in the case of the programme for UST ducts 21 grid points per row were used.

APPENDIX F

Computer programme for uniform surface heat flux ducts

The programme for uniform heat flux ducts is given in Fig. F.1. Information that is required on the data cards will be found in Statement No. 100 of the programme; reference should be made to Appendix C for the definitions of the symbols. It should be noted that the dimensionless volume flow (Q and not Q* in the programme) is no longer restricted to values less than $\Pi/8$ as in the case of uniform surface temperature ducts.

```
      PROGRAM JRD031M (INPUT,TAPE60=INPUT,OUTPUT,TAPE61=OUTPUT)
C     DYER MECH ENG DEPT U OF A TEL X439  COMPILE ON CDC6400
C     NATURAL CONVECTION THROUGH A CYLINDER WITH
C     UNIFORM WALL HEAT FLUX
C     JRD/031M
      DIMENSIONU(2,22),T(3,22),V(22),SU(22),TU(22),UU(22),WU(22),XU(22)
      DIMENSIONZU(22),AU(22),BU(22),CU(22),YU(22),DU(22),RU(22)
    1 FORMAT(4E10.3,F5.2,2I4,F9.6,E9.2,I4,I2)
    5 FORMAT(/1H1,5X,8HJRD/031M)
   10 FORMAT(1H ,5X,37HNATURAL CONVECTION THROUGH A CYLINDER)
   15 FORMAT(1H ,5X,35HWITH FLAT VELOCITY PROFILE AT INLET)
   18 FORMAT(1H ,5X,22HUNIFORM WALL HEAT FLUX)
   20 FORMAT(1H ,5X,26H21 EQUALLY SPACED STATIONS)
   25 FORMAT(1H ,5X,17HSTATION 22 - WALL)
   30 FORMAT(1H ,5X,24HSTATION  2 - CENTRE-LINE)
   35 FORMAT(1H ,5X,10HDATA CARD 4E10.3,F5.2,2I4,F9.6,E9.2,I4,I2)
   40 FORMAT(1H ,5X,4HQ  =F7.3,7X,18HUNHEATED LENGTH  =E9.2)
   45 FORMAT(1H ,5X,4HPR =F7.3,7X,5HPHI =F7.3)
   50 FORMAT(1H ,7X,44HX          DP/DX      P DIFF     HT/TRANS  FLOW,
     136X,17HD2U/DX2   H CHECK)
   55 FORMAT(/1H ,5X,5E10.3,I6,9X,I5,5X,I5,2E10.3)
   60 FORMAT(/1H ,5X,1E10.3,10X,3E10.3,I6,9X,I5,5X,I5,E10.3)
   65 FORMAT(1H ,5X,5E10.3,10X,5E10.3)
   70 FORMAT(/1H ,7X,44HL            GR*       GRPR*       NU TWM     PI,
     117X,47HLI/L        PR         Q          H          TW OUT)
   75 FORMAT(/1H ,5X,5E10.3,10X,5E10.3)
   80 FORMAT(/1H ,7X,18HTW MEAN   GRPR TWM)
   85 FORMAT(/1H ,5X,2E10.3)
  100 READ(60,1)Q,PR,DX,DCX,WT,LLL,III,PHI,XP,LX,LC0
      IF(Q.EQ.0.)GOTO360
      WRITE(61,5)
      WRITE(61,10)
      WRITE(61,15)
      WRITE(61,18)
      WRITE(61,20)
      WRITE(61,25)
      WRITE(61,30)
      WRITE(61,35)Q,PR,DX,DCX,WT,LLL,III,PHI,XP,LX,LC0
      WRITE(61,40)Q,XP
      WRITE(61,45)PR,PHI
      WRITE(61,50)
      DO120K=2,22
      Y=K-2
      YU(K)=Y*.05
      U(1,K)=U(2,K)=Q/3.141592654
  120 T(1,K)=T(2,K)=V(K)=0.
      IF(LX.EQ.0)121,122
  121 PI=0.
  122 X=P=H=D2U=0.
      DBX=DX
      AA=.0125/DX
      PRA=400./PR
      PR8=PRA*2.
      II=L=0
      LC=10
      LL=1
      WRITE(61,60)X,P,H,Q,LL,L,L,D2U
```

Fig. F.1-1 Sheet 1 of 4 of the computer programme for uniform surface heat flux ducts

```
      WRITE(61,65)(T(1,K),K=2,22)
      WRITE(61,65)(U(1,K),K=2,22)
      U(1,22)=U(2,22)=0.
      TM=0.
      CU(22)=.00125
      UU(2)=WU(2)=PRB
      AU(2)=BU(2)=800.
      DO126K=2,21
  126 DU(K)=(YU(K+1)*YU(K+1)-YU(K)*YU(K))*1.570796327
  128 LL=LL+1
      IF(LL.GT.201)GOTO100
      X=X+DX
      IF(LL.LT.LX.OR.LL.EQ.LX)GOTO130
  130 DO135K=3,21
      ZU(K)=(V(K)-1./(PR*YU(K)))/.1
      UU(K)=PRA+ZU(K)
      WU(K)=PRA-ZU(K)
      TU(K)=U(1,K)/DX
      XU(K)=TU(K)*U(1,K)
      BU(K)=(V(K)-1./YU(K))/.1
      AU(K)=400.-BU(K)
      BU(K)=400.+BU(K)
      CU(K)=1./(TU(K)+800.)
      RU(K)=TU(K)*T(1,K)
  135 TU(K)=TU(K)+PRB
      RU(2)=U(1,2)*T(1,2)/DX
      TU(2)=U(1,2)/DX+PRB*2.
      CU(2)=1./(U(1,2)/DX+1600.)
      XU(2)=U(1,2)*U(1,2)/DX
      R=0
      DO190K=2,21
      T(3,K)=T(2,K)*COSF(PHI)
  190 R=R+DU(K)*(CU(K+1)+CU(K))
      SU(22)=0.
      I=0
  200 I=I+1
      SUM=A=0.
      U(2,1)=U(2,3)
      DO210K=2,21
  210 SU(K)=(XU(K)+U(2,K+1)*AU(K)+U(2,K-1)*BU(K)+T(3,K))*CU(K)
      DO220K=2,21
  220 A=A+DU(K)*(SU(K+1)+SU(K))
      DPDX=(A-Q)/R
      SU(22)=DPDX/800.
      DO230K=2,21
      TEMP=SU(K)-DPDX*CU(K)
      TEMP=TEMP-U(2,K)
      SUM=SUM+TEMP*TEMP
  230 U(2,K)=U(2,K)+TEMP
      IF(SUM.LT.1.E-12)250,200
  250 DO260K=2,20
      V(K+1)=(U(2,K+1)+U(2,K)-(U(1,K+1)+U(1,K)))*(YU(K)+YU(K+1))*AA
  260 V(K+1)=(V(K)*YU(K)-V(K+1))/YU(K+1)
      P=DPDX*DX+P
      IF(LL-LX)280,262,264
  262 LL=1
      LC=10
      LX=0
```

Fig. F.1-2 Sheet 2 of 4 of the computer programme for uniform surface heat flux ducts

```
    GOTO280
264 L=0
    N=3
    FT=1.
    H=6.2831853*X/PR
265 HR=0.
    DO266K=2,19
266 HR=HR+DU(K)*(U(2,K+1)*T(2,K+1)+U(2,K)*T(2,K))
    TEMP=T(2,21)
    T(2,21)=(H-(HR+DU(20)*U(2,20)*T(2,20)))/((DU(20)+DU(21))*U(2,21))
    R=(TEMP-T(2,21))**2
    DO267M=1,N
    L=L+1
    SUM=R
    T(2,1)=T(2,3)
    DO267K=2,20
    TEMP=(T(2,K+1)*WU(K)+T(2,K-1)*UU(K)+RU(K))/TU(K)
    TEMP=FT*(TEMP-T(2,K))
    SUM=SUM+TEMP*TEMP
    T(2,K)=T(2,K)+TEMP
267 CONTINUE
    IF(SUM.LT.1.E-12)270,268
268 FT=WT
    N=1
    GOTO265
270 T(2,22)=(T(2,21)*TU(21)-(T(2,20)*UU(21)+RU(21)))/WU(21)
    TM=TM+(T(1,22)+T(2,22))*DX
280 IF(LL.EQ.1)281,282
281 DX=DBX
    AA=.0125/DX
    X=0.
    PI=P
    GOTO290
282 IF(LC0.EQ.1.AND.LL.GT.4)GOTO286
    IF(LL.LT.10)290,283
283 IF(LL.EQ.LC)284,286
284 LC=LC+10
    GOTO290
286 IF(P+4.0*DPDX*DX.GT.0..OR.LL.EQ.201)290,300
290 R=HC=0.
    DO292K=2,21
    HC=HC+DU(K)*(U(2,K+1)*T(2,K+1)+U(2,K)*T(2,K))
292 R=R+DU(K)*(U(2,K+1)+U(2,K))
    D2U=(U(2,3)-U(2,2))*800.
    WRITE(61,55)X,DPDX,P,H,R,LL,L,I,D2U,HC
    WRITE(61,65)(T(2,K),K=2,22)
    WRITE(61,65)(U(2,K),K=2,22)
    WRITE(61,65)(V(K),K=2,22)
300 IF(P.GT.0.)305,310
305 II=II+1
    IF(II-III)310,350
310 DO320K=2,22
    T(1,K)=T(2,K)
320 U(1,K)=U(2,K)
    PP=-P
    HP=H
    IF(LL.EQ.LLL)340,330
330 GOTO128
```

Fig. F.1-3 Sheet 3 of 4 of the computer programme for uniform surface heat flux ducts

```
340 DX=DCX
    AA=.0125/DX
    GOTO128
350 TM=TM/(2.*X)
    X=X-P*DX/(PP+P)
    GR=1./X
    GRPR=GR*PR
    H=HP+(H-HP)*PP/(PP+P)
    TO=T(1,22)+(T(2,22)-T(1,22))*PP/(PP+P)
    FU=1./TM
    R=XP/X
    WRITE(61,70)
    WRITE(61,75)X,GR,GRPR,FU,PI,R,PR,Q,H,TO
    GRPR=GRPR*TM
    WRITE(61,80)
    WRITE(61,85)TM,GRPR
    GOTO100
360 STOP
    END
```

Fig. F.1-4 Sheet 4 of 4 of the computer programme for uniform surface heat flux ducts

APPENDIX G

Entry restrictions yielding values of ℓ_i/ℓ in excess of 0.8

An entry restriction larger than that given by the 37 in. long unheated section of the duct was obtained, as shown in Fig. 6.7, by using either a smaller diameter entrance or an additional duct of smaller diameter.

Smaller diameter entrance

A smaller diameter entrance is suitable only for the laminar flow regime. The reason for this is that for the other flow regimes it is not possible to determine the volume flow (Q) whose value is required to obtain the equivalent length of this additional entry restriction.

The equivalent length of the combined entry restriction can be estimated in the following manner:

1. The dimensionless volume flow (Q) is obtained by plotting the experimental values of Nu and Ra on Fig. 4.2 .
2. Reynolds number (Re_r) is obtained from Eq. (3.30) .
3. The mean flow velocity in the duct (u_m) is obtained from Eq. (3.26) .

4. For fully developed flow in the unheated section of the duct, the pressure drop per unit length (Δp_1) (17) is

$$\Delta p_1 = \rho \frac{u_m^2}{2} \frac{1}{2r_w} \frac{32}{Re_r} \qquad \ldots (G.1)$$

5. The pressure drop (Δp_2) produced by the abrupt enlargement of the flow cross-section (17) is

$$\Delta p_2 = \left(\frac{r_w^2}{r_e^2} - 1 \right)^2 \rho \frac{u_m^2}{2} \qquad \ldots (G.2)$$

where r_e is the radius of the entry passage.

A very much smaller pressure drop (Δp_3) occurs in the entry passage. A bold assumption is made that this pressure drop is the same as that for fully developed laminar flow. Hence

$$\Delta p_3 = \rho \frac{u_{me}^2}{2} \frac{\ell_e}{2r_e} \frac{32}{Re_{re}} \qquad \ldots (G.3)$$

where the subscript e refers to the entry passage.

The combined equivalent length (ℓ_i) of the unheated section of length ℓ_1 and the smaller diameter entrance is given by

$$\ell_i = \ell_1 + \frac{\Delta p_2 + \Delta p_3}{\Delta p_1} \qquad \ldots \text{(G.4)}$$

It is clear from the foregoing equations that the equivalent length of the combined restriction (ℓ_i) is a function of Re_r. Hence it follows that ℓ_i will vary with Ra. This dependence of ℓ_i on Ra can be seen by inspecting the experimental results in Fig. 7.6; a 0.400 in. diameter entrance gave values of ℓ_i/ℓ ranging from 1.8 to 4.2, a 0.219 in. diameter from 8.7 to 20 and a 0.098 in. diameter in excess of 20.

Additional duct of smaller diameter

Since the equivalent length of an additional duct of smaller diameter can be obtained without requiring a knowledge of the volume flow Q, this entry restriction is suitable for tests in all flow regimes. However, the length and diameter of the additional restriction should be chosen so that the pressure drop produced by the abrupt enlargement of the flow area is sufficiently small to be ignored.

Referring to Fig. 6.7, the equivalent length of the combined restriction is estimated in the following manner. The flow in each of the unheated sections is

assumed to be laminar and fully developed. Therefore the pressure drop (Δp_4) in the larger diameter section, designated by the subscript 1, is (17)

$$\Delta p_4 = \rho \frac{u_{m1}^2}{2} \frac{\ell_1}{2\, r_{w1}} \cdot \frac{32}{Re_{r1}} \qquad \ldots \text{(G.5)}$$

and the pressure drop (Δp_5) in the smaller diameter section, designated by the subscript 2, is

$$\Delta p_5 = \rho \frac{u_{m2}^2}{2} \cdot \frac{\ell_2}{2\, r_{w2}} \cdot \frac{32}{Re_{r2}} \qquad \ldots \text{(G.6)}$$

Since the volume flow in each section is the same, dividing Eq. (G.5) by Eq. (G.6) yields

$$\frac{\Delta p_4}{\Delta p_5} = \frac{\ell_1}{\ell_2} \left(\frac{r_{w2}}{r_{w1}} \right)^4 \qquad \ldots \text{(G.7)}$$

The equivalent length of the combined restriction is given by

$$\ell_i = \ell_1 + \frac{\Delta p_5}{\Delta p_4} \ell_1 \qquad \ldots \text{(G.8)}$$

and using Eq. (G.7) gives

$$\ell_i = \ell_1 + \ell_2 \left(\frac{r_{w1}}{rw_2}\right)^4 \qquad \ldots \text{(G.9)}$$

In this case, Eq. (G.9) shows that the equivalent length of the combined entry restriction (ℓ_i) is independent of Re_r and consequently of Ra.

REFERENCES

1. J.R. Dyer: The development of natural convection in a vertical circular duct. Mech. and Chem. Engg. Trans. I.E. Aust., vol. MC4, No. 1, pp. 78-86 (1968)

2. J.R. Dyer: The development of laminar natural-convective flow in a vertical duct of circular cross-section that has a flow restriction at the bottom. Heat transfer 1970, vol. IV, Paper NC 2.8, Elsevier Publishing Company, Amsterdam (1970)

3. M.J. Lighthill: Theoretical considerations on free convection in tubes. Quart. Journ. Mech. and Applied Math., vol. 6, part 4, pp. 398-439 (1953)

4. W. Elenbaas: The dissipation of heat by free convection (from) the inner surface of vertical tubes of different shapes of cross-section. Physica, vol. 9, no. 8, pp. 865-874 (1942)

5. W. Elenbaas: Heat dissipation of parallel plates by free convection. Physica, vol. 9, no. 1, pp. 1-28 (1942)

6. J.R. Bodoia and F.J. Osterle: Development of free convection between heated vertical plates. Trans. A.S.M.E., Series C, Journ. of Heat Transfer, vol. 84, pp. 40-44 (1962)

7. J.R. Dyer and J.H. Fowler: The development of natural convection in a partially-heated vertical channel formed by two parallel surfaces. Mech. and Chem. Engg. Trans. I.E. Aust., vol. MC2, no. 1, pp. 12-16 (1966)

8. H. Schlichting: Boundary layer theory. 4th ed., McGraw-Hill Book Company, New York, 647 p. (1960)

9. E.C.R. Eckert and R.M. Drake: Heat and mass transfer. 2nd ed., McGraw-Hill Book Company, New York, 530 p. (1959)

10. W.H. McAdams: Heat transmission. 3rd ed., McGraw-Hill Book Company, New York, 532 p. (1954)

11. F.M. Leslie and B.W. Martin: Laminar flow in the open thermosyphon, with special reference to small Prandtl numbers. Journal of Mechanical Engineering Science, vol. 1, no. 2, pp. 184-193 (1959)

12. B.W. Martin and H. Cohen: Heat transfer by free convection in an open thermosyphon tube. British Journ. of Applied Physics, vol. 5, pp. 91-95 (1954)

13. B.W. Martin: Free convection in an open thermosyphon, with special reference to turbulent flow. Proceedings of the Royal Society of London, series A, vol. 230, pp. 502-530 (1955)

14. E.M. Sparrow and J.L. Gregg: Laminar free convection from a vertical plate with a uniform heat flux. Trans. A.S.M.E., vol. 78, pp. 435-440 (1956)

15. B.W. Martin and F.C. Lockwood: Entry effects in the open thermosyphon. J. Fluid Mech., vol. 19, pp. 246-256 (1964)

16. J.R. Bodoia: Finite difference analysis of confined viscous flow. Ph.D. thesis, Carnegie Institute of Technology, 117 p. (1959)

17. V.L. Streeter (ed.): Handbook of fluid dynamics, McGraw-Hill Book Company, New York (1961)